

2018 | Faculty of Sciences



**UHASSELT**

KNOWLEDGE IN ACTION

Doctoral dissertation submitted to obtain the degree of  
Doctor of Sciences, to be defended by

**Matthew McDonald**

**DOCTORAL DISSERTATION**

Study and properties of neural  
bi-directional interfaces,  
fabricated by cell engulfment  
of boron-doped nanodiamond  
nanostructures

IMO-IMOMEC  
 imec

**Promoter:** Prof. Dr Milos Nesladek

**Co-promoter:** Prof. Dr Ken Haenen

D/2018/2451/11

Doctoral dissertation

**Study and properties of neural bi-directional interfaces, fabricated by cell engulfment of boron-doped nanodiamond nanostructures**

Matthew McDonald

|                      |   |
|----------------------|---|
| Chair:               | Prof. Jan Colpaert<br><i>Universiteit Hasselt, Belgium</i>                        |
| Supervisor           | Prof. Milos Nesládek<br><i>Universiteit Hasselt &amp; IMEC vzw, Belgium</i>       |
| Co-promoter:         | Prof. Ken Haenen<br><i>Universiteit Hasselt &amp; IMEC vzw, Belgium</i>           |
| Members of the jury: | Prof. Hans-Gerd Boyen<br><i>Universiteit Hasselt, Belgium</i>                     |
|                      | Prof. An Hardy<br><i>Universiteit Hasselt, Belgium</i>                            |
|                      | Prof. Michele Giugliano<br><i>Universiteit Antwerpen, Belgium</i>                 |
|                      | Dr. Stoffel Janssens<br><i>Okinawa Institute of Science and Technology, Japan</i> |
|                      | Prof. Marcel Ameloot<br><i>Universiteit Hasselt, Belgium</i>                      |

# Table of Contents

|   |             |
|---|-------------|
| <b>Table of Contents</b> .....  | <b>iii</b>  |
| <b>Acknowledgements</b> .....   | <b>vii</b>  |
| <b>Journal Publications</b> .....   | <b>ix</b>   |
| <b>Training Activities</b> .....  | <b>x</b>    |
| <b>Nederlandse Samenvatting</b> .....                                     | <b>xi</b>   |
| <b>Summary</b> .....  | <b>xiii</b> |
| <b>List of Abbreviations</b> .....  | <b>xv</b>   |
| <b>List of Figures &amp; Tables</b> .....                                 | <b>xix</b>  |
| Figures .....   | xix         |
| Tables .....  | xxii        |
| <b>1 Introduction</b> .....   | <b>1</b>    |
| <b>2 Background: An Overview of Diamond &amp; Electrophysiology</b> ..... | <b>3</b>    |
| <b>Diamond</b> .....  | <b>3</b>    |
| 2.1 General properties of diamond .....                                   | 4           |
| 2.2 Diamond Synthesis.....  | 6           |
| 2.2.1 HPHT Synthesis of Single Crystal Diamond.....                       | 7           |
| 2.2.2 CVD of Polycrystalline Diamond .....                                | 8           |
| 2.3 Doping Diamond .....  | 11          |
| <b>Electrophysiology</b> .....  | <b>12</b>   |
| 2.4 Neurons and their Action Potential.....                               | 13          |
| 2.5 Intracellular recordings: patch clamp.....                            | 16          |
| 2.6 Extracellular recordings: micro-electrode arrays.....                 | 18          |

|          |  |           |
|----------|--|-----------|
| 2.6.1    | Basic Setup.....   | 18        |
| 2.6.2    | Electrode design .....   | 20        |
| 2.6.3    | Electrical model of cell-electrode interface .....   | 22        |
| 2.6.4    | Engulfment mechanism of mushroom electrodes .....  | 25        |
| <b>3</b> | <b>Materials and Experimental Techniques .....</b>   | <b>27</b> |
| 3.1      | Substrates and Preparation .....   | 27        |
| 3.1.1    | Cleaning .....   | 27        |
| 3.1.2    | Diamond Nanoparticle Seeding .....   | 28        |
| 3.2      | ASTeX MPECVD Systems.....  | 29        |
| 3.2.1    | In-situ thickness measurements .....   | 31        |
| 3.3      | Sputtering and Reactive-Ion Etching System .....   | 33        |
| 3.4      | Lithographic Process.....  | 35        |
| 3.4.1    | Photolithography procedures .....  | 36        |
| 3.4.2    | Electron Beam Lithography procedure .....  | 37        |
| 3.5      | Scanning Electron Microscopy .....   | 38        |
| 3.6      | Raman Spectroscopy .....   | 39        |
| 3.7      | Electrochemical Impedance Spectroscopy.....  | 41        |
| <b>4</b> | <b>Diamond substrates for culturing neurons .....</b>  | <b>45</b> |
| 4.1      | Motivation .....   | 46        |
| 4.2      | Contributions.....   | 47        |
| 4.3      | Article: Impact of differently modified nanocrystalline diamond on the growth of neuroblastoma cell.....                       | 48        |
| 4.3.1    | Contributions to the article "Impact of differently modified nanocrystalline diamond on the growth of neuroblastoma cell"..... | 48        |
| 4.3.2    | Main Body of "Impact of differently modified nanocrystalline diamond on the growth of neuroblastoma cell".....                 | 49        |

|          |   |           |
|----------|---|-----------|
| 4.4      | Article: Nanocrystalline diamond surfaces for adhesion and growth of primary neurons, conflicting results and rational explanation.....                       | 62        |
| 4.4.1    | Contributions to the article "Nanocrystalline diamond surfaces for adhesion and growth of primary neurons, conflicting results and rational explanation"..... | 62        |
| 4.4.2    | Main body of the article "Nanocrystalline diamond surfaces for adhesion and growth of primary neurons, conflicting results and rational explanation".....     | 63        |
| 4.5      | Polyethyimine surface treatment.....  | 83        |
| 4.5.1    | Contributions to Section 4.5 "Polyethyimine Surface Treatment"....  | 83        |
| 4.5.2    | Substrate fabrication.....  | 83        |
| 4.5.3    | Substrate preparation.....  | 84        |
| 4.5.4    | Primary neuronal cultures.....  | 85        |
| 4.5.5    | Cell biological analysis.....   | 85        |
| 4.5.6    | Cellular electrophysiology.....   | 87        |
| <b>5</b> | <b>Planar diamond MEAs.....</b>   | <b>89</b> |
| 5.1      | MEAs with NCD Passivation layer.....  | 90        |
| 5.1.1    | MEA Fabrication.....  | 90        |
| 5.1.2    | Substrate Preparation.....  | 90        |
| 5.1.3    | Primary Neuronal cultures.....  | 90        |
| 5.1.4    | Network Electrophysiology.....  | 91        |
| 5.2      | Article: Diamond microelectrode arrays for in-vitro neuronal recordings   | 94        |



# Acknowledgements

I would like to acknowledge a number of people who have helped me throughout this project, including colleagues and important collaborators who this project would not have been possible without. In the past four years, I have learned valuable lessons from colleagues and friends about what it means to be a scientist in the academic field. These people have helped me grow as both a researcher and as a person, have assisted in the laboratory, have shared knowledge, and have provided critical analysis that has helped me progress.

Firstly, I would like to thank my promoter Professor Milos Nesládek who gave me this opportunity and has guided me throughout it. I highly value his knowledge and expertise which has taught me many valuable lessons. I also appreciate the freedom and responsibility given to me that allowed me to develop my own ideas and challenged me to think critically.

I would also like to thank Professor Ken Haenen who has provided valuable insight into my research.

Thank you to Professor Jan Colpaert for chairing my defense committee. Also, thank you to the jury, especially Stoffel Janssens and Michele Giugliano as external referees for evaluating my thesis.

I have a lot of gratitude to Micha Spira and his lab for the strong collaboration that we have kept throughout this project. Without his valuable input and exchange of devices, much of this research would not have been possible.

Thank you to Michele Giugliano and his research group, especially Lowry Curly and Antonina Monaco, who have provided valuable testing of our devices and have provided a solid flow of ideas and communication.

I would like to thank all of the many colleagues who have made my stay at IMO a wonderful experience. Special thanks to Stoffel and Wiebke for being my mentors in diamond growing.

Paulius, thank you for teaching me about sputtering mechanisms and in-depth discussions about any topic that I came for help with.

Thank you Farnoosh for a valuable collaboration between our similar research topics, and always providing a positive attitude to our discussions.

Sien, thank you for contributing to the positive attitude at 1.06 and for your valuable contributions to the projects.

Thank you Christopher for taking over the continued work of my project and I wish you all the best in the future work.

I am also very grateful to all of my other colleagues, including Yaso, Wim, Quang, Weng-Siang, Rajesh, Elena, and Sankaran for providing valuable discussions and making my time at IMO a worthwhile experience.

Special thanks to the technicians, especially Johnny, who kept everything running smoothly and was always willing to help. Thank you Jan and Bart for introducing me to the SEM setup and continually helping improve my technique with it.

Thanks Hilde and Christel for keeping the laboratories safe and well stocked, and for providing help with chemicals or equipment.

Thanks to my friends Peter and Mark who joined me in this journey from Canada to Europe with me and were constant supports both academically and personally.

Thank you Relinde and Ellen, as well as their colleagues at IMEC, for helping me navigate the maze of administration.

My thanks go to all of the fellows of the NAMASEN and MERIDIAN projects including Laurent, Benjamin, Hayder, Rocco, Sreedhar, Peter, Chaitanya, Tutu, Silviya, Tiago, and Mauro.

Thank you Gitte for being a constant source of motivation and helping me through my hardest times. Without you, I don't think I would have been able to finish this PhD.

Thanks to all of the others that I have forgotten, I hope you will forgive me!

*Thanks everybody! Dank jullie wel!*

# Journal Publications

- Diamond microelectrode arrays for in vitro neuronal recordings  
*M. McDonald, A. Monaco, F. Vahidpour, K. Haenen, M. Giugliano, M. Nesladek*  
MRS COMMUNICATIONS, VOLUME 7, ISSUE 3, SEPTEMBER 2017, PAGES 683-690
- Biofouling resistance of boron-doped diamond neural stimulation electrodes is superior to titanium nitride *in vivo*  
*S. Meijs, M. Alcaide, C. Sorensen, M. McDonald, S. Sorensen, K. Rechendorff, A. Gerhardt, Milos Nesladek, N.J.M Rijkhoff, C.P. Pennisi*  
JOURNAL OF NEURAL ENGINEERING, VOLUME 13, NUMBER 5, AUGUST 2016, 056011
- Increased charge storage capacity of titanium nitride electrodes by deposition of boron-doped nanocrystalline diamond films  
*S. Meijs, M. McDonald, S.Sørensen, K. Rechendorff, V. Petrak, M. Nesladek, N. Rijkhoff, P. Pennisi*  
NEUROTECHNIX 2015 CONFERENCE PAPER, VOLUME 3, NOVEMBER 2015
- Evaluation of Theophylline Imprinted Polypyrrole Film  
*I. Baleviciute, V. Ratautaite, A. Ramanaviciene, Z. Balevicius, J. Broeders, D. Croux, M. McDonald, F. Vahidpour, R. Thoelen, W. Ceuninck, K. Haenen, M. Nesladek, A. Reza, A. Ramanavicius*  
SYNTHETIC METALS, VOLUME 209, NOVEMBER 2015, PAGES 206-211
- Impact of differently modified nanocrystalline diamond on the growth of neuroblastoma cells  
*A. Vaitkuvienė, M. McDonald, F. Vahidpour, J.P. Noben, K. Sanen, M. Ameloot, V. Ratautaite, V. Kasetā, G. Biziuleviciene, A. Ramanaviciene, M. Nesladek, A. Ramanavicius*  
NEW BIOTECHNOLOGY, VOLUME 32, ISSUE 1, JANUARY 2015, PAGES 7-12
- Impact of Diamond Nanoparticles on Neural Cells  
*A. Vaitkuvienė, V. Ratautaite, A. Ramanaviciene, K. Sanen, R. Paesen, M. Ameloot, V. Petrakova, M. McDonald, F. Vahidpour, G. Ramanauskaite, G. Biziuleviciene, M. Nesladek, A. Ramanavicius*  
MOLECULAR AND CELLULAR PROBES, VOLUME 29, ISSUE 1, FEBRUARY 2015, PAGES 25-30
- Nanocrystalline diamond surfaces for adhesion and growth of primary neurons, conflicting results and rational explanation  
*S. M. Ojovan, M. McDonald, N. Rabieh, N. Shmuel, H. Erez, M. Nesladek, M. E. Spira*  
FRONTIERS IN NEUROENGINEERING, VOLUME 7, ARTICLE 17, JUNE 2014

# Training Activities

- Neuroscience 2015, Chicago (USA), 19-21 Oct 2015 (Oral presentation)
- Hasselt Diamond Workshop 2015 SBDD XX, Hasselt (Belgium), 25-27 Feb 2015 (Poster Presentation)
- 4th NAMASEN Training Workshop, Heraklion (Greece), 1-4 July 2014.
- Hasselt Diamond Workshop 2014 SBDD XIX, Hasselt (Belgium), 19-21 Feb 2014
- International Conference on Micro and Nano Engineering, London (UK), 16-19th Sep 2013. (Poster Presentation)
- 2nd NAMASEN Training Workshop, Antwerpen (Belgium), 6-7th Jun 2013.
- Hasselt Diamond Workshop 2013 SBDD XVIII, Hasselt (Belgium), 27 Feb-1 Mar 2013
- 4th International Conference on Neuroprosthetic Devices, Freiburg (Germany), 19-20th Nov 2012.
- 8th International Meeting on Substrate-Integrated Microelectrode Arrays, Reutlingen (Germany), 11-13th Jul 2012.
- 1st NAMASEN Training Workshop, Reutlingen (Germany), 9-10th Jul 2012.
- European Summer School of Neuroengineering, Genova (Italy), 11-15th Jun 2012.
- Hasselt Diamond Workshop 2012 SBDD XVII, Hasselt (Belgium), 14-16 Mar 2012

# Nederlandse Samenvatting

In dit project wordt nano-kristallijne diamant (NCD) onderzocht voor toepassingen binnen bio-compatibele implanteerbare materialen, en geavanceerde neuro-elektrische apparaten bestemd voor actieve neurale koppelingen. Het primair objectief van het project spitst zich toe op de ontwikkeling van een functionele neurale koppeling gebruikmakende van 3D-microstructuur-geïmpregneerde diamanten. Deze koppelingen worden verwacht langdurige parallele opnamen te faciliteren met uiterst hoogwaardige signaalkwaliteit. De NCD-gebaseerde dunne films, die gebruikt worden als substraten voor de groei van neuroblastomacellen en neuronen, zijn gelijkaardig en/of beter als de conventionele glasoppervlakken. In tegenstelling tot de oppervlaktebehandeling vereist bij conventionele glasoppervlakken door middel van polyethylenimine (PEI) of poly-d-lysine / laminine voor niet-proliferende cellen, is er geen voorbehandeling vereist voor de goede groei en adhesie van profilerende cellen (neuroblastomen) op NCD-gebaseerde substraten. De NCD-gebaseerde films worden opgenomen op een multielektrode-array (MEA) als een isoleerlaag tussen de geleidende connecties, gebruikmakende van isolerend diamant als een passiveringslaag en gedopeerd diamant als een vlakke electrode voor de functionele MEA's. Deze apparaten zijn vergelijkbaar in performantie als standaard MEA's die gebruikelijk bestaan uit dikkere siliciumnitride-lagen. Aansluitend wordt borium-gedopeerde nano-kristallijne diamant (BNCD) geïntroduceerd als een geleidend elektrodemateriaal ter vervollediging van de diamanten koppeling. Deze apparaten worden met succes gebruikt voor de opname van primaire corticale neuronen van muizen. Om de elektrodeverzakking te stimuleren, en als gevolg, de signaalkwaliteit te versterken, worden apparaten met een driedimensionale elektrodegeometrie gefabriceerd. Hierbij wordt de elektrodeverzakking van de NCD beoordeeld door een matrix van gouden paddestoelvormige microstructuren te bedekken met een dunne laag van BCND. Deze matrices vertonen goede verzakkingseigenschappen. Tensloten worden functionele MEA met diamanten paddestoelvormige elektroden in vitro getest met primaire hippocampale

rattenneuronen. Preliminair resultaten tonen opnamen van hoge kwaliteit die kenmerkend zijn voor een verzwakt intracellulair signaal.

# Summary

In this work, nanocrystalline diamond (NCD) was investigated as a novel paradigm of biocompatible implantable materials and advanced neuroelectric devices were constructed to be used for active interfacing to neural cells. The primary objective of this project was aimed at developing a device with a full diamond interface, including 3D microstructures made from conducting diamond, for neuronal interfacing. It is expected that a device of this nature will enable long-term parallel recordings with extremely high quality signals. NCD thin films were used as substrates for the growth of neuroblastoma cells and neurons, and shown to be as good as or better than conventional glass surfaces. For proliferating cells (neuroblastoma) it was found that no pre-treatment of the NCD surface was necessary for good growth and adhesion, while for the non-proliferating neurons, a conventional glass surface treatment of polyethylenimine (PEI) or poly-d-lysine/laminin was necessary. These NCD films were then incorporated onto multielectrode array (MEA) devices as an insulation layer for the conductive leads, using a combination of insulating diamond as a passivation layer and doped diamond as a planar electrode material for functional MEAs. These devices were shown to have similar characteristics to standard MEAs that are employing a much thicker standard silicon nitride layer. Boron-doped nanocrystalline diamond (BNCD) was introduced as a conductive electrode material to complete a device with a full diamond interface. These devices were successfully used for recordings of primary cortical neurons from mice. Finally, devices with three dimensional electrode geometry were fabricated in order to promote engulfment of the electrode for increased signal quality. Engulfment of these electrodes with NCD was tested by coating an array of gold mushroom-shaped microstructures with a thin layer of BCND. These arrays showed good engulfment characteristics. Finally, a functional MEA with diamond mushroom shaped electrodes was tested *in vitro* with primary hippocampal rat neurons. Preliminary results showed high quality recordings, characteristic of an attenuated intracellular signal.



# List of Abbreviations

## Abbreviations

- AlN** – Aluminium nitride
- B<sub>2</sub>H<sub>6</sub>** – Diborane
- BMI** – Brain machine interfacing
- BNCD** – Boron-doped nanocrystalline diamond
- BS** – Blocking solution
- BSE** – Back-scattered electrons
- CAM** – Cell adhesion molecule
- CDL** – Double layer capacitance
- CNT** – Carbon nanotube
- CVD** – Chemical vapor deposition
- DI** – Deionized
- DIV** – Days in-vitro
- DMEM** – Dulbecco’s Modified Eagle Media
- DMSO** – Dimethyl sulfoxide
- DND** – Detonation nanodiamond
- EBL** – Electron-beam lithography
- ECM** – Extra-cellular matrix
- EDX** – Energy-dispersive x-ray spectroscopy
- EIS** – Electrochemical impedance spectroscopy
- FBS** – Fetal bovine serum
- FIB** – Focused ion-beam
- FS** – Fused silica
- GaAs** – Gallium arsenide
- GaN** – Gallium nitride
- GFAP** – Glial fibrillary protein
- H<sub>2</sub>O<sub>2</sub>** – Hydrogen peroxide
- HBSS** – Hank’s Balanced Salt Solution
- HPHT** – High temperature and high pressure

**HQD** – High quality diamond  
**HSP** – Heat shock protein  
**HSQ** - Hydrogen silsesquioxane  
**IBID** – Ion beam induced deposition  
**IBID** – Ion beam induced deposition  
**IPA** – Isopropyl alcohol  
**IrOx** – Iridium oxide  
**ITO** – Indium-tin oxide  
**K<sub>v</sub> channel** - voltage-gated potassium K<sub>v</sub> channel  
**LOR** – Lift-off resist  
**LQD** – Low quality diamond  
**MCD** – Microcrystalline diamond  
**MEA** – Microelectrode array  
**MFR** – Mean firing rate  
**MWPECVD** – Microwave plasma enhanced chemical vapor deposition  
**Na<sub>v</sub> channel**– Voltage-gated sodium channel  
**NCD** – Nanocrystalline diamond  
**NH<sub>4</sub>OH** – Ammonium hydroxide  
**PDL** – Poly-D-lysine  
**PEDOT** – poly(3,4-ethylenedioxythiophene)  
**PEI** – Polyethylenimine  
**PLL** – Poly-L-lysine  
**PMMA** – Poly(methyl metacrylate)  
**PtIr** – Platinum iridium  
**RCA1** – Silicon wafer cleaning technique  
**RCA2** – Silicon wafer cleaning technique  
**RIE** – Reactive-ion etching  
**R<sub>RMS</sub>** – Root mean squared surface roughness  
**Rs** – Solution resistance  
**Rseal** – Seal resistance  
**SE** – Secondary electrons  
**SEM** – Scanning electron microscopy  
**SiC** – Silicon carbide  
**SiOx** – Silicon oxide

**SNR** – Signal to noise ratio  
**TiN** – Titanium nitride  
**TMAH** – Tetramethylammonium hydroxide  
**TMB** – Trimethylborane  
**UNCD** – Ultrananocrystalline diamond  
**XPS** – X-ray photoelectron spectroscopy

## **Symbols & Constants**

**C<sub>e</sub>** – Electrode capacitance  
**C<sub>j</sub>** – Capacitance of junctional cell-electrode interface  
**C<sub>nj</sub>** – Capacitance of non-junctional cell-electrode interface  
**CPE** – Constant phase element  
**CPE<sub>DL</sub>** – Double-layer constant phase element  
**E(t)** – time dependent voltage  
**E<sub>m</sub>** – amplitude of sinusoidal voltage  
**i(t)** – Time dependent current  
**i<sub>m</sub>** – amplitude of sinusoidal current  
**R<sub>C</sub>** – Resistor-capacitor (in reference to a type of circuit)  
**R<sub>CT</sub>** – Charge transfer resistance  
**R<sub>e</sub>** – Electrode resistance  
**R<sub>j</sub>** – Resistance of junctional cell-electrode interface  
**R<sub>nj</sub>** – Resistance of non-junctional cell-electrode interface  
**R<sub>s</sub>** – Solution resistance  
**t** – time  
**t<sub>k</sub><sup>i</sup>** – Time of occurrence of an action potential of k-th channel  
**V<sub>k</sub>(t)** – Raw extracellular voltage waveforms of k-th channel  
**Y<sub>0</sub>** – pseudo-double-layer capacitance  
**Z** – impedance  
**Z<sub>w</sub>** – Warburg element  
**α** – Exponential factor related to degree of capacitance or resistance behavior  
**Φ** – phase shift  
**ω** – frequency



# List of Figures & Tables

## Figures

|   |    |
|---|----|
| Figure 2-1 – Unit cell of face-centered cubic diamond lattice structure.....  | 4  |
| Figure 2-2 – Carbon phase diagram. Adapted from [23]. .....   | 7  |
| Figure 2-3 – SEM images showing fine grain structure of ultra-nanocrystalline diamond, nanocrystalline diamond, and microcrystalline diamond.....                                   | 10 |
| Figure 2-4 – Schematic of (a) the physical and chemical processes occurring in the CVD reactor, and (b) the reaction process of stepwise addition occurring at diamond surface..... | 11 |
| Figure 2-5 – Schematic of cells lipid bilayer with the integral membrane proteins responsible for the ionic gradient between intracellular and extracellular space.. ..             | 14 |
| Figure 2-6 – Diagram of a typical action potential in a neuron. ....  | 15 |
| Figure 2-7 – Diagram showing the structure of a neuron with insert showing the transmission of signal through synapses by neurotransmitters. ....                                   | 16 |
| Figure 2-8 – (a) Typical MEA design with glass well for culturing. (b) Array pattern of 59 electrodes where recordings are made. ....   | 19 |
| Figure 2-9 – Schematic of a typical MEA stimulation and recording setup.....  | 20 |
| Figure 2-10 – Schematic of the electrical equivalent circuit of a neuron close to the electrode of a MEA. ....  | 23 |
| Figure 2-11 – Electrical model of the junction between a neuron and a mushroom shaped electrode. ....   | 24 |
| Figure 2-12 – Schematic showing (a) engulfment of a particle by phagocytosis, and (b) incomplete phagocytosis-like engulfment of a protruding electrode.....                        | 26 |
| Figure 3-1 – ASTeX 6500 MWPECVD system. ....  | 29 |
| Figure 3-2 – Schematic of thin-film interference, used for in-situ monitoring of diamond film growth. ....  | 32 |
| Figure 3-3 – Image of home built system at IMO used for both sputtering and reactive-ion etching. ....  | 34 |

|  |    |
|--|----|
| Figure 3-4 – (a) Schematic of SEM, and (b) schematic of origin of various radiation sources within sample by the electron beam. ....   | 39 |
| Figure 3-5 – Raman spectrum of nano-crystalline diamond at different excitation laser wavelengths. ....  | 41 |
| Figure 3-6 – (a) Schematic of Randles equivalent circuit used for modeling electrodes, (b) Nyquist plot of Randles circuit showing the real and imaginary parts of the impedance, and (c) typical Bode plots of the impedance magnitude and phase as a function of frequency ..... | 43 |
| Figure 4-1 - Hydrophobicity of nanocrystalline diamond and boron doped nanocrystalline diamond surfaces with oxygen and hydrogen terminations.....   | 55 |
| Figure 4-2 - Proliferation of SH-SY5Y cells after 72 h cultivation with NCD and B(1)NCD coatings of different termination.....   | 56 |
| Figure 4-3 - Light microscopy images of SH-SY5Y cells after 48 h cultivation on NCD coatings in medium with FBS.. ....   | 58 |
| Figure 4-4 - Light microscopy images of SH-SY5Y cells after 48 h cultivation on NCD coatings in medium without FBS.....  | 59 |
| Figure 4-5 - Proliferation of SH-SY5Y cells after 48 h cultivation on different NCD samples/substrates in medium with FBS (■) and without FBS (□).....   | 60 |
| Figure 4-6 - Characterization of the nanocrystalline surface. ....   | 69 |
| Figure 4-7 - Clusters of hippocampal neurons cultured on bare glass or NCD surfaces.. ....   | 71 |
| Figure 4-8 - Embryonic hippocampal neurons (7 DIV) cultured on: (A) PDL-laminin functionalized glass and (B) PDL-laminin functionalized NCD .....  | 73 |
| Figure 4-9 - The structural organization of cell–aggregates formed on bare NCD substrate.....  | 74 |
| Figure 4-10 - Confocal image of immunolabeled hippocampal cells.....   | 75 |
| Figure 4-11 - SEM image of embryonic hippocampal neurons cultured on PDL-laminin functionalized NCD, 7 DIV. ....   | 76 |
| Figure 4-12 - Connectivity map of 14 days old cultured embryonic neurons on PDL-laminin functionalized NCD surface.....  | 79 |
| Figure 4-13 – Biological analysis of diamond substrates vs. control, by cell-counting (left) and % viability with XTT assay (right). ....  | 86 |
| Figure 4-14 – Staining of cell nuclei (DAPI, blue), glia (GFAP, red) and neurons (β III Tubulin, green) at 14 DIV.....   | 87 |

|  |     |
|--|-----|
| Figure 4-15 – Intracellular (patch-clamp) recordings of primary cortical neurons on NCD and quartz control substrates. ....  | 88  |
| Figure 5-1 – Summary of all the action potentials recorded at 14 DIV, at each individual electrode (above) and as a histogram of spikes (below). ....  | 92  |
| Figure 5-2 – Mean firing rate and burst frequency of cortical neurons on NCD-MEAs and control MEAs. ....   | 93  |
| Figure 5-3 - Fully packaged BNCD/NCD MEA (left) and SEM image of the active sensing area (right). ....   | 96  |
| Figure 5-4 – Fabrication process of MEAs with BNCD electrodes and NCD passivation layer. ....  | 98  |
| Figure 5-5 – SEM image of BNCD electrode (left) and SEM image showing fine grain structure of BNCD electrode vs. NCD passivation layer. ....   | 101 |
| Figure 5-6 – Bode plot of a BNCD electrode with active area of 707 $\mu\text{m}^2$ . ....  | 103 |
| Figure 5-7 – a) Plot of impedance magnitude and phase of all microelectrodes before and after b) attaching a glass ring as a culture chamber. c) Impedance magnitudes for 5 MEAs, averaged over all their microelectrodes. ....  | 104 |
| Figure 5-8- Effect on neurons cell properties by culturing on BNCD films compared to control condition (n=6). ....   | 105 |
| Figure 5-9 - Spiking activity recorded on a diamond MEA compared to a control MEA with ITO electrodes. ....  | 106 |
| Figure 6-1 – SEM images of mushroom chips. ....  | 111 |
| Figure 6-2 – Fabrication steps involved in creating diamond MEAs with 3D mushroom shaped diamond electrodes. ....  | 112 |
| Figure 6-3 - (a) Liftoff structures with EBL b) Aluminum mask evaporation (c) lift-off and etching through SiO <sub>2</sub> /NCD to open electrode (d) Growth of BNCD stem through opened hole (e) continued BNCD growth to create mushroom head (f) removal of SiO <sub>2</sub> to reveal final structure. .... | 114 |
| Figure 6-4 – Cross section of NCD coated gold mushrooms of different sizes. ....   | 119 |
| Figure 6-5 – Recordings from 7 active mushroom shaped diamond electrodes after 12 DIV (above) and 16 DIV (below). ....   | 120 |
| Figure 6-6 – Recordings from two different mushroom shaped diamond electrodes<br>.....   | 121 |

# Tables

|  |    |
|--|----|
| Table 2-1 – Electrical properties of diamond compared to other semiconductors. Adapted from [17], [18], [21].        | 6  |
| Table 3-1 – Deposition parameters for sputtering of different materials and for reactive ion etching.                | 35 |
| Table 4-1 – Parameters applied for the deposition of NCD   | 52 |
| Table 4-2 – Hydrogenation conditions of NCD and BNCD samples   | 53 |
| Table 4-3 – Patch-clamp data comparing membrane potentials on various substrates. Measurements taken from DIV 14-21. | 88 |

# 1 Introduction

Brain-machine interfacing (BMI) is an exciting field with an enormous potential to impact human lives through coupling of the electrical circuits of the brain with external devices. This allows for a bidirectional communication between the digital world of computers and the biological realm of the brain. To fully utilize this potential, much improvement is needed in the tools used at the brain-machine interface, as well as in the understanding of the physiological workings of the brain. These two aspects will develop in tandem, as better devices allow for a more detailed analysis of the brain and its constituent cells. Electrophysiology is the study of this field, which integrates aspects of materials science, biology, chemistry, and engineering, to build the tools used in brain-machine interfacing. These tools can be used to elucidate the fundamental workings of the brain, provide potential solutions to neurodegenerative diseases such as Parkinson's disease, macular degeneration, and retinitis pigmentosa, or even to control prosthetic devices with haptic feedback loops directly to the brain.

Two primary approaches in electrophysiology are (1) recording of neuronal electrical signals and (2) evoking action potentials through electrical stimulation. High quality recordings require a low impedance, whereas efficient stimulation requires a high charge transfer capacitance; which are both dependent on the cell-electrode interface and the material properties of the electrode. 'Patch-clamping' is a technique that uses a micropipette to puncture cells in order to obtain high quality intracellular signal with complete control of the cell potential [1]. However, this technique suffers from the disadvantages of only being able to measure from a single cell at a time, as well as causing cells to die shortly after investigation. Microelectrode arrays (MEAs) have been developed as a tool in electrophysiology for highly parallel extracellular recordings with high spatial and temporal resolution; though due to this extracellular nature, MEAs suffer from poor signal quality and have typically been limited to spike counting of action potentials [1, 2]. For high spatial resolution, the electrodes must be made quite small, on the order of a cell, which leads to a high impedance and low capacitance. Furthermore, typical planar electrodes are passive in the formation of neural

networks and a significant cleft if formed between the cell and electrode, massively degrading the quality of electrical recordings. It has been shown that 3D microelectrodes in the shape of mushrooms can be used to promote an engulfment type mechanism by the neurons to minimize the cleft and drastically enhance the signal quality to that of intracellular recordings [3–5]. On the other hand, the electrode material plays a large role as well. Recently, diamond has attracted attention as a potential electrode material in electrophysiology due to its inert chemistry, incredible biocompatibility, and exceptional electrochemical and electrical properties which make it suitable for chronic use [6–12]. Additionally, the surface of diamond is naturally anti-fouling and can be easily functionalized using standard carbon chemistry techniques for adhesion promotion or to reduce immune response.

After a brief introduction in Chapter 1, the theory and background related to this multifaceted topic is laid out in Chapter 2. Chapter 2 covers theory on diamond and its synthesis and gives a background of electrophysiology in terms of neuron physiology and recording/stimulation techniques, focused on MEAs and the current state of the art. In Chapter 3, the techniques used for fabrication and characterization are described with a theoretical explanation of the technique followed by practical implementation used in this thesis.

Chapters 4-6 follow a progression of milestones leading to the overarching goal of this work. Chapter 4 shows that NCD can be used as an effective platform for neuronal growth with use of a proper surface treatment, characterized by staining experiments and cell counting assays. Chapter 5 demonstrates both that diamond can be used as an effective insulator and as a conductive electrode material towards MEA devices. This is shown by producing MEA devices and using them to record signal characteristics and compared to control devices. Chapter 6 verifies that neurons will engulf 3D mushroom-shaped structures made from a diamond interface, and establishes a robust fabrication process for creating 3D protruding electrodes from doped diamond to be used for the electrical recording and stimulation of neural cells. Chapter 7 goes on to summarize the work, highlighting the novelties and providing an outlook for future work on this topic.

# 2 Background: An Overview of Diamond & Electrophysiology

## Diamond

Carbon is a truly outstanding atom which not only makes up the backbone of life as we know it, but also creates the strongest materials known to man. The versatility of carbon lies in its unique electronic structure which allows it to form up to four covalent bonds through molecular orbital hybridization. The electronic ground state of carbon is  $1s^2 2s^2 2p^2$ , which leaves two unpaired electrons; according to valence theory this would typically allow for only two bonds to be formed [13]. However, through hybridization of the 2s orbital with the 2p orbitals, different kind of bonding patterns are available. This hybridization leads to predictable molecular geometries based on the number of bonds formed, caused by the repulsion of valence shell electrons [14]. When the 2s orbital hybridizes with only one p-type orbital, it creates two sp bonds which form linear molecules ( $180^\circ$  bond angle) such as acetylene [14]. If, however, two of the p-type orbitals hybridize with the 2s orbital, then three  $sp^2$  bonds are formed, which arrange into the trigonal pattern ( $120^\circ$  bond angle) responsible for the structure of graphene and carbon nanotubes. When all three p-type orbitals hybridize with the 2s orbital, it creates four  $sp^3$  bonds, which arrange into a tetrahedral shape ( $109.5^\circ$  bond angle). When each carbon  $sp^3$  bond is attached to another carbon  $sp^3$  bond and repeated, the resultant material is known as diamond. The tetrahedral bonding pattern of diamond leads to a face-centered cubic crystallographic structure with eight carbon atoms per unit cell, as shown in Figure 2-1.

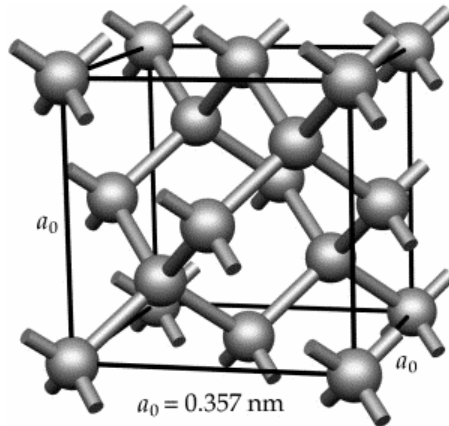


**Figure 2-1** – Unit cell of face-centered cubic diamond lattice structure. Adapted from [15] .

At room temperature, the diamond unit cell has a length of  $3.57 \text{ \AA}$  and a C-C bond length of  $1.53 \text{ \AA}$ , giving an atomic density of  $1.76 \times 10^{23} \text{ atoms/cm}^2$ , the highest density of all known materials. The main crystallographic planes used to describe the structure of diamond, which are also often the orientation of samples, are (100), (110), and (111).

## 2.1 General properties of diamond

Diamond is commonly used for cutting tools and abrasives due to its exceptional hardness and stiffness, which ultimately stems from the high binding energy of the  $sp^3$  bonding structure [13]. However, the unique C-C  $sp^3$  bonds give rise to many other superlative properties which make diamond interesting for electrical, thermal, mechanical, optical, and biological applications. The strong bonding between carbon atoms in the diamond lattice also gives rise to an extreme chemical inertness, which gives it a high degree of biocompatibility [13]. Furthermore, the dangling  $sp^3$  bonds at the surface typically terminate with hydrogen or oxygen. However, these can also be bonded with molecules using standard carbon chemistry to functionalize the surface, for example, to enhance protein adsorption or target specific biomarkers [16]. The tetrahedral structure, high energy bonding and short bond length of diamond results in a dense, high mass, non-polar crystal with extreme phonon velocity; giving rise to a low thermal

expansion coefficient and the highest thermal conductivity of any material at room temperature [13]. These properties also give diamond high optical phonon energies and a long acoustic phonon relaxation period, resulting in high charge carrier mobility for electrons ( $2200 \text{ cm}^2/\text{Vs}$ ) and holes ( $1800 \text{ cm}^2/\text{Vs}$ ) [17, 18]. When the molecular orbitals of a carbon atom hybridize, it forms not only four sigma bonding orbitals, but another four sigma anti-bonding orbitals which are at a higher energy [14]. When there is network of carbon atoms  $sp^3$  bonded together, the energy difference between bonding and anti-bonding orbitals is quite large and gives rise to a wide band gap of 5.47 eV [13]. This gives diamond a large breakdown voltage and low band-to-band carrier generation/recombination noise, making it attractive for high power or low-noise electrical devices. However, the electrical properties of diamond can be modified by incorporating specific impurities through a process called doping (described in Section 2.32.3), to lower the band-gap or even eliminate it, and give metallic conductivity. Many of the electrical properties of diamond are summarized in Table 2-1. Recently, diamond has attracted much attention in the field of quantum optics due to its color-center defects which can be used as qubits in quantum computing, or sensitive optical sensors in many different applications [19, 20]. Furthermore, diamond is wide-spectrum optically transparent, between wavelengths of 220 nm and  $80 \mu\text{m}$  [13]. Each of these properties of diamond alone is quite outstanding, but the truly remarkable thing is the potential to use these properties in conjunction to provide integrated solutions for a variety of applications.

**Table 2-1** – Electrical properties of diamond compared to other semiconductors. Adapted from [17], [18], [21].

| <b>Material Property</b>  | <b>Si</b> | <b>GaAs</b> | <b>SiC<br/>(6H)</b> | <b>SiC<br/>(4H)</b> | <b>GaN</b> | <b>Diamond</b> |
|---|-----------|-------------|---------------------|---------------------|------------|----------------|
| <b>Band gap (eV)</b>  | 1.12      | 1.42        | 2.86                | 3.26                | 3.39       | 5.47           |
| <b>Dielectric Constant</b>  | 11.9      | 13.1        | 9.7                 | 9.7                 | 10.4       | 5.7            |
| <b>Breakdown field (MV·cm<sup>-1</sup>)</b>                             | 0.3       | 0.4         | 3                   | 2.7                 | 2.7        | 10             |
| <b>Hole mobility (cm<sup>2</sup>·V<sup>-1</sup>·s<sup>-1</sup>)</b>     | 370       | 400         | 100                 | 120                 | 24         | 1800           |
| <b>Electron mobility (cm<sup>2</sup>·V<sup>-1</sup>·s<sup>-1</sup>)</b> | 1450      | 8500        | 370                 | 981                 | 1245       | 2200           |
| <b>Thermal conductivity (W·cm<sup>-1</sup>·K<sup>-1</sup>)</b>          | 1.15      | 0.46        | 3.6                 | 3.6                 | 2          | 21.9           |

## 2.2 Diamond Synthesis

Though diamond is such a hard and inert material, it is actually only a metastable allotrope of carbon, as the  $sp^2$  bonding of graphite is energetically more favorable [22]. However, once diamond is formed, the kinetic barrier to overcome the transition back to  $sp^2$  carbon is large enough that temperatures over 1620 °C at atmospheric pressure would be required [22]. There are two main techniques for making diamond: high temperature and high pressure (HPHT), and chemical vapor deposition (CVD). HPHT works by using bulk graphite under extreme conditions to convert into a large single crystalline diamond, while CVD builds diamond layer by layer by reacting a gaseous carbon form onto the growing surface. Figure 2-2 shows a phase diagram for carbon with the temperature and pressure regions for the various synthesis methods.

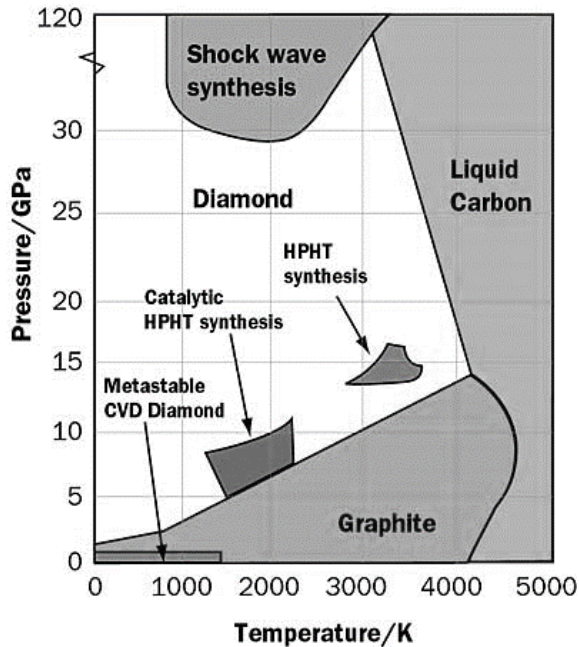


**Figure 2-2** – Carbon phase diagram. Adapted from [23].

### 2.2.1 HPHT Synthesis of Single Crystal Diamond

Diamond forms naturally deep under the earth's surface where high temperature and high pressure give favorable conditions for the transition between  $sp^2$  to  $sp^3$  carbon. The HPHT method emulates these conditions by applying temperature of ca. 1600 K at ca. 55 kbar in combination with a molten metal catalyst to lower the transition barrier between the two phases [24]. Without this catalyst (typically cobalt, nickel, iron, chromium, platinum, or palladium), the transition would require conditions of >130 kbar at ca. 3300 K [24]. This process is performed by discharging a large electrolytic capacitor through graphite in order to heat it while avoiding melting of, or reactions with, the surrounding chamber. This method was first demonstrated by General Electric in 1955 and shortly after in 1960 in Sweden by Allmänna Vesak Elektriska Aktiebolaget [22]. This method has succeeded as the most common technique in industrial fabrication of diamonds for use in polishing and cutting. HPHT is also sometimes used to change or enhance the colors of certain diamond gemstones in order to increase their value.

### 2.2.2 CVD of Polycrystalline Diamond

The basic mechanism behind chemical vapor deposition of diamond is that a gaseous carbon source decomposes onto an existing diamond lattice under low pressure and mild temperatures (200-1100 °C), building it layer upon layer. This technology was first reported in 1962, when Eversole described a method to fabricate diamond using a methyl gas source at pressures between 70-140 bar and temperatures of 900-1100 °C [22]. However, this technique suffered from a large amount of black carbon deposition and needed frequent interruptions during growth to remove it. It was not until 1982, when Matsumoto et al. incorporated hydrogen into the gas mixture of a hot filament reactor as a means to etch the graphitic  $sp^2$  phase carbon, that CVD diamond became a commercially viable technology and gained traction as an international topic of research [22]. Hot filament reactors use a tungsten filament at ca. 2000 °C to generate the hydrogen and methyl radicals that work together to add carbon to the  $sp^3$  template while etching  $sp^2$  carbon. Only a year later, microwave plasma enhanced CVD (MWPECVD) reactors were developed, which used a microwave power source to generate the radicals, eliminating the contamination caused by a hot tungsten filament. Though MPECVD is now the preferred method for large area, high quality thin film diamond deposition, hot filament CVD is still widely used, as are a number of other technologies, including: Direct current-plasma, Radio frequency-plasma, and electron cyclotron resonance microwave plasma CVD [22].

CVD diamond growth starts by nucleation on the surface and this is quite difficult without an existing diamond template to grow onto. In early development, large single crystal diamond fabricated by HPHT methods were used as substrates for the CVD diamond to grow. Hetero-substrates were also of great interest for growing diamond onto and Mitsuda et al. developed a technique to scratch the substrate surface with a solution of diamond microparticles in alcohol in order to enhance nucleation density [25]. This was thought to work by both increasing the substrates surface area by scratching, and embedding diamond particles as templates for diamond nucleation. Osawa et al. later developed another seeding technique which spincoats an aqueous diamond nanoparticle solution on the substrate [25]. This technique was found to typically give a higher seeding density and more uniform film growth. Yugo et al. also reported on nucleation of diamond

on hetero-substrates through ion bombardment using an electric field in the plasma reactor to enhance nucleation density [26].

Polycrystalline diamond films are a good compromise to single crystal diamond, as they retain many of the desirable properties, but can be deposited on a wide variety of surfaces that would not otherwise be possible. These diamond films can be generally categorized by their grain size, as shown in Figure 2-3. The initial diamond grains are composed of many facets which are randomly oriented and grow at different rates. In a survival of the fittest type growth, the faster growing facets swallow the slower facets, resulting in the grain size increasing with the film thickness, as larger grains dominate the growth and swallow smaller ones [27]. If these grains are greater than ca. 1  $\mu\text{m}$  than they can be considered microcrystalline diamond (MCD). If they are, however, between ca. 100 nm-1 $\mu\text{m}$  they are typically called nanocrystalline diamond (NCD); though it is typically of the same type of structure as MCD and continued growth would result in MCD. Ultrananocrystalline diamond (UNCD) growth occurs when the grains are very small (<100 nm) and typically independent of the thickness of the film. This is due to renucleation of diamond grains as the film grows, resulting in new grain formation [27]. As grain size of polycrystalline diamond films decreases, more of the material becomes composed of grain boundaries which are typically made of  $\text{sp}^2$  bonded carbon. High  $\text{sp}^2$  incorporation can lead to some desirable properties, such as low surface roughness, but comes at a loss of many bulk diamond properties, such as the high carrier mobility (due to increased carrier scattering); whereas low  $\text{sp}^2$  can give many material properties that approach that of bulk diamond. This composition and morphology can be controlled by the growth conditions, including: pressure, power, temperature, and gas composition.

Methane is a common carbon gas source for diamond growth and is the source used for all diamond growth contained within this thesis. Typically, methane makes up 0.5-10 % of the gas mixture in an excess of hydrogen, which is used to etch graphitic or amorphous carbon that deposits. Small quantities of oxygen can also be added to the gas mixture to help suppress  $\text{sp}^2$  carbon from forming while increasing the growth rate by lowering the concentration of acetylene in the reaction chamber. Argon is also often used, either as a replacement or in combination with hydrogen; this is typically used to generate UNCD, as the argon

helps to renucleate grains as the film grows. Many active species are present during growth, including:  $\text{CH}_4^+$ ,  $\text{CH}_3^+$ ,  $\text{CH}_2^+$ ,  $\text{CH}^+$ ,  $\text{C}^+$ ,  $\text{CH}_5^+$ ,  $\text{H}^+$ ,  $\text{H}_2^+$  and  $\text{H}_3^+$ , which leads to a complex series of kinetic reactions from the plasma to the growing diamond surface, described in Figure 2-4 [24].

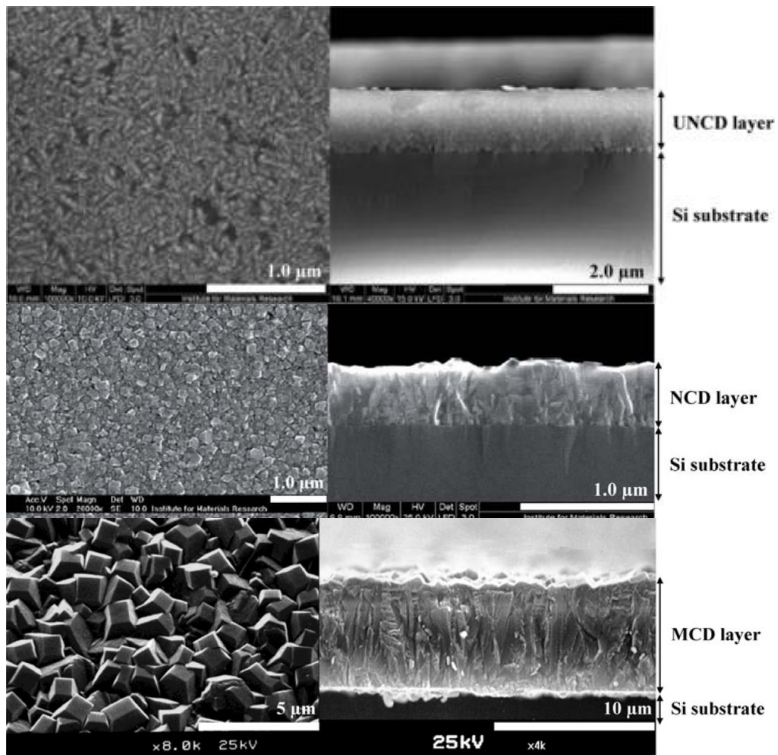


**Figure 2-3** – SEM images showing fine grain structure of ultra-nanocrystalline diamond, nanocrystalline diamond, and microcrystalline diamond. Adapted from [27].

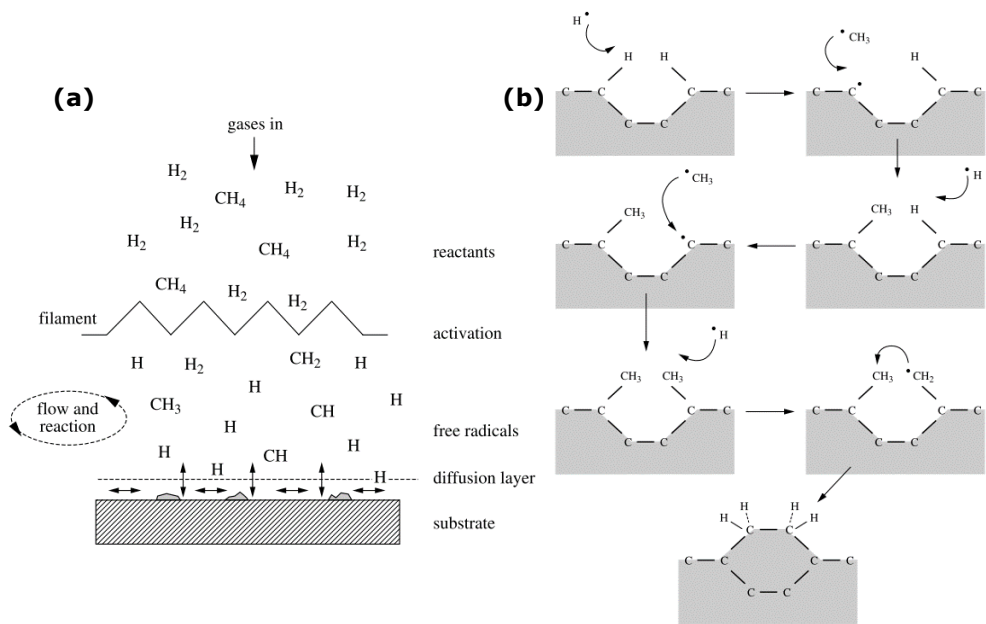


**Figure 2-4** – Schematic of (a) the physical and chemical processes occurring in the CVD reactor, and (b) the reaction process of stepwise addition occurring at diamond surface. Adapted from [24].

## 2.3 Doping Diamond

Intrinsic diamond is a wide bandgap semiconductor with a bandgap of 5.47 eV, making it a superb insulating material [13]. However, through substitutional replacement of carbon atoms in the lattice with dopant molecules, we can give diamond a metallic type conductivity. This is achieved by introducing dopant gases into the plasma reaction chamber during growth. Diamond is somewhat limited to this doping method, as heating to the temperatures required to form vacancies and interstitial atoms for doping by in-diffusion can disturb the metastability of diamond [15]. Furthermore, the short C-C bond length of diamond means that substitutional doping is also difficult, limiting the possible dopant atoms. The most common dopant atoms are boron for p-type doping and nitrogen, and phosphorus for n-type doping. Boron is a group-III element which acts as an electron acceptor and easily incorporates into the diamond lattice due to its similar atomic radius to carbon [15]. The acceptor activation energy of boron in diamond is ca. 0.37 eV,

which is large enough that only a small fraction of boron is thermally activated at room temperature [15]. Doping levels for boron range between  $10^{14}$  atoms/cm<sup>3</sup> to  $10^{21}$  atoms/cm<sup>3</sup>, with good electrical conductivity appearing around  $10^{19}$  atoms/cm<sup>3</sup> [28, 29]. At doping levels of ca.  $10^{20}$  atoms/cm<sup>3</sup>, the boron impurity band overlaps with the valence band, resulting in characteristic metallic like electrical conductivity. Trimethylborane (TMB) and diborane (B<sub>2</sub>H<sub>6</sub>) are commonly used sources of boron that are fed into the reaction chamber for boron doping. Nitrogen and phosphorous are both group-V donors that are able to fit in the diamond lattice and have successfully been used as dopant atoms [30]. Nitrogen substitutes well into the diamond lattice due to its small size but suffers from a deep activation energy of 1.7 eV, which renders it useless for electronic applications at room temperature. Phosphorus is next in the list of group-V elements and has been difficult to incorporate into the diamond lattice due to the strain caused by its larger atomic radius. Under the right plasma conditions, it is however possible to get effective phosphorus doping, which results in an activation energy of 0.46 eV [15]. Phosphorous is the most promising n-type dopant and has made major progress in recent years. However, boron doping remains the most common for diamond electrodes due to its ease of doping, negligible morphological changes and metallic-like conductivity. The incorporation of dopant into the structure of diamond also depends heavily on the growth conditions. The pressure, temperature, and relative concentrations of hydrogen, carbon, and boron are all important parameters that influence the doping efficiency. Given the granular structure of NCD, it is possible for dopant atoms can be incorporated into the grain boundaries in addition to the crystal structure itself. It has been shown that for suitable growth conditions of BNCD, that boron is well incorporated into the diamond crystal lattice [31, 32].

## **Electrophysiology**

The aim of electrophysiology is to study the electrical properties of biological cells and tissues. In this section, the basic theory of electrogenic cells and the tools used to study them are detailed. Electrogenic cells are capable of producing an electrical response, typically from mechanical, optical, chemical, thermal, or

electrical stimuli. There are two main types of electrogenic cells: the neurons which make up the main phenotype of the nervous system, and the cardiomyocytes which are muscle cells that make up the cardiac muscle. The focus in this chapter will be on: neural cells, the mechanism they use to create a signal, and the cell structures that allow this signal to propagate. Methods of neuronal recording will also be discussed. These can be separated into invasive intracellular recordings (patch-clamp) and non-invasive extracellular recordings (multi-electrode arrays). Furthermore, a brief discussion about intracellular patch-clamp recordings will be given, followed by a more in-depth review of multi electrode arrays with comparison of planar vs 3D electrode geometry.

## **2.4 Neurons and their Action Potential**

Neurons are electrically excitable cells and are the basic unit of signaling within the nervous system. They use electrical and chemical signals to process and transmit information through vastly interconnected networks. Typical neurons consist of a cell body (soma), an axon, and multiple dendrites [1]. Dendrites carry signals from other neurons, which are connected by a special junction called a synapse. These signals are carried toward the cell body, which integrates the juxtaposition of the incoming signals and determines whether to fire an action potential along its axon towards other neurons. The action potential is the fundamental electrical signal in electrophysiology, which is made possible by the unique membranes of electrogenic cells. The cell membrane is a lipid bilayer which is integral to the function of all cells as a diffusion barrier that physically separates the intracellular domain of the cell from the extracellular environment. The membrane can passively transport some small atoms and molecules directly through the lipid bilayer, but also contains embedded proteins to passively and actively transport specific ions and larger molecules. This membrane is electrically insulating, giving rise to a voltage across it when there is an imbalance of charge between the intracellular and extracellular regions, referred to as the membrane potential [1]. At an equilibrium of ionic flow, a resting potential is established, which is typically between -40 to -80 mV with respect to the extracellular domain [1]. This potential is maintained by a variety of passive ion-channels and active

ion-pumps in the membrane, which work together to create a concentration gradient between the two sides of the membrane [1]. There are three main membrane proteins relating to action potentials in neural cells: the voltage-gated sodium channel, the voltage-gated potassium channel, and the sodium-potassium pump, shown in Figure 2-5.

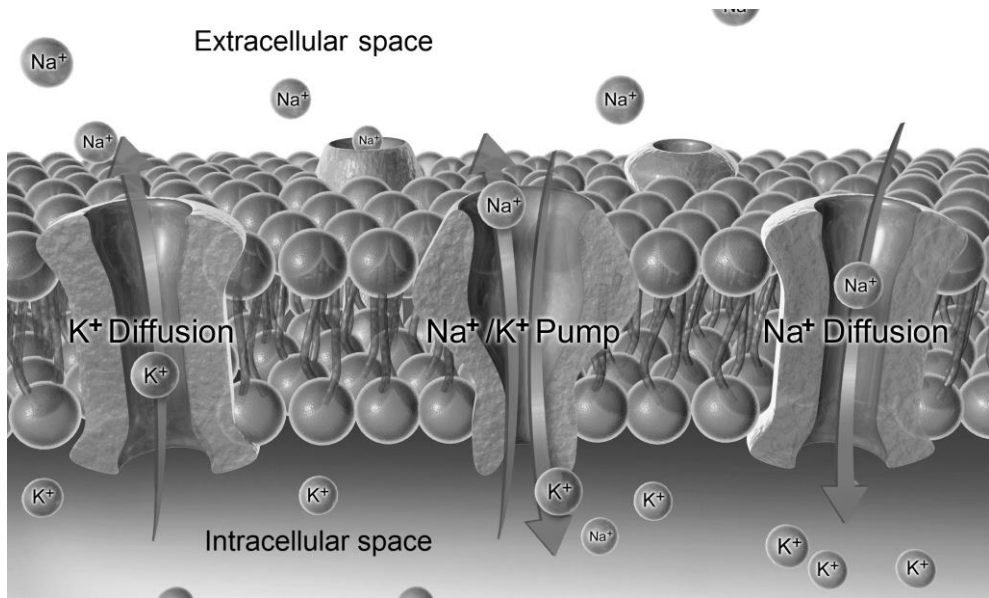


**Figure 2-5** – Schematic of cells lipid bilayer with the integral membrane proteins responsible for the ionic gradient between intracellular and extracellular space. Adapted from [33].

The voltage-gated sodium ( $\text{Na}_v$ ) channel has three possible configurations: deactivated, activated, and inactivated. At a resting potential of  $-70$  mV, most  $\text{Na}_v$  channels are in the deactivated state and are not-permeable to sodium ions [1]. As the membrane potential increases most  $\text{Na}_v$  channels remain closed until a threshold potential of  $-55$  mV is reached, whereupon there is a drastic increase in the activated population of  $\text{Na}_v$  channels [1]. As the  $\text{Na}_v$  channels allow sodium to enter the cell, this further increases the membrane potential and the number of open  $\text{Na}_v$  channels, leading to an explosive positive feedback loop called the depolarization phase [1]. This is also known as the “all-or-nothing” response. During depolarization, voltage-gated potassium ( $\text{K}_v$ ) channels also begin to open,

but more slowly than the  $\text{Na}_V$  channels [1]. Therefore, depolarization can occur, due to more sodium ions diffusing in than potassium ions diffusing out. At the peak of the action potential, the high potential causes the  $\text{Na}_V$  channels to enter the inactivated state, reducing sodium ion flow while  $\text{K}_V$  channels remain open, allowing potassium to diffuse out of the cell [1]. Potassium continues to diffuse out of the cell until slightly past the membrane resting potential (-90 mV) where the cell enters a refractory period [1]. During this period,  $\text{K}_V$  channels close and  $\text{Na}_V$  channels return to the deactivated state. The sodium-potassium pumps use energy to actively transport sodium out of the cell and potassium back into the cell to re-establish the concentration gradient and return to the resting potential in preparation for the next depolarizing stimulus. The different stages of the action potential are shown in Figure 2-6.

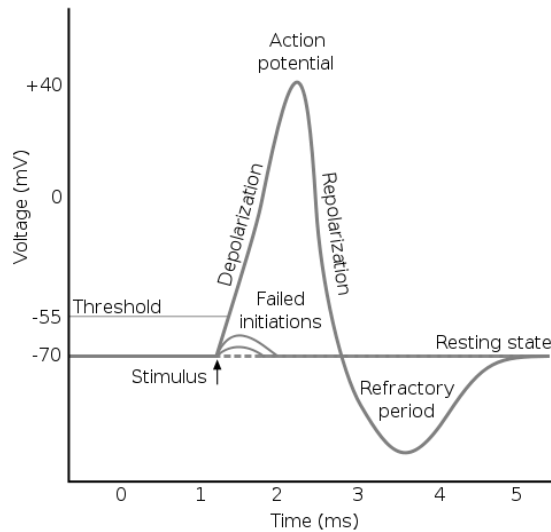


**Figure 2-6** – Diagram of a typical action potential in a neuron. Adapted from [34].

This action potential signal propagates across the axon by triggering action potentials to fire at periodic spatial intervals called Nodes of Ranvier. These nodes are separated by a special insulating Myelin sheath that allows conduction to propagate in a saltatory function as opposed to a continuous wave [1]. This increases the speed and efficiency of the electrical signal and is essential for the

proper functioning of the nervous system [1]. As the electrical signal reaches the end of the axon, it reaches the pre-synaptic site where it is converted into a chemical signal by releasing neurotransmitters into the synaptic cleft. The neighboring neuron receives these neurotransmitters at the postsynaptic cleft where it is converted back into an electrical signal that propagates towards the cell body, as shown in Figure 2-7.

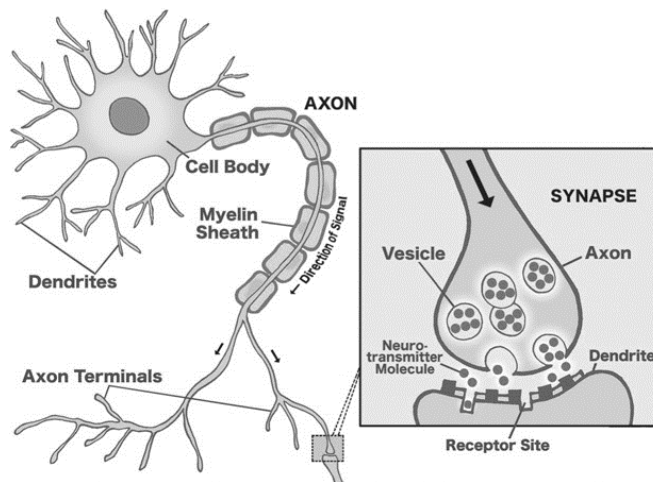


**Figure 2-7** – Diagram showing the structure of a neuron with insert showing the transmission of signal through synapses by neurotransmitters. Adapted from [35].

## 2.5 Intracellular recordings: patch clamp

The patch clamp technique is a method developed by Neher and Sakmann in the late 1970s that allowed the study of single or multiple ion channels in cells [1]. These techniques are especially suitable for studying electrically excitable cells, such as neurons, and Neher and Sakmann went on to win the Nobel Prize in Physiology and Medicine in 1991 for this work. The technique works by bringing a glass micropipette, filled with a metal electrode and electrolyte, close to the cell and applying a light suction to attach the cell membrane onto the tip. This forms a tight junction between the tip and cell membrane leading to a high resistance seal on the order of gigaohms. In this configuration it is called *cell-attached* patch and has the benefit of high seal-resistance and no disruption of the inside of the cell. The attached cell membrane can be detached from the rest of the cell to give

the *inside-out* patch configuration. This allows study of single ion channels with exposure of the intracellular side of the membrane to the external media [36]. In this way, the intracellular environment can be manipulated by changing the bath composition. From the cell-attached configuration it is also possible to apply either more suction or a voltage pulse to rupture the cell membrane and enter the *whole-cell* patch configuration. This configuration is used to obtain high quality recordings as the resistance is drastically reduced by removing the cell membrane. An inherent problem with this configuration is that the contents of the electrode will slowly replace the inside of the cell and alter its properties. *Perforated* patch is a compromise between whole-cell and cell-attached configurations. Instead of rupturing the cell membrane, antifungal or antibiotic agents are used to form small pores in the membrane which lowers access resistance while keeping the flow of molecules intact and retaining the regular signaling mechanisms [36]. The *outside-out* patch configuration starts from the whole-cell configuration and the micropipette is slowly withdrawn to pull parts of the membrane with it, which reform into a convex membrane at the tip. In this configuration the fluid of the micropipette is used to simulate the intracellular fluid. In this way, it is possible to study the current through the same membrane as it is exposed successively to different bath solution [36]. In all of these configurations, it is possible to perform the measurements using either *voltage-clamp* mode or *current-clamp* mode. In *voltage-clamp* mode the voltage is held constant while observing changes in current. In *current-clamp* mode the current is kept constant while the voltage is monitored. Though patch clamp techniques give unparalleled quality in signal recording, and allow study of membrane properties, they suffer from the drawbacks of allowing only acute recordings from single cells at a time. In the next section, we talk about how multi-electrode arrays have been used to fill the gap of multisite recordings over a long period of time to study network level electrophysiology.

## 2.6 Extracellular recordings: micro-electrode arrays

Multi-electrode arrays are another important tool used in electrophysiology which is complimentary to patch-clamping techniques. MEAs are chip based biosensors that have multiple micro- or nano- electrodes in a matrix through which neural signals can be recorded or delivered [37, 38]. These electrodes are non-invasive and signals are recorded extracellularly so it does not harm the cells or cause non-physiological changes in cell function; this enables long-term recordings over days or months. Another major advantage is the ability to record from multiple sites simultaneously in a small spatial area. However, the extracellular nature of the recording inherently leads to loss in signal quality. The two general classes of MEAs are those used for cell-culturing and tissue slices (*in vitro*), and those used for implantation into living animals (*in vivo*). With implanted MEAs, there are several impairing biological responses which depend on the MEA size, composition, and period of implantation. These responses include neuronal cell lose, glial scarring, and loss of functional electrodes [1]. Unlike in patch-clamp, the electrode is typically stationary, playing a passive role in cell placement relative to the electrode. However, recent work has shown that the electrode geometry can play an active role in enticing the cell closer to the interface through the cell's own mechanisms of engulfment [4]. In this section, the basic setup of multi-electrode array technologies will be described, followed by a discussion of the electrode design. An electrical model of the cell-electrode interface will then be detailed and a brief description of the engulfment mechanism for 3D electrodes will be given.

### 2.6.1 Basic Setup

Multi-electrode arrays typically consist of a matrix of electrodes which interface with the cells, connected to metal pads which interfaces to the outside world, allowing a neural interface to electronic circuitry. The tracks between the electrode matrix and the pads are generally insulated with a dielectric material. On *in-vitro* MEAs, a glass ring is typically placed on top to provide a chamber for cell culturing to prevent short-circuits from the culturing liquid. A typical MEA is shown in Figure

2-8 This provides only two material interfaces for the cells, that of the electrode, and that of the insulating (passivation) layer. Both of these layers should be biocompatible and bioinert, and the electrode material should be electrochemically stable.

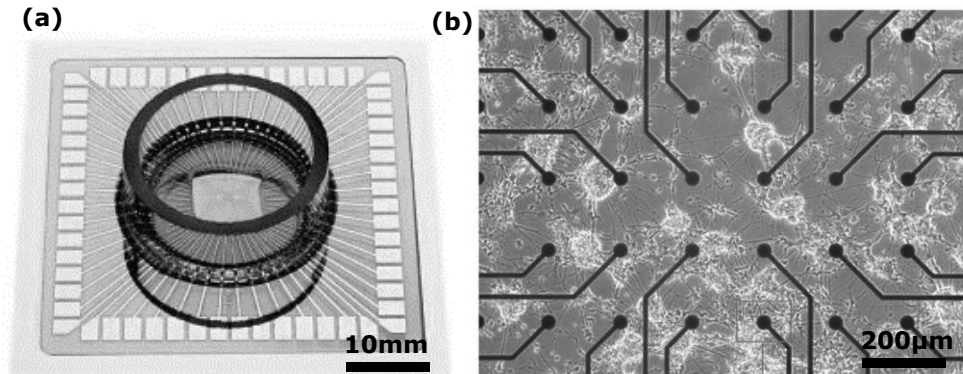


**Figure 2-8** – (a) Typical MEA design with glass well for culturing. (b) Array pattern of electrodes where recordings are made. Adapted from [39, 40]

Electrodes can be passive elements coated with various different conducting materials, or active transistors which are gated by neural signals. The signals are passed through the pads to an amplifier which filters and amplifies the signal. The amplitude and shape of recorded signals, as well as the charge injection capabilities for stimulation typically depend on the electrode material, surface area, and coupling with the cell. The amplification system also plays a role in the recording efficiency, but is limited by the sophistication of the setup and not by the electrode design. A typical scheme for a MEA recording system is shown in Figure 2-9.

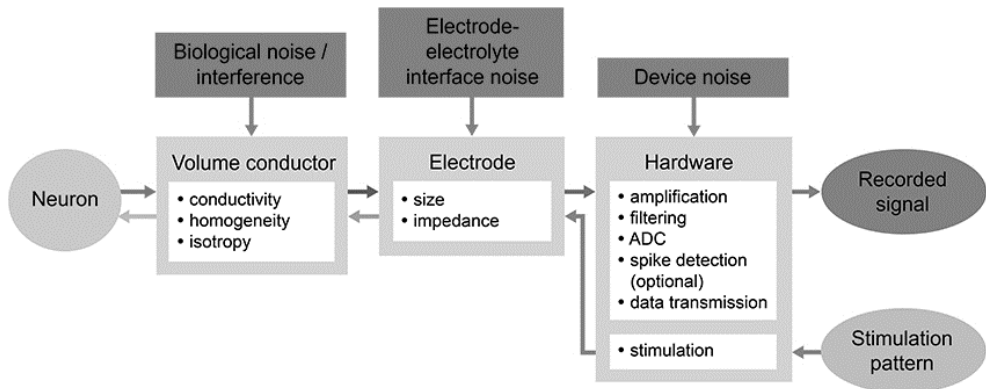


**Figure 2-9** – Schematic of a typical MEA stimulation and recording setup, showing the flow of signal and sources of noise. Adapted from [8].

### 2.6.2 Electrode design

The electrode-cell interface of MEAs is an important area of research in electrophysiology that draws from many fields, including: materials science, electrochemistry, biochemistry, and cellular biology. Electrodes sit extracellularly and thus record potential profiles from the entire cellular environment. Slow field potentials and action potentials from cells that sit close enough to the electrode are picked up as signals on the order of 100  $\mu\text{V}$ , while those further away contribute to the background or “neural-noise” [38]. The signal-to-noise ratio also depends on the electrode impedance and thus it is desirable to minimize this quantity. A voltage can also be applied to the electrodes which creates a potential gradient that can be used to depolarize neuron membranes and invoke an action potential. For this stimulation, voltages need to be kept low to avoid electrochemical reactions that could damage electrodes or cause side reactions that could damage cells. This means that electrodes need to have a large charge-storage capacitance so that an adequate charge can be delivered for stimulation. However, in order to achieve high spatial resolution, electrodes must be made as small as possible, which increases impedance and lowers the charge storage capacity. This trade-off of impedance and charge-storage capacity vs. spatial resolution has been the driving factor for research into new electrode designs and materials [8, 38, 39]. One of the main approaches towards this issue is the use of highly porous electrode materials which have high surface areas and

drastically reduce impedance while increasing charge storage capacity [37, 40]. Another approach has been to entice cells towards the electrode through electrode geometry, surface functionalization with biomolecules or growth factors, or a combination of both [4, 41].

Commonly used electrode materials include: gold (Au), platinum (Pt), platinum iridium (PtIr), iridium oxide (IrOx), indium-tin oxide (ITO) and titanium nitride (TiN) [8]. More recently, carbon based materials have been used, including: graphene, carbon nanotubes (CNTs), conducting polymers, and boron-doped diamond [38, 40]. Pt and PtIr electrodes have large impedances and relatively low charge injection limits of 50-150  $\mu\text{C}\cdot\text{cm}^{-2}$  and are not completely electrochemically stable [44]. IrOx was developed as an electrode material using a faradaic charge injection mechanism by the redox reaction of  $\text{Ir}^{3+}$  to  $\text{Ir}^{4+}$  to deliver charge capacities up to 750  $\mu\text{C}\cdot\text{cm}^{-2}$  [44]. TiN has gained widespread use due to its fractal microstructure which gives it a large surface area, leading to a charge injection capacitance of ca. 900  $\mu\text{C}\cdot\text{cm}^{-2}$  and impedances of ca. 40 k $\Omega$  for a typical microelectrode of 30  $\mu\text{m}$  diameter [42, 43, 44]. CNTs coated in the conductive polymer poly(3,4-ethylenedioxythiophene) (PEDOT) is one of the most promising recently developed electrode materials [45, 46]. These electrodes can obtain charge injection capacities up to 2-10 mF $\cdot\text{cm}^{-2}$ , with impedances as low as 14 k $\Omega$  on a typical microelectrode. However, CNT toxicity is a known issue that could limit the application of these electrodes for *in-vivo* implantation. Recently it has been shown that nanostructured boron-doped diamond electrodes can also reach charge storage capacities of ca. 10 mF $\cdot\text{cm}^{-2}$  with impedances below 50 k $\Omega$  for a typical microelectrode [11].

Typically, MEAs employ a circular planar style of electrode, though recently, smaller electrodes with different geometries have been developed including, needle, nail, and mushroom shapes [38]. The closer a cell sits to the electrode the better the signal will be compared to the neural-noise, allowing a greater impedance and thus smaller electrode size. The idea is to use the cells own mechanisms to attract it to the electrode, giving tight cell adhesion and improved signal quality. The electrical recordings from these electrode designs give direct evidence of the cell interaction with the 3D shape of these electrodes. Particularly, Hai et al. have recorded signals comparable in amplitude and shape to intracellular

patch-clamp recordings from gold mushroom shaped electrodes on the order of 1 $\mu$ m diameter [3]. This has led to the term 'in-cell' recordings for signals that are extracellularly recorded from microelectrodes but have similar shape and quality of intracellular patch-clamp recordings. Depending on the material, geometry may be necessary but not sufficient for this engulfment behaviour and may need surface functionalization. Proteins such as poly-D-lysine (PDL) and poly-L-lysine (PLL) are commonly used to promote general neural adhesion, though other more sophisticated biomolecules can be used for signaling specific biological pathways [38]. The electrical description of the cell-electrode interface and why engulfment of 3D electrodes gives improvement will be detailed in the following section. The actual engulfment mechanism of the cell will be briefly discussed in the section after.

### **2.6.3 Electrical model of cell-electrode interface**

In order to simplify the electrical description of the cell-electrode interface, we only consider a single cell in close proximity to the electrode and build an equivalent circuit relating different physiological elements to electrical elements, as seen in Figure 2-10.

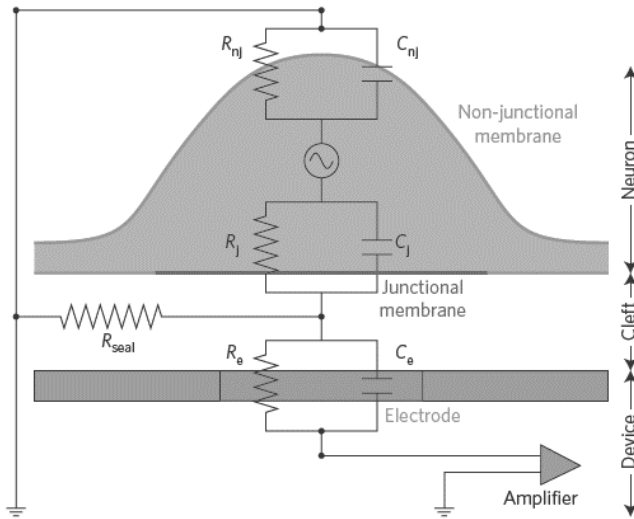


**Figure 2-10** – Schematic of the electrical equivalent circuit of a neuron close to the electrode of a MEA. Adapted from [38].

In this model, the neurons plasma membrane can be considered to have two domains: the junctional membrane which faces the electrode and the non-junctional membrane which faces the surrounding media. Each of these membrane regions is modeled by a resistor in parallel with a capacitor:  $R_j$  and  $C_j$  for the junctional membrane and  $R_{nj}$  and  $C_{nj}$  for the non-junctional membrane. Between the membrane components a current generator is added to model the current generated by an action potential. The electrode is also modeled by a resistance ( $R_e$ ) and a capacitance ( $C_e$ ) in parallel. The electrode circuit is connected on one end to the junctional membrane and to an amplifier on the other. However, between the neuron and the electrode there is a cleft which is filled with cell media full of electrolytic species which generates a resistance to ground called the seal resistance ( $R_{seal}$ ). If the seal is not tight, then currents will leak to the extracellular medium in quantities proportional to the voltage drop across the equivalent resistor. To minimize this current, there should be a high seal resistance, which physically means tight binding to the electrode surface. Typically, this cleft is in the range of 40-100 nm for planar electrodes, leading to  $R_{seal}$  values in the 1-2 M $\Omega$  range [3]. The aim of 3D microelectrodes is to improve signal quality by increasing the seal resistance and decreasing the junctional

resistance. A coupling coefficient can be used to determine the quality of the cell-electrode coupling and is defined as the ratio between the maximum recordable voltage by the electrode in response to a voltage generated by the cell. Figure 2-11 shows simulations of the coupling coefficient for different values of the seal resistance and junctional resistance at a low and high frequency signal.

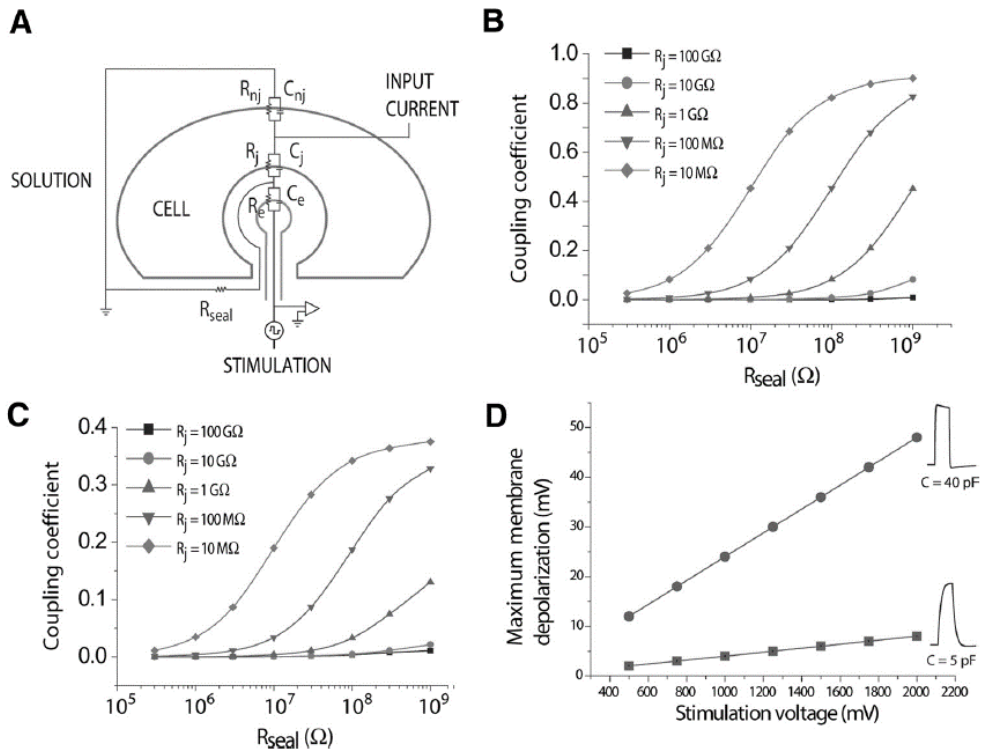


**Figure 2-11** – Electrical model of the junction between a neuron and a mushroom shaped electrode: (a) the equivalent electrical circuit of electrode-neuron junction, (b) coupling coefficient as a function of seal resistance and junctional resistance at high frequency (100 Hz), (c) coupling coefficient as a function of seal resistance and junctional resistance at low frequency (1 Hz), (d) Maximum membrane depolarization as a function of the stimulation voltage for electrodes with high (circles) and low (squares) capacitance. Adapted from [3].

In the model presented in Figure 2-11, junctional resistances were chosen to range between 10 M $\Omega$  and 100 G $\Omega$  based on values calculated for an action potential in a frequency range of 100 Hz to 1 kHz with a seal resistance of 100 M $\Omega$  and coupling coefficients between 0.05 to 0.5. As can be seen, the coupling

coefficient increases by about an order of magnitude by changing from a planar electrode coupling ( $R_{\text{seal}} \sim 1 \text{ M}\Omega$ ) and 3D electrode coupling ( $R_{\text{seal}} \sim 100 \text{ M}\Omega$ ). It has been shown that with gold mushroom shaped electrodes, the junctional resistance decreases by at least an order of magnitude, which is likely due to a recruitment of voltage-independent ion channels to the cell-electrode interface. Furthermore, the seal resistance is enhanced and stabilized by the formation of an actin ring around the stalk of these mushroom shaped electrodes which holds it in place. The engulfment mechanisms that lead to these improvements in electrical properties will be discussed in the following section.

#### **2.6.4 Engulfment mechanism of mushroom electrodes**

Mushroom shaped electrodes have been developed in recent years to solve the challenge of weak electrical coupling of the cell and electrode. This is based on taking advantage of the cells natural mechanisms to induce a phagocytosis type event [4, 5]. These types of electrodes emulate the shape and dimensions of dendritic spines, which are small protrusions scattered along dendrites where synaptic connections are made. Phagocytosis is a mechanism used by cells to internalize particles such as bacteria, dead tissue cells, and mineral particles for nutrients. The size, shape, and biomolecular coating of the particles are all determining factors in the uptake of particles by phagocytosis and can be specific to the type of cell. This process starts by the interaction of the cells' extracellular receptor molecules with the targets molecules which tether the two together. The engaged receptors increase as more of the cells receptors are recruited to the target and this signals recruitment of a family of proteins responsible for internalization. As the proteins drive the engulfment further, a ring of actin filaments pulls the membrane closed and finally pinches it off from the cell membrane. Engulfment of mushroom shaped electrodes is based on this mechanism where it engulfs the head of the mushroom but can not finish. The actin filaments form a ring around the base of the mushroom and immobilize it, which creates a mechanically stable interface. The dimensions and the surface functionalization are thus important parameters for these types of electrodes in order to successfully induce engulfment; shown in Figure 2-12.

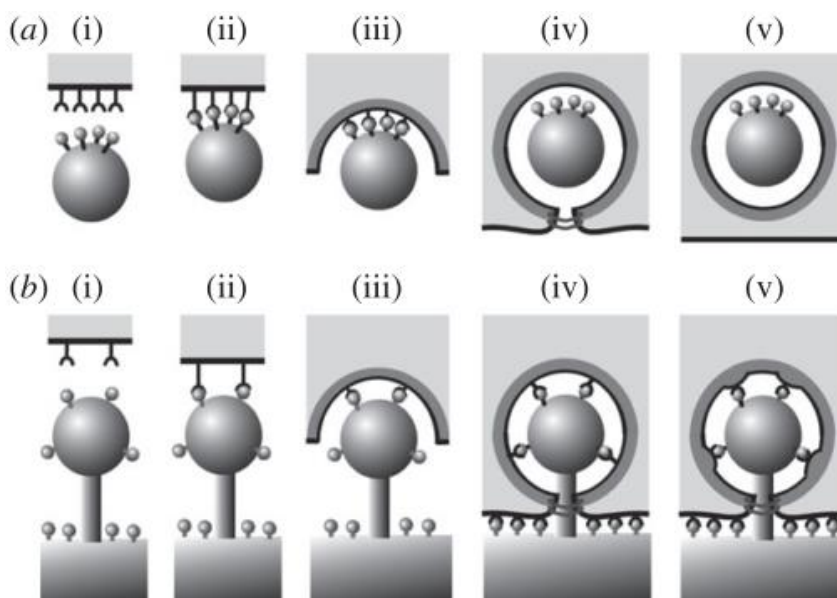


**Figure 2-12** – Schematic showing (a) engulfment of a particle by phagocytosis, and (b) incomplete phagocytosis-like engulfment of a protruding electrode. Adapted from [4].

Hai et al. Found that neurons readily engulf gold mushrooms with a height of  $1.5\ \mu\text{m}$ , head with of  $1.84\ \mu\text{m}$  and base width of  $800\ \text{nm}$  and a coating of cysteine-terminated peptide with a number of RGD repeats [3]. Santoro et al. have shown that the ratio between the dimensions of the mushroom is critical and also that the engulfment mechanism depends on which area of the cell is in contact with the electrode [5]. Combining the engulfment mechanisms with the desirable electrochemical properties of diamond allows for an ideal cell-electrode interface. The highly inert diamond surface gives a large potential window and low background current, which allows pure capacitive coupling with no damage from Faradaic charge injection [49]. Furthermore, the diamond surface is highly biocompatible and allows biomolecular functionalization.

# 3 Materials and Experimental Techniques

## 3.1 Substrates and Preparation

In order to fabricate devices based on NCD technology, substrates were needed that are able to withstand the high temperature conditions of the CVD reactors. Conventional MEA devices are typically made of thin-films deposited on transparent glass substrates, which is a highly beneficial property, allowing for visualization of cells. Within the scope of this thesis, the substrates used for NCD deposition were typically made of fused silica. Fused silica (FS) was the preferred form of glass because its lack of impurities gives it a high working temperature which is suitable for diamond growth conditions. One important limitation of FS substrates is the stresses that are introduced upon cooling after growth due to the differences in the thermal expansion coefficients of diamond and FS. FS has a very low coefficient of thermal expansion compared to diamond and this limits the thicknesses of the prepared NCD films to  $\sim 200$  nm before intrinsic stresses cause film delamination. FS is also easily available in high purity, at low cost, with a smooth surface finish. Typically, studies on neural growth on diamond were performed on 10 mm X 10 mm x 0.5 mm FS substrates which were the standard in-house size. Studies with MEAs were done by using either in-house 49 mm X 49 mm x 0.5 mm FS substrates, or 49 mm X 49 mm X 1 mm FS substrates from MultiChannel Systems (MCS) GmbH with metal tracks pre-deposited.

### 3.1.1 Cleaning

Proper substrate cleaning is essential to ensure dense, highly uniform, reproducible NCD layers. Bare FS substrates are cleaned by using the standard RCA cleaning procedure, one of the most commonly used set of wafer cleaning

steps in microfabrication [50]. This clean consists of two steps: RCA-1 for removal of organic contamination and RCA-2 for removal of ionic contaminants. RCA-1 uses a mixture of deionized (DI) water, ammonium hydroxide ( $\text{NH}_4\text{OH}$ ) and hydrogen peroxide ( $\text{H}_2\text{O}_2$ ) in a ratio of 5:1:1 at a temperature of  $\sim 80$  °C for 10 minutes. RCA-2 uses a mixture of DI water, hydrochloric acid (HCl) and  $\text{H}_2\text{O}_2$  in a ratio of 6:1:1 at a temperature of  $\sim 80$  °C for 10 minutes. Typically, this cleaning process is used for silicon wafers, but is also commonly used for glass cleaning, such as in the display industry [50]. This process is as effective with fused silica as with silicon, and leaves the glass with a silica-rich surface.

RCA cleaning can strip many metals due to the  $\text{H}_2\text{O}_2$  and HCl and thus is not suitable to clean MEAs obtained from MCS that have already have metal tracks. These samples were instead cleaned with a general solvent clean by sonicating and boiling in acetone and then isopropyl alcohol (IPA) for 5 minutes each. Acetone is effective at removing organic contaminants, and IPA is used to remove potential residues left by acetone. This is followed by thoroughly flushing with DI water to prevent residues from IPA, and finally dried with a nitrogen gun. This cleaning process was found to be effective enough to obtain a dense uniform NCD layer.

### **3.1.2 Diamond Nanoparticle Seeding**

Diamond nucleation is a critical step in order to achieve dense, uniform layers of NCD. Samples were seeded with diamond nanoparticles to cover the surface in a dense, uniform layer of diamond crystallites, based on the method of Osawa et al. [51]. An aqueous based colloidal suspension of detonation nanodiamond (DND) was pipetted onto each sample surface and left for  $\sim 60$  s before spincoating while flushing with DI. Flushing is done to improve the uniformity by redispersing particles not directly attached to the surface during spinning. This method allows DND attachment to a large variety of surfaces through van der Waals and electrostatic forces. A stable suspension was prepared by ultra-sonicating DND powder (provided by the NanoCarbon Institute Co., Ltd., Japan) in DI water at a concentration of  $0.33 \text{ g}\cdot\text{L}^{-1}$  for 3 hours. The specified particle size was  $3.8\pm 0.7$  nm and dynamic light scattering using a ZetaPALS 90Plus/NI-MAS showed a particle

size distribution of 5-10 nm in the final solution; showing that there is very little aggregation of particles. The zeta-potential was measured to be  $49\pm 5$  mV at a pH of 4.8, showing a positive surface charge. Thus, the substrate's surface charge can strongly determine the seeding density. It is even possible to selectively seed areas on a substrate by depositing materials with positive surface charge that repel the diamond nanoparticles [52].

### 3.2 ASTeX MPECVD Systems

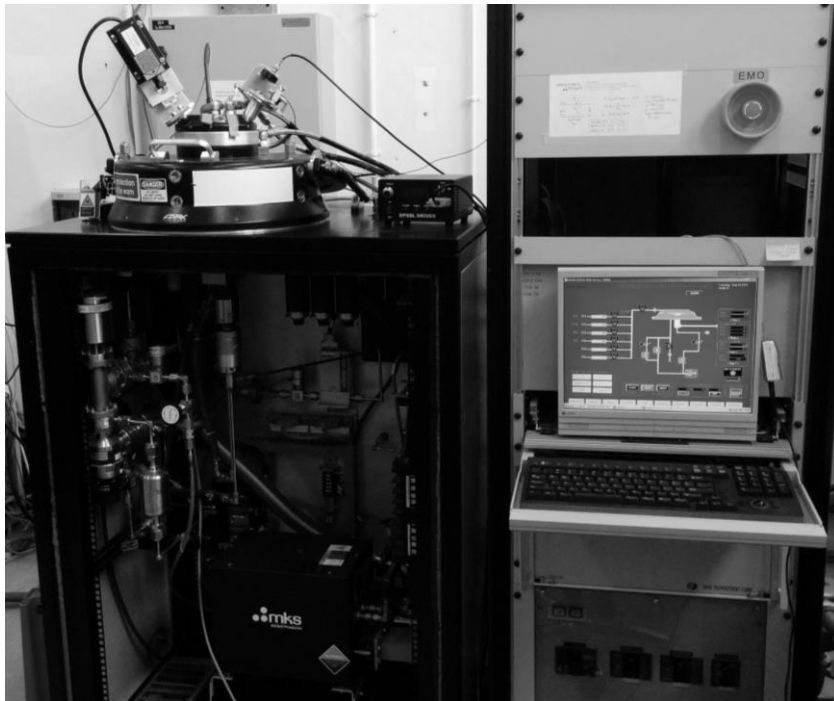


**Figure 3-1** – ASTeX 6500 MWPECVD system used for intrinsic diamond growth at IMO.

All NCD films were grown using commercial ASTeX 6500 microwave plasma enhanced chemical vapour deposition reactors. IMO is equipped with two of these types of reactors, one for growing undoped NCD (ASTeX-3), and another for

growing NCD doped with boron (ASTeX-2). The separation of these two systems is to ensure that no impurities are introduced during the growth of undoped diamond from residual dopant atoms on reactor walls. Figure 3-1 shows one of these reactors. The reactors consist of four main components: the vacuum chamber, the microwave source, the gas supply, and the pressure regulation system. The vacuum chamber is made from a steel dome with a copper stage which are both cooled by water. Samples are placed within a molybdenum holder which is 7 mm in height and sit at the centre of the stage. A quartz ring sits around the copper stage to act as a microwave resonator to create and contain the plasma ball. There is also plenum hole which sits in the middle of the stage to allow a partial vacuum under the molybdenum holder in order to lower thermal losses by convection. Microwaves are introduced from below the stage through a waveguide system by a microwave generator operating at 2.45 GHz, with output power between 500-5000 W possible. In ASTeX-3, the vacuum chamber is connected to a floor pump which allows base pressures of  $\sim 3.0 \times 10^{-3}$  mbar. In ASTeX-2, there is an additional turbopump, to allow for lower base pressures of  $\sim 2.0 \times 10^{-6}$  mbar, for higher purity doping. In both systems, there is a throttle valve connected to allow fine control of the chamber pressure in the reactor, typically between 10-100 Torr. Astex-3 has 2 gas channels, each with an individual mass flow controller. Channel 1 feeds atomic hydrogen (H) provided by a hydrogen generator with 7N purity to the chamber at a maximum flowrate of 500 sccm. Channel 2 is used for the carbon source, which is pure methane (CH<sub>4</sub>) and has a maximum flow rate of 50 sccm. Astex-2 has the same first two channels (H<sub>2</sub> and CH<sub>4</sub>) with the third channel used to feed tri-methyl boron (TMB) as the boron dopant source. The TMB feed line is diluted with H<sub>2</sub> at a ratio of 1:1000 and has a maximum flowrate of 100 sccm. The individual gas channels are combined before being fed into the reactor chamber. Typically, the total gas flow is maintained at 500sccm, with C:H concentrations between 0.5-5%. For highly boron-doped NCD, typical B:C ratios of 5000-10,000 ppm in the gas mixture were used. Through the control of microwave power and working pressure, the plasma shape and power density can be controlled. The concentration of different species in the plasma is also affected by these parameters, but also largely by the gas composition and flow rate. The temperature of the stage can also be controlled independently of the plasma characteristics by applying a vacuum at the plenum. All of these

parameters give many ways in which the growth conditions of diamond films can be influenced.

In the top of the ASTeX 6500 type reactors, there are 4 windows installed which can be used for optical readouts for in-situ monitoring of the growth. Substrate temperatures were read out using a handheld dual-wavelength pyrometer. Additionally, a laser and photo-diode were used to measure interference patterns during growth for in-situ thickness measurements which is detailed in the following section.

### **3.2.1 In-situ thickness measurements**

It is possible to measure the thickness of diamond films in-situ by using the principles of optical interferometry. A gallium nitride (GaN) laser (405 nm) is directed to the sample through a glass window in the reaction chamber and is reflected to a photo-diode through a window in the other side. The photo-diode is equipped with a filter to minimize the radiation background. The growing diamond film creates two interfaces: the diamond-substrate interface and the diamond-air interface. Some of the laser light will be reflected at the diamond-air interface and some will pass through the diamond and be reflected at the diamond-substrate interface and back out through the diamond. The extra distance travelled by the second wave will create a phase shift between the two beams. The beams will interfere with each other with a phase-shift that varies with the film thickness, resulting in constructive and destructive interference patterns as shown in Figure 3-2 [53].

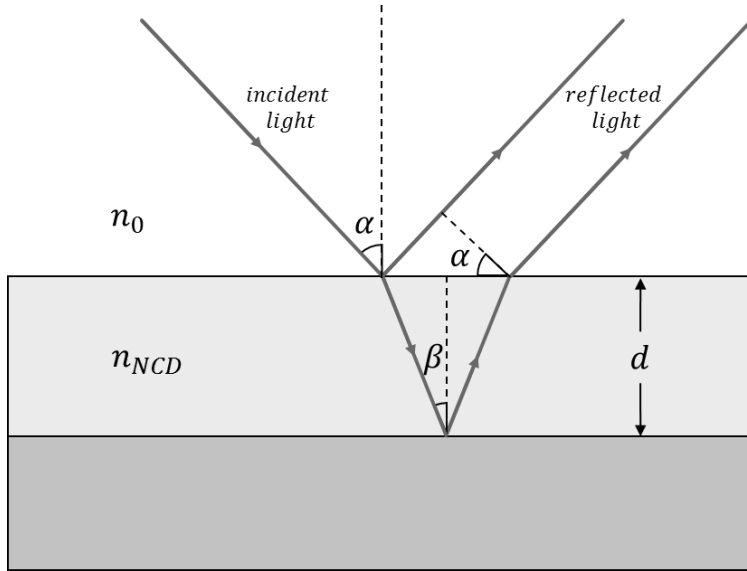


**Figure 3-2** – Schematic of thin-film interference, used for in-situ monitoring of diamond film growth.

For integer multiples,  $m$ , of the incident wavelength  $\lambda$ , constructive interference occurs when:

$$2n_{NCD}d \cos(\beta) = m\lambda$$

And destructive interference occurs when the phase is shifted by half a period of the wavelength of the light:

$$2n_{NCD}d \cos(\beta) = \left(m - \frac{1}{2}\right)\lambda$$

Where  $n_{NCD}$  is the refractive index of NCD,  $d$  is the film thickness,  $\beta$  is the angle of reflection within the diamond layer. The angle of reflection within the NCD layer is calculated by:

$$\sin(\beta) = \frac{n_0}{n_{NCD}} \sin(\alpha)$$

Where  $\alpha$  is the incident laser angle to the surface normal and  $n_0$  is the refractive index of the plasma above the diamond layer, which is  $\sim 1$ . In the case of ASTeX 6500 systems, the laser is at an angle of  $28.3^\circ$  to the surface normal. The

refractive index of NCD at room temperature for light with a 405 nm wavelength is 2.4619. This gives a reflected angle of  $11.1^\circ$  for  $\theta_2$ . The refractive index changes with temperature, but the room temperature value gives a good approximation of  $\sim 84$  nm film thickness for each period in the interference pattern, as confirmed through SEM of a cross-section.

### **3.3 Sputtering and Reactive-Ion Etching System**

Sputtering is a process for thin film deposition that uses high energy particles to bombard a target material and eject atoms from it onto the sample. Typically, an electrostatic potential field is applied across two electrodes in a gas, accelerating electrons that then collide with gas atoms. This leads to ionization or excitation of the gas atoms. Ionized atoms are then accelerated by the potential field towards the target, resulting in a high momentum collision that ejects atoms from the target. Reactive-ion etching (RIE) uses a similar mechanism as sputtering, though the stage becomes the target in order to remove material from the sample. When removal is done physically with an inert gas it is called ion-milling, but when the ionized gas species reacts with the surface to etch it, it is called reactive-ion etching. The system in Figure 3-3 was built in-house at IMO and houses two stages, one for sputtering and a second for etching.



**Figure 3-3** – Image of home built system at IMO used for both sputtering and reactive-ion etching.

For simple metal sputtering, argon is used as it is an inert gas and leads to purely physical sputtering. However, additional gases can be introduced that also ionize and react with the sputtered material to form materials such as aluminium nitride (AlN) and silicon oxide ( $\text{SiO}_x$ ). However, these compound materials also form on the target surface and in the case of dielectrics such as these, can lead to charge accumulation and arcing problems. The system used at IMO utilizes a DC-pulsed power source which applies inverse voltage pulses to the cathode in order to discharge the surface. Positively pulsed voltages are 1600 ns long and the cycle frequency between pulses is 250 kHz. There are a number of experimental parameters which affect the deposition rate and the grain structure of the deposited material, including: power, working pressure, target-stage distance, substrate temperature, and gas ratio. Parameters for different materials in this system have previously been optimized and are summarized in Table 3-1.

**Table 3-1** – Deposition parameters for sputtering of different materials and for reactive ion etching.

| Material         | Target | Gas                                      | P (mbar) | Power (W) | Target Stage distance (cm) | Substrate Temp (°C) | Rate (nm/min) |
|------------------|--------|--|----------|-----------|----------------------------|---------------------|---------------|
| Ti               | Ti     | Ar<br>50sccm                             | 4.0E-3   | 150       | 13                         | RT                  | 10            |
| Cr               | Cr     | Ar<br>50sccm                             | 4.0E-3   | 150       | 12                         | RT                  | 15            |
| AlN              | Al     | Ar<br>10sccm<br>N <sub>2</sub><br>40sccm | 4.0E-3   | 300       | 6                          | RT                  | 8-10          |
| SiO <sub>x</sub> | Si     | Ar<br>25sccm<br>O <sub>2</sub><br>75sccm | 1E-2     | 100       | 6                          | 300                 | 1-2           |

### 3.4 Lithographic Process

Lithography here refers to the patterning techniques used for structuring materials on a micro- or nano-scale. Typically, this is done by coating a wafer in a thin polymer layer which changes solubility to a specific developer solution under irradiation. If the areas exposed to irradiation become more soluble to the developer, then it is called a positive resist. Polymers that crosslink/polymerize under irradiation and become less soluble to the developer are called negative resists. The energy used to cross-link or degrade the resist typically comes from light (photolithography) or from a beam of electrons (electron-beam lithography). Photolithography has the advantage of using large masks to cover large areas for high throughput, though resolution is limited by the wavelength of light used. Electron-beam lithography on the other hand is a maskless technology that can draw custom patterns with sub-10nm resolution, but suffers from low-throughput as it writes directly, pixel by pixel [53]. Once the pattern is established, it can be used to transfer the pattern to the underlying material through etching, or

depositing material in the opened areas by a lift-off process. Etching requires that the resist be stable in the chemical or plasma used to etch the underlying material. For lift-off techniques, the polymer is stripped away after the material is deposited, leaving only material on the desired pattern. For successful liftoff, an undercut of the resist is typically necessary to avoid sidewall deposition; this can be achieved either by using specific resists for lift-off, or first adding a lift-off resist (LOR) that is not photosensitive but its solubility is controlled by baking temperature and duration. The most widely used technique for depositing resists is by spin coating, which is done by applying the resist on the centre of the substrate and spinning at high speeds to achieve uniform film thickness. This is followed by prebaking the wafer at a specific temperature to evaporate the excess solvent. The sample is then exposed and put in a developer solution to remove the soluble areas.

### **3.4.1 Photolithography procedures**

Two photolithography procedures were developed for patterning of multi-electrode arrays. The first used a standard negative photoresist procedure to define a lift-off pattern for the metal track deposition and is summarized below [53]:

- 1) Spincoat the adhesion promoter MCC Primer 80/20 at 4000 rpm for 30 s.
- 2) Bake on hotplate at 110 °C for 120 s.
- 3) Spincoat photoresist ma-N 1420 at 3000 rpm for 30 s (thickness 2.0 µm).
- 4) Bake on hotplate at 110 °C for 120 s.
- 5) Exposure with i-line (365 nm) light of a 350 W bulb for 60 s (exposure dose: 400 mJ·cm<sup>-2</sup>).
- 6) Develop in ma-D 533/S developer for 5 minutes.
- 7) Rinse with flowing DI water for 60 s and dry with nitrogen gun.
- 8) Deposit material.
- 9) Immerse sample in acetone for lift-off. Sonicate to help removal if necessary.
- 10) Rinse with acetone and IPA and dry with nitrogen gun.

The second used a bilayer stack of LOR and a positive photoresist for deposition of a hard-mask to define the planar electrodes of the MEAs and is summarized as follows [54]:

- 1) Dehydrate sample surface by baking on hotplate at 180 °C for 5 minutes.
- 2) Spincoat lift-off resist LOR3B at 2500 rpm for 45 s (thickness 350 nm).
- 3) Bake on hotplate at 180 °C for 60 s.
- 4) Spincoat positive resist S1818 at 6000 rpm for 30 s (thickness 1.5 µm).
- 5) Bake on hotplate at 115 °C for 60 s.
- 6) Exposure with i-line (365 nm) light of a 350 W bulb for 7.3 s (exposure dose:  $\sim 50 \text{ mJ}\cdot\text{cm}^{-2}$ ).
- 7) Develop in solution of 1:10 H<sub>2</sub>O:TMAH (25%) for 80 s.
- 8) Rinse with flowing DI water for 60 s and dry with nitrogen gun.
- 9) Deposit material.
- 10) Immerse sample in acetone for lift-off. Sonicate to help removal if necessary.
- 11) Rinse with acetone and IPA and dry with nitrogen gun.

### **3.4.2 Electron Beam Lithography procedure**

A technique for negative electron beam lithography was developed using a polymer called hydrogen silsesquioxane (HSQ) on top of a poly(methyl methacrylate) (PMMA) layer [53–59]. HSQ is polymerized by electron beams and is thus a negative e-beam resist. HSQ is developed in a TMAH solution which has no effect on the underlying PMMA layer. PMMA is etched by an oxygen plasma, which does not etch the HSQ layer. The undercut of the PMMA can be controlled by the etching conditions and time to create a lift-off structure. Details of the SEM can used for EBL can be found in the following section. The procedure for this process is listed below:

- 1) Dehydrate sample surface by baking at 180 °C for 5 minutes.
- 2) Spincoat PMMA 950 C4 at 3000 rpm for 45 s (thickness 500 nm).
- 3) Bake on hotplate at 180 °C for 60 s.
- 4) Spincoat negative electron-beam resist HSQ (XR-1541 6%, Dow Corning) at 4000 rpm for 45 s (thickness  $\sim 100 \text{ nm}$ )

- 5) Bake on hotplate at 80 °C for 5 minutes.
- 6) Expose with electron beam with a dose of 1500  $\mu\text{C}/\text{cm}^2$  (30 keV accelerating voltage, 2 nm spot size)
- 7) Develop in aqueous solution of 3.33% TMAH by weight, for 60 s.
- 8) Rinse with flowing DI water for 60 s and dry with nitrogen gun.
- 9) Deposit material.
- 10) Immerse sample in Remover PG for lift-off. Sonicate to help removal if necessary.

### **3.5 Scanning Electron Microscopy**

Scanning electron microscopy (SEM) is a technique that allows high-resolution imaging by scanning with a focused beam of electrons. SEM gives much higher resolution and depth of field than optical microscopy, making it an indispensable tool for visualizing fine structures in micro- and nano- fabrication [62]. Electrons interact with the sample to produce various signals that give information of the surface topography and atomic composition. The most common imaging mode makes use of secondary electrons (SE) which are generated in the first few nanometers of the sample through inelastic scattering of electrons from the specimen atom's k-shell by the incident electrons. Back-scattered electrons (BSE) are electrons from the incident beam that have been reflected or back-scattered through elastic interaction with the specimen atoms. Detection of back-scattered electrons is useful in showing contrast between areas of different chemical compositions due to heavier elements backscattering electrons more strongly than light ones. Characteristic x-rays can also be produced by the electron beam by exciting inner-shell electrons of the atom, which emit x-rays upon relaxation [62]. Since these transitions are highly specific to each element, the number and energy of x-rays collected can be used to measure the surface chemistry through a technique called energy-dispersive x-ray spectroscopy (EDX). Figure 3-4a shows a schematic of a typical SEM setup in which a beam of electrons is produced by an electron gun and focused by a combination of electrostatic condensers and apertures. Figure 3-4b shows where the various signals produced originate from within the specimen.

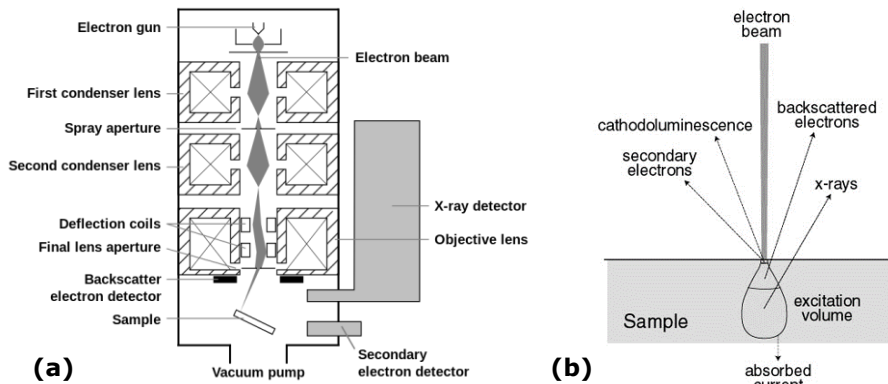


**Figure 3-4** – (a) Schematic of SEM, and (b) schematic of origin of various radiation sources within sample by the electron beam and the signals that can be collected. Adapted from [63],[64].

A FEI Quanta 200 FEG SEM was used to prepare all images contained in this thesis, as well as for the electron-beam lithography. The electron gun is capable of producing a beam with energies from as low as 200 eV up to 30 keV. Typical operating conditions for imaging sample were a beam energy of 15 keV, spot size of 4 nm, and working distance of 10 mm. For EBL, a beam energy of 30 keV, spot size 2 nm, and working distance of 10 mm were used.

### 3.6 Raman Spectroscopy

Raman spectroscopy is a common technique employed in diamond film analysis, as it allows identification of the different forms of carbon. It can be used to measure the quality of NCD by quantifying the ratio of  $sp^2$  to  $sp^3$  bonded carbon [65]. Additionally, the film stress or doping effects can be elucidated from Raman spectra. The technique works by using a monochromatic laser that interacts with low-frequency modes, such as molecular vibrations or phonons, to create inelastic scattering of the photons [66]. This causes a shift in energy of the scattered photon either lower (Stokes) or higher (anti-Stokes) depending on whether the interaction results in a higher or lower vibrational molecular state, respectively. The light is collected and filtered to remove the much stronger signal from elastic

(Rayleigh) scattering, which is the same wavelength as the exciting beam. The change in energy corresponds to a change in the photon wavelength and this can be used to plot a spectrum with peaks corresponding to characteristic modes, together making up a “fingerprint” of a molecule.

Pure diamond contains only  $sp^3$  bonds, which corresponds to a single Raman line at  $1332\text{ cm}^{-1}$  [65]. Nano-crystalline diamond contains grain-boundaries containing amorphous  $sp^2$  carbon which adds corresponding peaks to the spectra of pure diamond. There is a prominent peak at  $1350\text{ cm}^{-1}$  which is called the D-band for disordered carbon [65]. There is also a peak related to graphitic carbon, called the G-band, between  $1550$  and  $1600\text{ cm}^{-1}$  [65]. Another peak attributed to  $sp^2$  carbon is found at  $1480\text{ cm}^{-1}$  [65]. Finally, a peak is found at  $1150\text{ cm}^{-1}$ , which is thought to be specific to the fine grain nano-crystalline structure of NCD [65]. Furthermore, lattice strain and defects in NCD cause a downshift or upshift in the diamond peak. The relative intensities of these peaks is strongly dependent on the excitation wavelength of the laser, as shown in Figure 3-5. Excitation in the visible range gives intense peaks for  $sp^2$  bonded carbon which can make it hard to identify the diamond peak in the spectra. This is believed to be due primarily to a resonance effect, caused by proximity of the excitation wavelength to an electronic transition of  $sp^2$  bonded carbon material [65, 66]. UV excitation can give much higher ratios ( $\sim 25\times$ ) of the diamond to non-diamond peaks by eliminating this resonance, and this can be used to quantify the relative amount of each phase [65].

A Lexel SHG-95 Ar-ion laser with  $488\text{ nm}$  wavelength was used in conjunction with a confocal microscope for the excitation. Spectra was recorded by a Horiba Jobin-Yvon T64000 micro-Raman spectrometer. The charge coupled device detector is cooled by liquid nitrogen and equipped with an optical grating ( $1800\text{ mm}^{-1}$ ) to disperse the beam. Intensity of the incident beam is controlled with a slit on the microscope lens. Each set of data contains at least 3 scans in order to improve signal-to noise ratio.

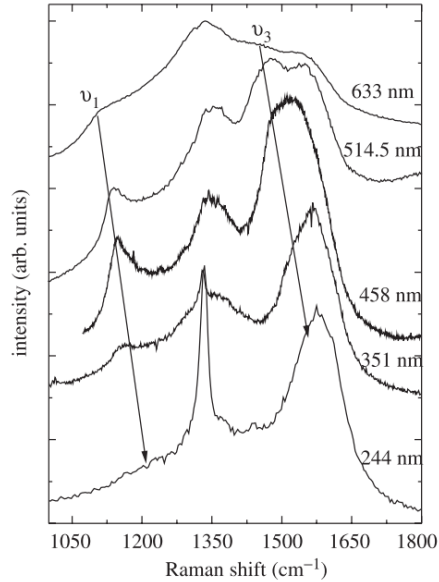


**Figure 3-5** – Raman spectrum of nano-crystalline diamond at different excitation laser wavelengths. The peaks at 1332 cm<sup>-1</sup>, 1350 cm<sup>-1</sup>, 1550-1600 cm<sup>-1</sup>, and 1480 cm<sup>-1</sup> are clearly shown. Adapted from [69].

### 3.7 Electrochemical Impedance Spectroscopy

Electrochemical impedance spectroscopy (EIS) is a powerful tool to characterize the properties of electrodes and is commonly used to evaluate MEA electrodes. The principle of EIS is to apply a small sinusoidal voltage in an electrochemical cell given by the equation [45, 68, 69]:

$$E(t) = E_m \sin(\omega t)$$

The resultant current is measured, which will have a different amplitude and phase shift depending on the material properties of the electrode and is given by:

$$i(t) = i_m \sin(\omega t - \phi)$$

This gives an impedance of the system defined by:

$$Z = \frac{E(t)}{i(t)} = \frac{E_m \sin(\omega t)}{i_m \sin(\omega t - \phi)} = Z_0 \frac{\sin(\omega t)}{\sin(\omega t - \phi)}$$

Using Euler's relationship,

$$e^{j\phi} = \cos \phi + j \sin \phi$$

The potential can be written as:

$$E = E_m e^{j\omega t}$$

and current response as:

$$I = I_m e^{j(\omega t - \phi)}$$

Giving the impedance in complex form given to give a real and imaginary part of the impedance as:

$$Z = \frac{E}{I} = |Z|e^{j\phi} = Z_0(\cos \phi + j \sin \phi) = Z' + jZ''$$

Where  $Z'$  and  $Z''$  are the real and imaginary part of the impedance respectively which are independent of time and are a function of the phase shift, which depends on the frequency of the driving voltage. Typically, an electrode can be considered as a mixture of resistive and capacitive elements which give different amplitude and phase responses depending on the frequency. EIS uses a sweep across a range of frequencies to find a characteristic curve that can be used to model the electrode and find the values of the various elements. A Bode plot graphs the impedance magnitude or the phase shift versus frequency, whereas a Nyquist plot gives a graph of the imaginary vs real part of the impedance (Figure 3-6b) [72]. Nyquist plots can be used to fit a curve to the electrical model by complex nonlinear least-squares procedures and extract material properties from the resultant values. Typically, a Randles circuit can be used (Figure 3-6a) to model the electrode.

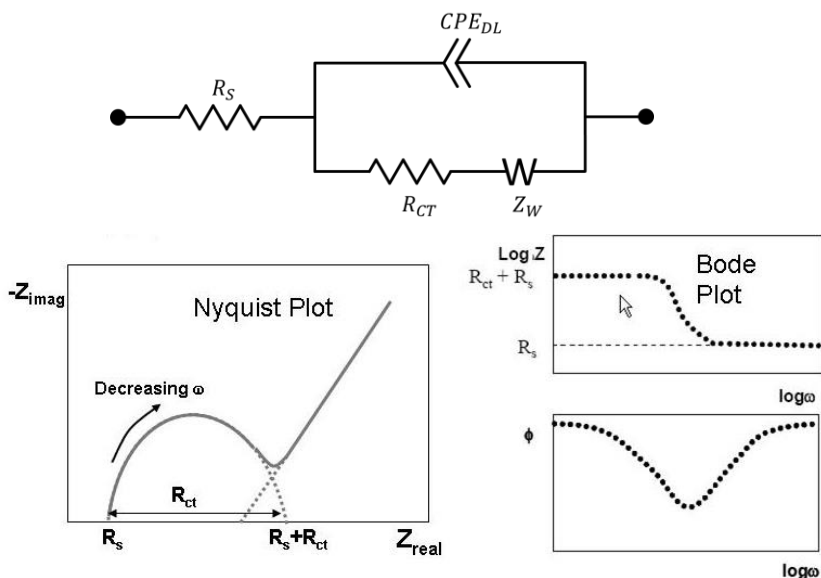


**Figure 3-6** – (a) Schematic of Randles equivalent circuit used for modeling electrodes, (b) Nyquist plot of Randles circuit showing the real and imaginary parts of the impedance, and (c) typical Bode plots of the impedance magnitude and phase as a function of frequency. Adapted from [72].

This circuit contains a resistor representing the solution resistance ( $R_S$ ) connected to a RC circuit which represents the charge transfer resistance ( $R_{CT}$ ) and double layer capacitance ( $C_{DL}$ ). For macroelectrodes, there is typically a Warburg element ( $Z_W$ ) in series with the charge transfer resistance which is used to describe the diffusional resistance for a diffusion layer of semi-infinite thickness [2, 70, 71]. This impedance is characterized on a Bode plot as a straight line at 45° and only has a strong effect at low frequencies. For microelectrodes, the mass transport to and from the electrode is much greater compared to macroelectrodes and  $Z_W$  can often be neglected, especially at low frequencies. Often, the interfacial impedance can not be modeled by a pure capacitor and a constant phase element ( $CPE$ ) must be introduced instead of  $C_{DL}$ . For diamond electrodes a CPE is typically used, which accounts for the complicated surfaced morphology, including grain boundaries, edges, and facets [71]. The impedance of a CPE can be given by the following:

$$Z_{CPE} = \frac{1}{(j\omega)^\alpha Y_0}$$

Where  $j$  is the imaginary number,  $\omega$  is the frequency,  $Y_0$  is a measure of the capacitance and  $\alpha$  is an exponential factor between 1 (pure capacitor) and 0 (pure resistor). Typically  $Y_0$  is quoted as a pseudo-double-layer capacitance value for diamond electrodes in units of  $F \cdot \text{cm}^{-2} \cdot \text{s}^{-\alpha}$ .

## 4 Diamond substrates for culturing neurons

In this section, the neuronal-diamond interface is investigated in order to determine an effective solution to culturing neurons diamond-based devices. From the results of these investigations, two papers have been published with partner institutes, both of which I am the second author. These articles have been reproduced here with permission of all authors. Additionally, a section detailing unpublished work on an effective diamond surface treatment is detailed in section 4.5.

Together, these articles demonstrate that some types of neural cells (neuroblastoma) can adhere well to bare diamond, while primary neurons require a surface functionalization technique. Furthermore, effective surface functionalization techniques for primary neuronal cultures are detailed in this chapter. The first article, entitled: *Impact of differently modified nanocrystalline diamond on the growth of neuroblastoma cell*, is a study of human neuroblastoma cells on hydrogen-terminated and oxygen-terminated NCD substrates. It shows that neuroblastoma cells, which are representative of neural cells, grow as well or better as the control glass substrates. However, neuroblastoma cells are proliferating and these results can not be extended to primary neurons which do not proliferate. Indeed, when studies were performed on primary hippocampal cells of rats or mice, unfunctionalized NCDs caused clustering of neurons, indicative of poor cell adhesion and growth. These results are described in the second article contained within this chapter, entitled: *Nanocrystalline diamond surfaces for adhesion and growth of primary neurons, conflicting results and rational explanation*. The article also shows that PDL-laminin functionalization can be used to successfully promote adhesion and growth. Finally, this chapter describes the work that has been done by functionalizing NCD with polyethylimine (PEI)

as an adhesion promoter for primary neural cells, which is shown here to be successful in promoting neural adhesion and growth as compared to control samples.

## 4.1 Motivation

The motivation for this project came from a need for biocompatible, low-biofouling materials with high robust electrochemical properties for in-vivo preclinical applications. Through the MERIDIAN project, coordinated by Milos Nesladek at IMO-MEC, nano-crystalline diamond was identified as a potential material for a new class of carbon materials for this application. Furthermore, the project set out to investigate the intimate cellular-substrate contact and develop a highly advanced concept of these interactions.

Diamond has been shown to be a promising material as a platform for cellular interfacing due to its chemical and biochemical inertness, high corrosion resistance, mechano-optical properties, and large surface area [74]. Diamond is intrinsically electrically insulating but it can be doped to become metallically conducting, making it an ideal material to create devices for brain-machine interfacing [75]. Furthermore, it is possible to tune the surface chemistry of diamond, for example, with simple hydrogen or oxygen termination, or with more complex biomolecules like proteins or DNA [76]. Typically, some type of attachment promoter (PDL, PLL, PEI, etc.) is necessary to functionalize substrates for successful neuronal attachment and growth. The literature shows that proliferating cells, including epithelial cells, fibroblasts and various other cell lines adhere and develop well on unfunctionalized NCD substrates[77]–[79]. However, this can not necessarily be extrapolated to post mitotic primary neural cells, and this chapter is dedicated to an investigation of NCD substrates towards this end. A diamond surface that promotes neuronal growth and adhesion is integral to the development of functional devices for recordings and stimulation, as neurons will tend to either cluster or die on poor surfaces. The main challenge here is to address which types of neuronal cells will adhere well to different types of diamond surfaces, and what surface treatments can be used to create a more attractive surface for the cells.

## 4.2 Contributions

The concept of developing the diamond substrate as a material for bidirectional neuronal interfacing for this project was set out at IMO-MEC, though due to the interdisciplinary nature of the project, other partner laboratories were involved with the cellular testing of the devices. The facilities for neuronal testing were not immediately available during the time of the project and thus three other partner laboratories were involved for testing of these diamond devices. The three institutes that were involved in this portion of the project were Vilnius University, the Hebrew University of Jerusalem, and the University of Antwerp. My personal laboratory contributions to this project were mostly the electrode devices design, the device engineering, fabrication and materials characterization of all devices, physical and electrochemical measurements and modelling of device performance, taking part in design of biological experiments. I have collaborated on the biological testing which was the critical element to this narrative and thus I felt it was important to include these results in the thesis; even if the actual biological testing was conducted by other institutes (to some of the measurements I was present and executed them at these laboratories jointly). Towards this end, two research articles have been included in this chapter on the topic of NCD substrates as a platform for adhesion and growth of neurons. Due to the nature of the biological testing of the devices being the critical scientific revelations, these two papers were published with the lead author as the person doing the actual biological testing, but the papers have been included in the thesis with permission of all the coauthors due to the multi-disciplinary nature of the project. We feel that with the device fabrication and characterization, combined with the original motivation for the project originating at IMO-MEC, that the articles are relevant and worthy of being included in this thesis. My specific contributions for each of these works is detailed at the beginning of each section.

## 4.3 Article: Impact of differently modified nanocrystalline diamond on the growth of neuroblastoma cell

**New Biotechnology, Volume 32, Issue 1, January 2015, Pages 7-12**

Aida Vaitkuviene<sup>1,4</sup>, Matthew McDonald<sup>2</sup>, Farnoosh Vahidpour<sup>2</sup>, Jean-Paul Noben<sup>3</sup>, Kathleen Sanen<sup>3</sup>, Marcel Ameloot<sup>3</sup>, Vilma Ratautaite<sup>1</sup>, Vytautas Kaseta<sup>4,5</sup>, Gene Biziuleviciene<sup>4</sup>, Almira Ramanaviciene<sup>6</sup>, Milos Nesladek<sup>2</sup> and Arunas Ramanavicius<sup>1,7</sup>

1 Department of Physical Chemistry, Faculty of Chemistry, Vilnius University, Naugarduko 24, LT-03225 Vilnius, Lithuania

2 Hasselt University, Institute for Materials Research, Division IMOMEC, Wetenschapspark 1, B-3590 Diepenbeek, Belgium

3 Hasselt University, Biomedical Research Institute, Agoralaan Building C, Diepenbeek B-3590, Belgium

4 Department of Stem Cell Biology, State Research Institute Centre for Innovative Medicine, Zygimantu 9, LT-01102 Vilnius, Lithuania

5 Laboratory of Biomedical Physics, Institute of Oncology, Vilnius University, Santariskiu 1, LT-08660 Vilnius, Lithuania

6 NanoTechnas-Center of Nanotechnology and Material Science, Faculty of Chemistry, Vilnius University, Naugarduko 24, LT-03225 Vilnius, Lithuania

7 Laboratory of NanoBioTechnology, Department of Materials Science and Electronics, Institute of Semiconductor Physics, State Scientific Research Institute Centre for Physical Sciences and Technology, Vilnius, Lithuania

### 4.3.1 Contributions to the article "Impact of differently modified nanocrystalline diamond on the growth of neuroblastoma cell"

This project started with the goal of determining whether the two main functionalization's (hydrogen- and oxygen-terminated) of diamond may play a role on the neuronal-substrate interactions. We also wanted to look at whether boron doping may affect this interaction as well. At IMO-MEC I optimized the growth conditions for NCD in order to get a homogeneous pin-hole free layer. This involved seeding clean glass substrates with the nanodiamond particle solution and growing in either the Astex-2 or Astex-3 reactor. After calibrating the growth conditions carefully, I determined with SEM (even though SEM results are not included in the article) that the layers have a good coverage and uniform crystal size. The diamond quality was also confirmed with Raman spectroscopy to ensure a high percentage of sp<sup>3</sup> carbon concentration, though again, these results were not included in the article. Additionally, I measured film thickness in-situ using optical interference, and confirmed afterwards with profilometry. Surface angle measurements were then recorded on the diamond substrates at IMO-MEC. These

measurements were first started by myself and later continued by Vilma Ratautaite during a visit to IMO-MEC. After the fabrication and material characterization were finished at IMO-MEC, samples were tested biologically by Aida Vaitkuviene, with the help of other co-authors.

#### **4.3.2 Main Body of “Impact of differently modified nanocrystalline diamond on the growth of neuroblastoma cell”**

##### **Abstract**

The aim of this study was to assess the impact of nanocrystalline diamond (NCD) thin coatings on neural cell adhesion and proliferation. NCD was fabricated on fused silica substrates by microwave plasma chemical vapor deposition (MWPECVD) method. Different surface terminations were performed through exposure to reactive hydrogen and by UV induced oxidation during ozone treatment. Boron doped NCD coatings were also prepared and investigated. NCD surface wettability was determined by contact angle measurement. To assess biocompatibility of the NCD coatings, the neuroblastoma SH-SY5Y cell line was used. Cells were plated directly onto diamond surfaces and cultured in medium with or without fetal bovine serum (FBS), in order to evaluate the ability of cells to adhere and to proliferate. The obtained results showed that these cells adhered and proliferated better on NCD surfaces than on the bare fused silica. The cell proliferation on NCD in medium with and without FBS after 48 h from plating was on average, respectively, 20 and 58 % higher than that on fused silica, irrespective of NCD surface modification. Our results showed that the hydrogenated, oxygenated and boron-doped NCD coatings can be used for biomedical purposes, especially where good optical transparency is required.

##### **Introduction**

Nanodiamond has a number of the properties, which are characteristic for bulk diamond, including superior hardness, resistance to harsh environments, advanced Young’s modulus, interesting optical properties, high thermal

conductivity, electrical resistivity, chemical stability, and excellent biocompatibility [80]. Extraordinary physiochemical, mechanical and electrical properties of nanostructured diamond make this material attractive to bioengineers and medical researchers. The possibility of functionalizing the diamond surface at the nanoscale by hydrophobic and electrical conductive hydrogen termination or hydrophilic and electrically highly resistive oxygen-termination, make this material ideal to develop new high sensitivity cell-based biosensors [27–29]. Diamond coatings can also be made conductive by doping with boron. Nanocrystalline diamond (NCD) coatings produced by microwave plasma chemical vapor deposition (MWPECVD) exhibit many desirable properties favorable to orthopedic implants, such as excellent wear resistance, minimal surface roughness, and chemical inertness [84]. It was demonstrated that diamond coatings based on NCD structures improve cytocompatibility properties [85]. It was shown that coating of simulated temporomandibular joint implants with either a single-layer nanocrystalline or a multilayer diamond thin film improved their lifetimes [86]. Thus NCD could be used as a coating for prosthetic implants, because the biocompatibility is a significant advantage of diamond-based coatings [33, 34]. The biocompatibility is much better in comparison to some metals and many alloys, which are commonly used in implantable devices [87]. Moreover, diamond coatings have the chemical inertness and impermeability required to reduce the crevice corrosion that is commonly seen in conventional metallic implants [89]. The suitability of NCD for osteoblast adhesion, proliferation and stimulation of differentiation has been proven [36, 37]. Amaral et al. claimed that the nanometric featuring of NCD, which is usually based on its chemical modification, are most important topics in bone regeneration [91]. Such surface properties as topography and surface-chemistry of diamond coatings might be controlled in order to promote or inhibit osteoblast functions [92]. This fact implies that some forms of diamond coatings might be used in order to support or inhibit bone growth in selected regions [92]. Furthermore, the nanodiamond monolayers have been shown as suitable platform for neuronal growth similar to protein-coated materials [39–41]. Thus, the relatively easy fabrication and functionalization of nanocrystalline diamond coatings makes it an interesting material for many biomedical applications. However, before the application of any

material for medical purposes it is necessary to perform advanced evaluation of biocompatibility.

In this work, biocompatibility of the diamond-based surfaces with different chemistry was investigated to assess their suitability as transparent substrates for the growth and maintaining of neural cells. The human neuroblastoma cell line SH-SY5Y is representative of neural cells and relevant for the development of biosensing devices. NCD coatings were synthesized on fused silica by MPCVD. The surface wettability was assessed by contact angle measurement. Cell adhesion and viability/proliferation on native and boron-doped nanocrystalline diamond surfaces with oxygen and hydrogen terminations were evaluated. In order to better assess the capability of cells to adhere and to proliferate on different terminated NCD substrates, cell culture medium with and without fetal bovine serum (FBS) was used.

## **Materials and methods**

### *Fabrication of nanocrystalline diamond coatings*

NCD coatings were grown by MPCVD process in an ASTEX (Applied Science and Technology Company). The detailed deposition parameters of NCD and of boron doped NCD (BNCD) on the fused silica substrates of 1 cm × 1 cm area are listed in Table 4-1.

**Table 4-1** – Parameters applied for the deposition of NCD

| <b>Deposition parameters</b>    | Values                     |
|---------------------------------|----------------------------|
| <b>NCD</b>                      |                            |
| Gas: hydrogen (H <sub>2</sub> ) | 490 cm <sup>2</sup> (98 %) |
| Gas: methane (CH <sub>4</sub> ) | 10 cm <sup>2</sup> (2 %)   |
| Power                           | 2800 Watt                  |
| Pressure                        | 30 Torr                    |
| Temperature                     | ~700 °C                    |
| Thickness                       | ~150 nm                    |
| <b>BNCD</b>                     |                            |
| Gas: hydrogen (H <sub>2</sub> ) | 410 cm <sup>2</sup> (82 %) |
| Gas: methane (CH <sub>4</sub> ) | 10 cm <sup>2</sup> (2 %)   |
| Gas: trimethylboron (TMB)       | 80 cm <sup>2</sup> (16 %)  |
| Total boron in B(1)NCD          | 8000 ppm                   |
| B(2)NCD                         | 1000 ppm                   |
| B(3)NCD                         | 10 000 ppm                 |
| Power                           | 3500 Watt                  |
| Pressure                        | 35 Torr                    |
| Thickness                       | ~150 nm                    |

#### *NCD surface modification*

After the deposition of NCD coatings, surfaces were hydrogenated, oxygenated or boron-doped under conditions described in Table 4-2.

The NCD and BNCD was oxidized by UV induced ozone treatment during 30 min with PSD series digital UV-ozone system (Novascan Technologies, Inc.). The digital UV-ozone system was equipped with UV emitting high voltage mercury vapor lamp and produced high energy ultraviolet light at wavelengths of 185 nm and 254 nm. After UV induced ozone treatment oxygen-terminated NCD (NCD:O) and oxygen-terminated BNCD (BNCD:O) were obtained.

**Table 4-2** – Hydrogenation conditions of NCD and BNCD samples

| <b>Hydrogenation parameters</b>                         | Values                                   |
|---|--|
| <b>Gas: hydrogen (H<sub>2</sub>)</b>                    | 500 cm <sup>2</sup>                      |
| <b>Surface cleaning and producing reactive hydrogen</b> | 3500 Watt, 2 min, 30 Torr H <sub>2</sub> |
| <b>Hydrogen bonding with carbon surface</b>             | 2500 Watt, 5 min, 15 Torr H <sub>2</sub> |
| <b>Surface stabilization</b>                            | 30 min in H <sub>2</sub> atmosphere      |

*NCD surface analysis by contact angle measurement*

Hydrophobicity of NCD and BNCD surfaces was measured by contact angle measurements of ultra-pure water. For contact angle measurements Contact Angle System OCA DataPhysics (Filder-stadt, Germany) was used. To assume that the contact angle measurement is representative for the full sample surface, hydrophobicity was evaluated at four different points for each sample.

*Preparation/sterilization of NCD slides*

The oxygenated NCD and bare fused silica (control) slides were sterilized by incubation of them in 70 % ethanol for 30 min followed by exposure to ultraviolet light for 30 min.

*Neuroblastoma cell line*

SH-SY5Y cells were cultured in a 1:1 DMEM and nutrient mixture F-12 from Sigma (Taufkirchen, Germany) containing 10 % FBS, and 1 % penicillin/streptomycin. Medium was changed every 2–3 days until the monolayer reached 80–90% confluency. SH-SY5Y cells were then trypsinized for reseeding or experimentation. The SH-SY5Y cells were maintained at 37 °C in a humidified atmosphere containing 5 % CO<sub>2</sub> for the entire duration of culture.

### *Cell adhesion and proliferation studies*

For the assessment of the leakage of possible toxic substances from NCD coatings, SH-SY5Y cells were seeded in 96-well flat-bottom microassay plates at a concentration of  $3.1 \times 10^3$  cells/well, and cultured for 24 h. The medium was then replaced with 120  $\mu$ L of different medium, where NCD samples (1 cm  $\times$  1 cm) were soaked (in 1 ml of medium for 72 h), and incubated at 37°C in 5% CO<sub>2</sub> for 72 h. After that, medium was discarded and 100  $\mu$ L of new medium with 10  $\mu$ L MTT dye (5 mg/ml) was added to each well and reincubated for 3.5 h at 37°C. After this time, the medium was removed and 150  $\mu$ L of DMSO with 25  $\mu$ L glycine was added to each well. Absorbance was measured using a microplate reader (Fluostar Optima, BMG Labtech, Ortenberg, Germany) at 540 nm. The assay was performed in triplicate.

For the adhesion and proliferation assays, the cells were seeded in 24-well plates onto NCD-coatings and fused silica (as control) in the medium with and without FBS. Prior to cell seeding, all slides were soaked overnight in the culture medium at 37°C. SH-SY5Y cells were seeded at a density of  $1.65 \times 10^5$  cells/ml, and then allowed to adhere to the substrates undisturbed in a humidified incubator (at 37°C, 5% CO<sub>2</sub>). After 48 h cell incubation on the NCD coatings, XTT reagent was added. The absorbance values were measured in quadruplicate at 450 nm using a microplate reader (Fluostar Optima, BMG Labtech, Ortenberg, Germany). To evaluate the cell adhesion and morphology, we used a micro-scope Nikon T1-SM (Tokyo, Japan).

### *Statistical analysis*

The results were expressed as the arithmetic mean  $\pm$  SD. Differences between groups were evaluated by Student's t-test.  $P < 0.05$  was considered as significant.

## **Results and discussion**

The purpose of this study was to evaluate an impact of differently terminated NCD coatings on adhesion and growth of human neuroblastoma SH-SY5Y cells. NCD

surface terminations were evaluated by contact angle measurements of interactions with water. Oxygen termination gives rise to a highly hydrophilic surface on which water spreads quickly. Hydrogen-terminated surfaces are hydrophobic. The corresponding contact angles on the differently terminated NCD and BNCD surfaces are listed in Figure 4-1.

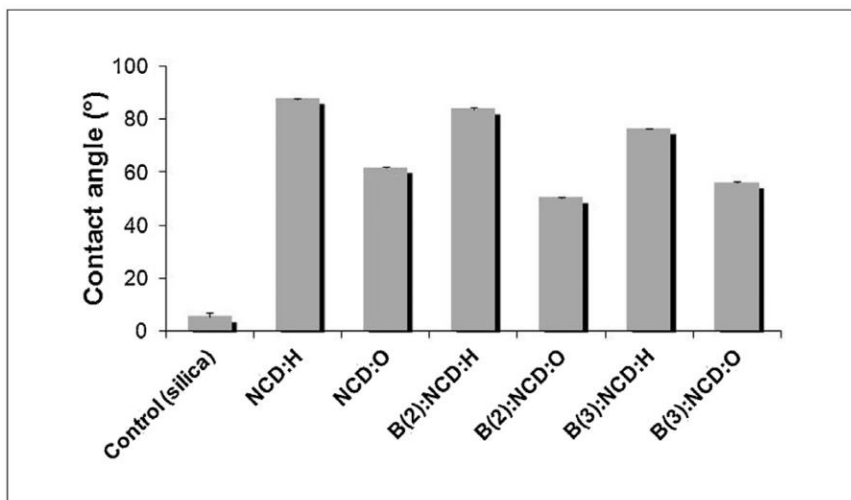


**Figure 4-1** - Hydrophobicity of nanocrystalline diamond and boron doped nanocrystalline diamond surfaces with oxygen and hydrogen terminations.

In Figure 4-1 results of hydrophobicity are represented. Fused silica control samples were very hydrophilic and contact angle with water was less than 5°. All other samples were more hydrophobic. Contact angle of hydrogenated NCD was 88°, and hydrophobicity of hydrogenated boron-doped NCD was lower 84° and 76° (B(2)NCD:O and B(3)NCD:O, respectively). During UV induced ozone treatment the surface of NCD and BNCD was oxidized. As a consequence, these samples became more hydrophilic. Contact angle of NCD:O samples decreased to 62°; B(2)NCD:O and B(3)NCD:O decreased to 50° and 56°, respectively. For control slides based on fused silica no surface modification procedures were applied. The slides were sterilized under standard sterilization procedure to avoid any contamination. The fused silica slides with NCD and BNCD were hydrogenated or oxygenated before cell seeding. Hydrogenated surfaces are described as

hydrophobic and oxygenated – as hydrophilic. It is well known that hydrophilic surfaces usually are more biocompatible in comparison with hydrophobic ones.

SH-SY5Y cell line, as an appropriate experimental model of the neural cells, has been used in order to evaluate biocompatibility of the NCD coatings, and their potential for biomedical applications. Hydrogen-terminated or oxygen-terminated NCD and boron-doped NCD coatings (NCD:H, NCD:O, BNCD:H and BNCD:O) were applied.

Firstly, in order to evaluate the possible trace pollutions from NCD coatings, we determined cell proliferation rate in the medium, where NCD samples were soaked for 72 h. No toxic leakages from NCD coatings were detected, that could affect the cell growth. Cell proliferation rate was similar to control cell proliferation rate on standard tissue culture polystyrene with untreated medium (Figure 4-2). Figure 4-2 illustrates that all tested samples supported cell proliferation.

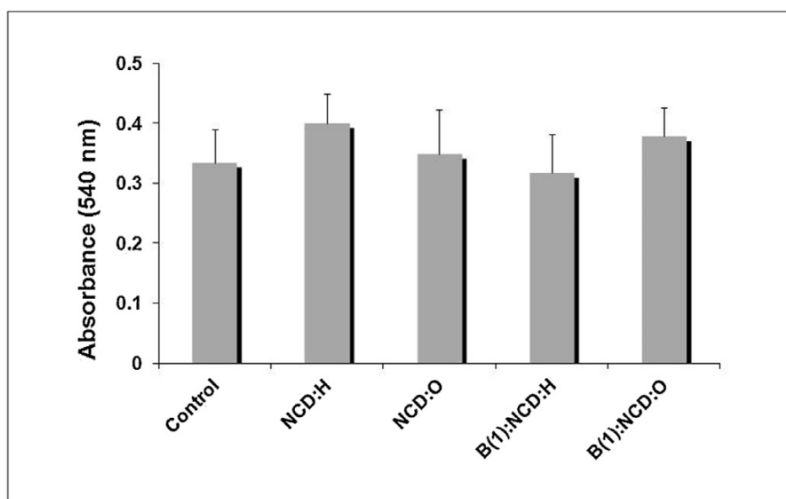


**Figure 4-2** - Proliferation of SH-SY5Y cells after 72 h cultivation with NCD and B(1):NCD coatings of different termination. Proliferation rate was evaluated applying the MTT test; light absorbance was measured at 540 nm. Error bar represents standard deviation of the mean value of three measurements.

We also assessed the capacity of neuroblastoma cells to adhere and to proliferate on NCD coatings. Cellular adhesion is very important for many biological processes, because the adhered cells can sense, integrate, interpret and respond

to some extracellular signals due to specific interaction between features present on the NCD-based surface and cell surface receptors [96]. Physical and chemical properties of the substrate (including their topography, surface energy, hydrophilicity and electrostatic charge) are playing critical role in regulation of cell proliferation and biological activity [89]. In our experiments SH-SY5Y cells were maintained in the standard culture medium with 10 % FBS. It is known that the proteins, which are present in the medium, may adsorb to the surfaces of different substrates and then they can significantly influence cell adhesion and growth. Consequently, we assessed cell adhesion on the differently terminated NCD surfaces not only in medium with FBS, but in FBS-free medium also. The nanocrystalline diamond deposited on fused silica has a good optical transmittance, which is important for efficient observation of cell cultures by standard inverted microscope. Obtained results showed that SH-SY5Y cells adhered well on all tested NCD surfaces in the medium with FBS, and in serum-free medium. In medium with FBS we observed an increase in cell adhesion on all surfaces as compared with those grown in FBS-free medium. It is known that the most neuronal cells cannot attach and maintain their functional properties for longer terms exceeding several days if samples are placed in serum-free medium [82]. Therefore, in all our studies we used DMEM containing F-12 Ham's nutrient mixture, and assessed the adherence and proliferation of cells 48 h after they have been seeded. Figures 3 and 4 show that cells adhered on all substrates after 48 h, regardless of NCD modification and presence of FBS in the medium. These photographs show that cells maintained a normal morphology showing that the different NCD coatings used are biocompatible. The optical images of cells growing on transparent samples are shown below.

Other authors demonstrated that hydrogen-terminated NCD surfaces inhibited human renal epithelial cells (HK-2 cell line) adhesion, whereas oxygen-terminated NCD improved attachment of these cells, as compared to borosilicate glass [97]. The data of our experiments show that SH-SY5Y cells adhered not only to oxygen-terminated NCD, but to hydrogen-terminated NCD also. Our results are consistent with the data of previous studies reporting that the adhesion and growth of neuronal GT1-7 cells on NCD surfaces does not depend on surface H- or O-termination [82]. The suitability and noncytotoxicity of ultra-nanodiamond films as a support surface for cell growth and proliferation has been proven [43, 44].

There are a number of studies *in vitro* have already revealed biocompatibility of NCD, but the most of them have been performed by using cell growth medium with the addition of FBS [44, 45]. Our experiments were performed not only in medium with FBS but in serum-free medium also. Obtained results showed that SH-SY5Y cells adhered on the all tested NCD surfaces as in medium with FBS (Figure 4-3), as in serum-free medium (Figure 4-4). These findings contradict the results obtained with another type of cells by other investigators, which claimed that cell attachment in FBS-free medium is possible only on hydrophilic surfaces [100]. Our results showed that SH-SY5Y cells can adhere on hydrophobic surfaces in FBS-free medium also. Moreover, we found that the adhesion and growth potential of SH-SY5Y cells in serum-free medium correlates with their seeding density. When the cell seeding density is higher, the cell adhesion and proliferation potential is greater (data not shown) due to increased intercellular contacts and cell produced proteins, which create more favorable conditions for cell growth. The disparities between our results and those reported by other authors were probably influenced by differences in experimental conditions and cell lines. For example, Frewin et al. determined that NCD showed a good level of viability with the neural H4 line, but a poor viability with the PC12 line [101].

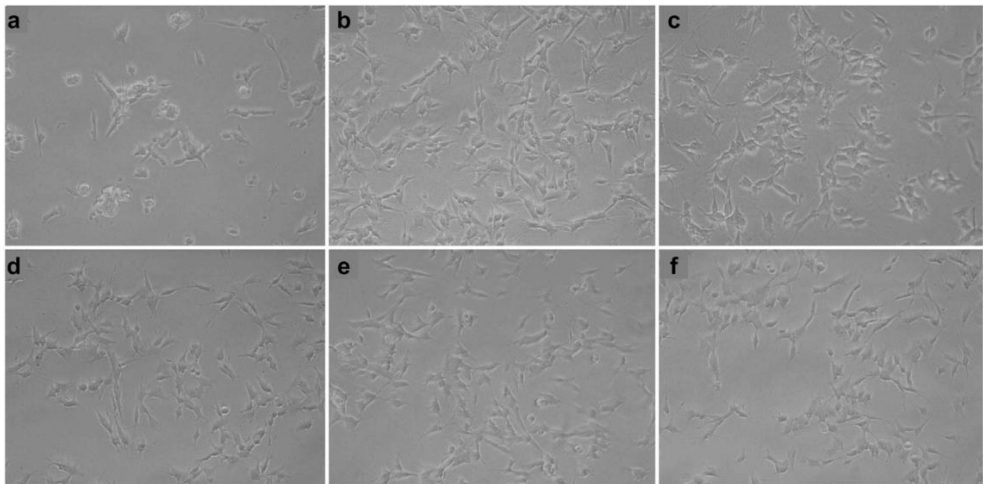


**Figure 4-3** - Light microscopy images of SH-SY5Y cells after 48 h cultivation on NCD coatings in medium with FBS. Images show the adhesion and morphology of SH-SY5Y cells on: (a) fused silica substrate (control), (b) NCD:O coating, (c) NCD:H, (d) B(3):NCD:O, (e) B(3):NCD:H, and (f) B(2)NCD:O coatings.

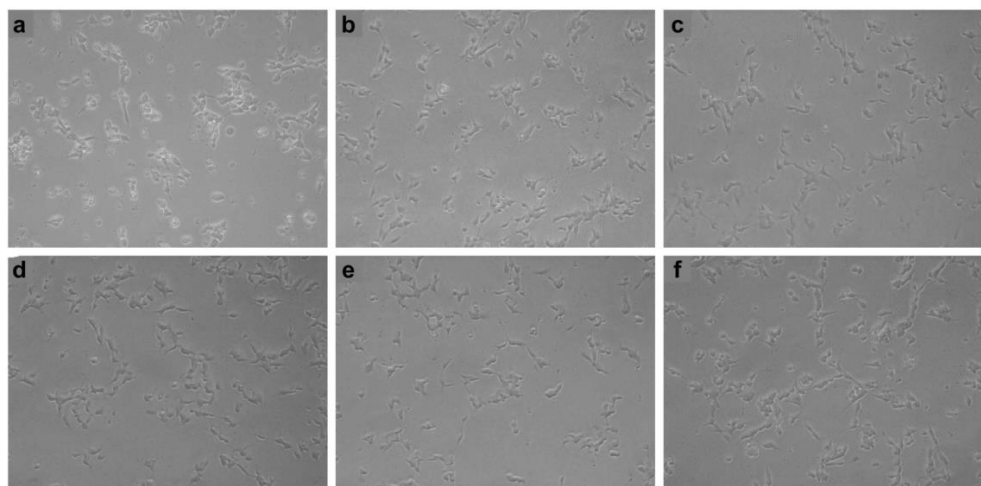


**Figure 4-4** - Light microscopy images of SH-SY5Y cells after 48 h cultivation on NCD coatings in medium without FBS. Images show the adhesion and morphology of SH-SY5Y cells cultured on: (a) fused silica substrate (control), (b) NCD:O coating, (c) NCD:H, (d) B(3):NCD:O, (e) B(3):NCD:H, and (f) B(2):NCD:O coatings.

Cell proliferation rate 48 h after cell seeding onto differently terminated NCD is shown in Figure 4-5.

Data presented in Figure 4-5 illustrate that after adding FBS in culture medium, cell proliferation has increased. It is evident that serum-free medium creates stressful conditions for cell growing. This fact is confirmed by mass-spectrometry protein analysis (data not shown) of the differently terminated NCD surfaces/samples with or without FBS. We found that SH-SY5Y cells growing on O- or H-terminated NCD and boron-doped NCD in medium without FBS expressed much higher level of different proteins as compared with those growing on the same NCD coatings in medium with FBS. We noticed a notable elevated abundance of heat shock protein (HSP) in the samples in the FBS-free medium only. It is known that the HSPs are highly conservative molecular chaperones, which are constitutively expressed [102]. The HSPs are present mainly in different subcellular compartments, and in unstressed cells they may constitute up to 2 % of the total cellular protein mass [102]. After physiological, thermal and/or other kind of stress, the expression of HSPs increases substantially, enabling cells to survive even very harsh conditions [102]. Moreover, we determined that in the medium with FBS, SH-SY5Y cells produced elastin microfibril interface located

protein (EMILIN-1). It is known that EMILIN-1 is an extracellular matrix glycoprotein [24]. This protein has significant adhesive capacity, but its other biological activities are still not well defined [103]. We think that the favorable cell growth conditions (medium with FBS) enabled neuroblastoma cells to produce this protein to enhance cell adhesion to NCD surfaces. Meanwhile, in stress conditions (serum-free medium) cells were forced to produce a lot of HSPs in order to survive.

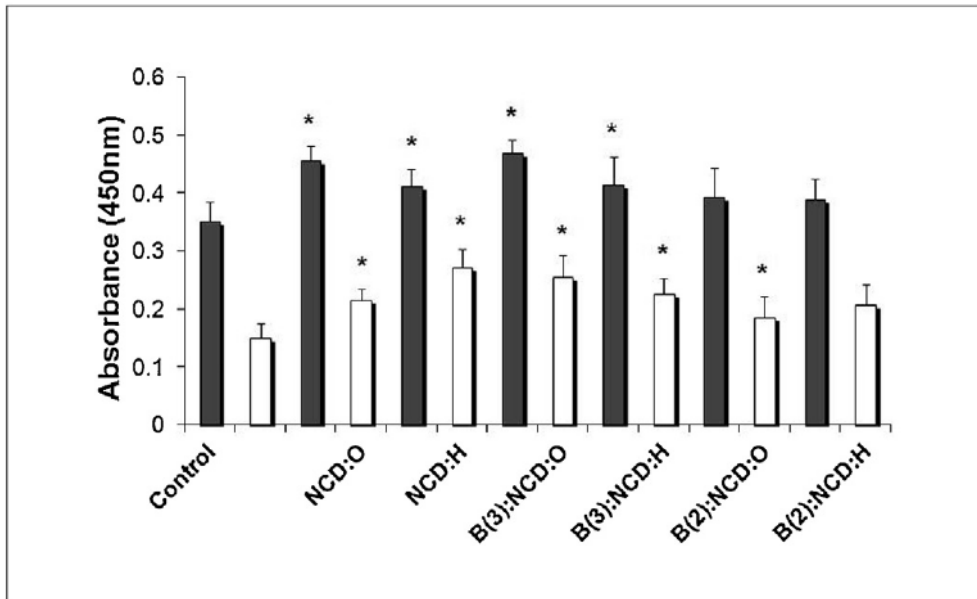


**Figure 4-5** - Proliferation of SH-SY5Y cells after 48 h cultivation on different NCD samples/substrates in medium with FBS (■) and without FBS (□). Proliferation rate was evaluated using the XTT test, and absorbance was measured at 450 nm. Error bar represents standard deviation based on four measurements. \* statistically significant difference between the control and sample ( $P < 0.05$ ).

Morphological and biochemical analysis performed with a neuroblastoma SHSY5Y cell line seeded on the differently terminated NCD coatings showed that cells adhered well on these coatings, maintained their metabolic activity, and the ability to proliferate. The cell proliferation rate on nanocrystalline diamond in medium with and without FBS after 48 h from plating was on average, respectively, 20 and 58 % higher than that on fused silica.

In summary, the presented results demonstrate that NCD coatings have significant influence on neural cell culture. Both H- and O-terminated NCD and boron-doped NCD coatings significantly promote the efficiency of neural cell adhesion and proliferation as compared with the fused silica, even in the medium without FBS. The results obtained show that the tested NCD coatings could be used as such without further modification for neural cell culture. Our data demonstrate that NCD have a potential for biomedical applications. The proposed coatings, which are highly biocompatible and capable to maintain cell adhesion, viability and proliferation, may be also interesting in tissue engineering. However, further studies are needed to validate this hypothesis.

### **Acknowledgements**

European Union Structural Funds project 'Postdoctoral Fellowship Implementation in Lithuania' within the framework of the Measure for Enhancing Mobility of Scholars and Other Researchers and the Promotion of Student Research (VP1-3.1-S<sup>MM</sup>-01) of the Program of Human Resources Development Action Plan.

## **4.4 Article: Nanocrystalline diamond surfaces for adhesion and growth of primary neurons, conflicting results and rational explanation**

**Frontiers in Neuroengineering, Volume 7, Article 17, June 2014**

Silviya M. Ojovan<sup>1</sup>, Mathew McDonald<sup>2</sup>, Noha Rabieh<sup>1</sup>, Nava Shmuel<sup>1,3</sup>, Hadas Erez<sup>1</sup>, Milos Nesladek<sup>2</sup> and Micha E. Spira<sup>1,3</sup> \*

1 Department of Neurobiology, The Alexander Silberman Institute of Life Science, The Hebrew University of Jerusalem, Jerusalem, Israel

2 Institute for Materials Research in MicroElectronics – Interuniversity Micro Electronics Centre, Hasselt University, Antwerp, Belgium

3 The Harvy M. Kruger Family Center for Nanoscience, The Hebrew University of Jerusalem, Jerusalem, Israel

### **4.4.1 Contributions to the article “Nanocrystalline diamond surfaces for adhesion and growth of primary neurons, conflicting results and rational explanation”**

Much of the work carried out at IMO-MEC for this article was similar in nature detailed in the previous section. However, SEM and Raman results were included in this article to demonstrate the high quality of the NCD substrates. The results of this article however, were the result of a back-and-forth dialogue and testing of many different samples. Based on an article by Thalhammer et al. [30] both institutes had assumed that primary neurons would grow easily on a NCD surface treated with a nanodiamond particle solution. However, after many trials done at IMO-MEC coating substrates with different particle sizes and concentrations, we were unable to reproduce Thalhammer’s results and thus an alternative treatment strategy was developed by HUJI. These unsuccessful trials are not included in the article, though were important in developing the case that nanodiamond particle treatment must only be effective under specific conditions with an unknown factor, which we were not able to replicate.

#### **4.4.2 Main body of the article “Nanocrystalline diamond surfaces for adhesion and growth of primary neurons, conflicting results and rational explanation”**

##### **Abstract**

Using a variety of proliferating cell types, it was shown that the surface of nanocrystalline diamond (NCD) provides a permissive substrate for cell adhesion and development without the need of complex chemical functionalization prior to cell seeding. In an extensive series of experiments, we found that, unlike proliferating cells, post-mitotic primary neurons do not adhere to bare NCD surfaces when cultured in defined medium. These observations raise questions on the potential use of bare NCD as an interfacing layer for neuronal devices. Nevertheless, we also found that classical chemical functionalization methods render the “hostile” bare NCD surfaces with adhesive properties that match those of classically functionalized substrates used extensively in biomedical research and applications. Based on the results, we propose a mechanism that accounts for the conflicting results; which on one hand claim that unfunctionalized NCD provides a permissive substrate for cell adhesion and growth, while other reports demonstrate the opposite. The ideas behind this work were initiated by IMO – UHasselt (M. McDonald, M. Nesladek) and discussed with Hebrew University (M. Spira, S. Ojovan), contribution to this work is 50 % from each of the institutes.

Keywords: nanocrystalline diamonds, cultured neurons, poly-d-lysine, cell adhesion, calcium imaging, network connectivity

##### **Introduction**

The construction of efficient brain-machine interfaces (BMI) relies, to a large extent, on the use of biocompatible materials that can withstand the harsh biological solutions comprising the environment in which living cells operate. A promising substrate for such BMIs is the family of nanocrystalline diamond (NCD) which is a continuous layer of nanoscopic diamond crystals embedded in a nanoscale matrix of  $sp^2$  and disordered carbon (1–10 %) [104]. NCD exhibits chemical and biochemical inertness, high corrosion resistance, excellent

mechano-optical properties and large surface area [105]. While intrinsic NCD is electrically insulating, it can be doped with boron to form semiconducting or even metallically conducting films with tunable surface chemistry [52, 53]. These properties make NCD and Boron-Doped NCD (BNCD) a very attractive material for electrodes or electrode coatings for the development of implantable electrodes for the restoration of sensory functions such as in cochlear or retinal implants [54–56], to electrically communicate between neurons or muscles and peripheral prosthesis [82] and for deep brain stimulation and recordings.

A major concern for using NCD coatings for multi-electrode arrays (MEAs) is whether it can serve as a permissive surface for post mitotic neuron adhesion and regenerative regrowth.

The general impression from the literature is that NCD substrates have superior biocompatible and adhesion permissive properties. Thus, it was reported that proliferating cells, including fibroblast, epithelial cells, and various cell lines, adhere and develop on bare (chemically non-functionalized) NCD surfaces. For example, Amaral et al. (2009) demonstrated that fibroblast cell line L929 (a mouse permanent cell line) and human gingival fibroblast adhere and proliferate on NCD surfaces without hydrophilic treatment or surface functionalization [78]. Klauser et al. (2010), revealed that epithelial cells attach within 24–72 h onto oxygen-terminated NCD substrates without further surface functionalization and without the addition of fetal bovine serum (FBS) to the growth medium [100]. Using the GT1-7 proliferating cell line, which was used to represent neurons, Ariano et al. (2009) documented that these cells adhere to H- or O-terminated NCD substrates without surface functionalization [82]. In an apparent consistency with the above observations, Thalhammer et al. (2010) reported that chemically un-functionalized monolayers of diamond nanoparticles, prepared by the minute detonation synthesis (the so called detonation nanodiamond-DND; Mochalin et al., 2012), promote adhesion and growth of cultured post mitotic hippocampal neurons; emphasizing that chemical surface functionalization does not improve the culture [26, 57]. This conclusion was recently supported also by Edgington et al. (2013) [112]. In the context of the potential use of NCD substrates for bidirectional electrical coupling of neurons or muscles with microelectrodes, it is important to note that beside the mechanical, chemical, and biological

compatibilities of a given interface, the interfacing material for BMIs should be also electrically tunable. Although both materials (NCD and DND) are of the same chemical composition, e.g., carbon in  $sp^3$  bonding configuration with  $sp^2$  inclusions at the grain (NCD) or particle (DND) boundary they differ in the term of technological capabilities [104], [65]. DND do not integrate into a compact layer; they cannot be used to construct flat or three-dimensional electrically conducting tracks. DND could be mainly used in combination with BNCD as a neuron adhesion promoting coating, however, DND can alter surface chemical properties of BNCD, by augmenting the Faradic currents. For example, it has been demonstrated by Holt et al. (2008) that DND particles on gold substrate surface lead to enhancement of redox reactions that can influence cellular processes by promoting the reduction of oxygen with potential production of harmful reactive oxygen species [113].

Driven by the potential use of NCD for fabrication of *in vitro* and *in vivo* bio-electronic platforms, we undertook here the examination of NCD surfaces (rather than DND particles) as substrates for post-mitotic primary vertebrate neurons. In contrast to the expectations based on the literature, we found that it is practically impossible to culture primary neurons, in a defined culture medium, on hydrogen or oxygen terminated NCD. Nevertheless, in view of the physical and chemical advantages of NCD for *in vitro* and *in vivo* applications, we have investigated whether chemical functionalization of NCD surfaces can confer permissive substrate properties for adhesion and growth of post mitotic neurons. We report that the problem of bare NCD to promote adhesion and growth of cultured primary neurons can be overcome using conventional poly-D-lysine (PDL)-laminin functionalization. Based on the results, we propose a mechanism that could account for the conflicting results, which on the one hand claim that unfunctionalized NCD provides a permissive substrate for adhesion and growth of cells, while other reports demonstrate the opposite.

## **Materials and Methods**

### *NCD Fabrication*

The diamond films were grown using an Astex AX6550 microwave plasma enhanced chemical vapor deposition system (MWPECVD) working at H<sub>2</sub> (99 %)/CH<sub>4</sub> (1 %) gas mixture and substrate temperature of 700 °C. The substrate was cleaned using standard RCA1 and RCA2 (Radio Corporation America, Kern, 1990) wafer cleaning techniques and subsequently seeded by detonation nanodiamond (DND, 7 nm size) by spin-coating from an aqueous DND mono-dispersion (NanoAmando®B, NanoCarbo Research Institute, Japan) prior to the deposition. Hydrogen terminated NCD films were achieved by allowing pure hydrogen plasma in the system for 30 min after stopping the CH<sub>4</sub> flow and subsequently cooling in hydrogen. UV ozone treatment for 30 min (Novascan, PSD digital Ozone system) was used on hydrogen terminated films to give NCD films an oxygen terminated surface. Surface termination was confirmed by XPS and the contact angle measurement, showing hydrophobic surfaces for H-terminated films with the contact angle of 15° and of 90–92° for O-terminated NCD films.

### *Surface Functionalization*

Glass or NCD chips were washed and sterilized by incubation in ethanol 75 % for 2 h. Thereafter the ethanol was thoroughly rinsed with double distilled water and then functionalized by 0.1 mg/ml PDL (Sigma–Aldrich) and 25 µg/ml laminin (Sigma–Aldrich) in sodium borate solution for 12 h prior to cells seeding.

### *Cell Culture*

Rat hippocampal neurons were obtained either from one day old new born rats or from 17 days old embryos, as described by Kaech and Banker (2006) [114]. Briefly, for embryonic hippocampal cultures the pregnant female was anesthetized, the embryos removed and decapitated. The embryonic or new born hippocampus were removed and treated with papain for 45 min (Sigma–Aldrich),

and serially triturated. Cell density at plating was 250,000–500,000 cells/ml. Cells were seeded in attachment/seeding medium [Neurobasal medium, 5 % FBS, 2 % B27, 1 % GlutaMAX (All from Life technologies), 1 % Penicillin-Streptomycin Amphotericin B Solution (Biological Industries)]. 24 h (1 DIV) after culturing the seeding medium was replaced with serum-free maintenance/feeding medium (Neurobasal medium, 2 % B27, 1 % GlutaMAX, 1 % Penicillin-StreptomycinAmphotericin B Solution). At 3 DIV 5  $\mu$ M ara-c (Sigma–Aldrich) was added to prevent glial cell's proliferation. Half of the maintenance medium was replaced every 3–5 days by astroglial conditioned medium. Hippocampal cultured cells were kept at 37 °C in a humidified atmosphere of 5 % CO<sub>2</sub>. Cultures were kept till 7–21 DIV. All procedures were approved by the Committee for Animal Experimentation at the Institute of Life Sciences of the Hebrew University of Jerusalem.

### *Immunohistochemistry*

Cultured hippocampal cells were immunolabeled as previously described [115]. Briefly, samples were fixed by 4 % paraformaldehyde (Sigma–Aldrich) in Hank's Balanced Salt Solution (HBSS, Biological Industries) for 30 min, washed with HBSS before membrane permeabilization with 0.1 % TritonX-100 (BDH Chemicals) in HBSS for 30 min. After washes with Tween 0.1 % (J.T.Baker) in HBSS, cells were incubated for 1 h in blocking solution [BS, 2 % chicken albumin (Sigma–Aldrich) in Tween 0.1 %]. Then samples were incubated with primary antibodies in 1 % BS, overnight at 4 °C: neurons were labeled for neuron-specific intermediate filaments with mouse anti neurofilament antibodies; Glial cells were labeled for glial fibrillary acidic protein (GFAP) with primary anti-GFAP rabbit monoclonal antibodies. The next day the samples were washed repeatedly with 0.1 % Tween and incubated with secondary antibodies in 1 % BS for 1 h: goat anti-mouse secondary antibodies conjugated to Cy2 (Jackson ImmunoResearch Laboratories, Inc), and goat anti-rabbit secondary antibodies conjugated to Cy3 (Life technology). Cells were counterstained with the nuclear marker DAPI (Sigma–Aldrich) for 1 h, at room temperature. Samples were washed with HBSS, and stored at 4 °C in anti-fade n-propyl gallate (Sigma–Aldrich) solution in 50 % glycerol till imaging. Confocal imaging of the immunolabeled cultures was done

using D-Eclipse C1 imaging system (Nikon) mounted on an Eclipse TE-2000 microscope (Nikon). Images were collected and processed using EZ-C1 software (Nikon). Scanning was done in sequential mode: red was excited with 543 nm He-Ne laser and collected with  $605 \pm 75$  nm band pass filter; green was excited with 488 nm Argon laser and collected with  $515 \pm 30$  nm band pass filter; blue excited with 405 nm Diode and collected with  $450 \pm 35$  nm band pass filter. Images were prepared using the open source image analysis program ImageJ (NIH,USA) and Photoshop CS6.

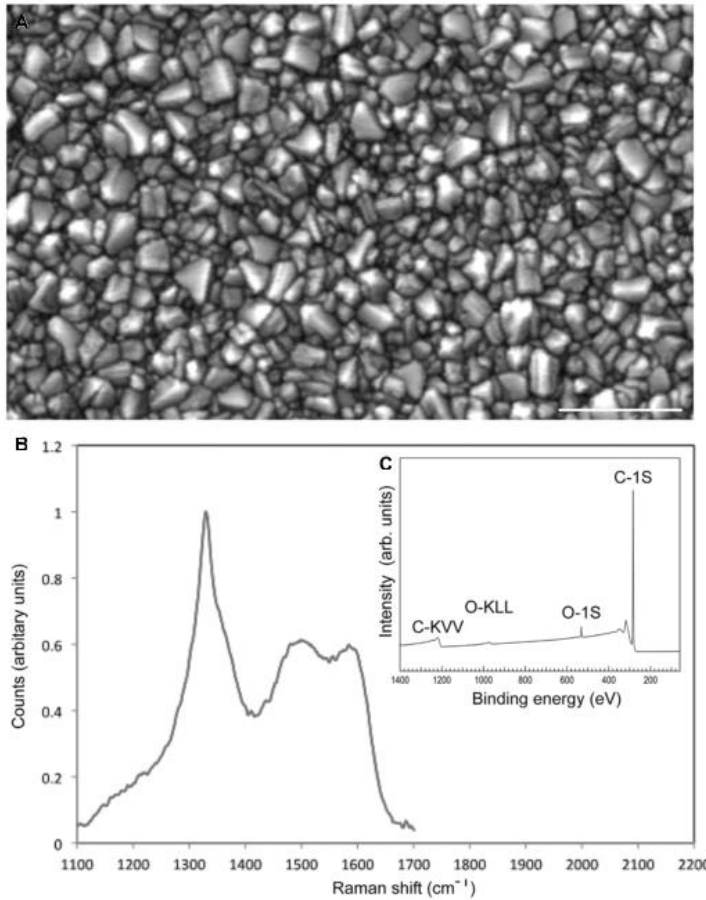


**Figure 4-6** - Characterization of the nanocrystalline surface. (A) SEM image of the nanocrystalline diamond (NCD) film morphology with Rmns ~17 nm. (B) The Raman spectra of the NCD film showing the zone-center phonon  $sp^3$  diamond line at  $1332\text{ cm}^{-1}$  and a higher wave number signal, consisting of disordered and  $sp^2$  bonded carbon at diamond grain boundaries. Content of non-diamond carbon is estimated to be 0.7 %. (C) shows an XPS spectrum of oxidized NCD surface. Bar in A =  $0.5\ \mu\text{m}$ .

#### *Calcium Imaging and Formation of a Connectivity Map*

Ten to 14-day-old cultures were incubated for 45 min in a  $37\text{ }^\circ\text{C}$  incubator in a  $5\ \mu\text{M}$  fluo-4 (AM; Molecular Probes) dissolved in HBSS. The fluo-4 AM solution was washed away with HBSS and the culture was then incubated in fluo-4 free medium

for 15 min. Cells were imaged with a 20 × objective (NA = 0.75) using the confocal microscope system described above. Seconds long stimulation of a single neuron at the center of the field of view was applied with a fire polished patch electrode and the response imaged by the frame-scan modes. The second long stimulation led to a buildup of intracellular calcium levels that could be detected by the low NA objective and the slow laser scan used (3.9 s/frame). Sequential confocal fluo-4 images were used to generate a neuronal connectivity map of a relatively large field of view. Upon cessation of the stimulation the fluorescent signal recovered to control level.

The connectivity map (Figure 4-12) was generated by subtracting each image from the previous one. Eight consecutive subtracted frames, from the stimulation onset, were then sequentially color coded in accordance to a lookup color table. The total number of cell bodies activated by the stimulation was counted and the largest distance between the stimulated cell and the follower cells within the field of view was measured.

### *Scanning Electron Microscopy*

For SEM analysis cells cultured on the NCD or glass substrate were fixed, dehydrated, within the culturing dish as previously described [116]. Briefly, hippocampal primary cultured cells were fixed by 3 % glutaraldehyde (Electron Microscopy Science) in cacodylate buffer (Agar Scientific, Stansted) at pH 7.4. The cells were then washed in cold 0.1 M cacodylate buffer, pH 7.4. The cells were post-fixed in 1 % osmium tetroxide (Electron Microscopy Science) and 1.5 %  $K_3Fe(CN)_6$  (Sigma–Aldrich). Dehydration was carried out through a series of ethanol solutions and washed two times for 30 min with fresh 100% ethanol before critical point drying with liquid  $CO_2$  in a SAMDRI-PVT-3D (Tousimis, USA). Once dry the samples were sputtered with gold in an SPI-Module<sup>TM</sup> Sputter Coater Module (SPI Supplies, USA). Images were taken with an Extra High Resolution Scanning Electron Microscopy Magellan<sup>TM</sup> 400L using an accelerating voltage of 5 kV.

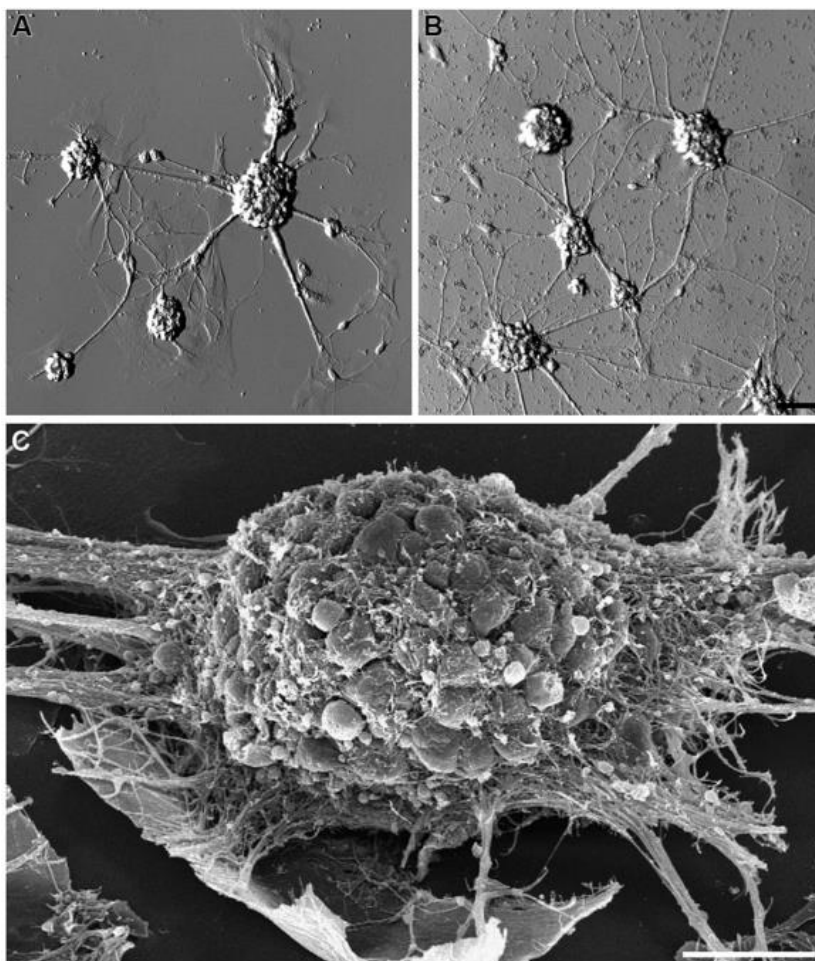


**Figure 4-7** - Clusters of hippocampal neurons cultured on bare glass or NCD surfaces. Embryonic (E17) hippocampal neurons cultured on bare glass (A) and bare NCD (B), 3 DIV; bar = 50  $\mu\text{m}$ . (C) SEM image of hippocampal neurons cultured on bare glass, 7 DIV; bar = 20  $\mu\text{m}$ .

### *Statistical Analysis*

The averaged density of cells adhering to PDL functionalized control glass or NCD substrates were calculated by averaging the densities (cells number/standard surface area of  $607 \times 607 \mu\text{m}$ ) obtained from five randomly selected areas on days 3, 7, and 10 in culture (DIV). The data are presented as mean  $\pm$  standard deviation. t-tests was performed using Excel software.

## Results

### *Synthesis of NCD Films*

For the present study, 150 nm thick high quality NCD films were synthesized on fused silica substrate (10 mm × 5 mm × 0.5 mm size). Substrates were seeded in an aqueous suspension of DND particles to promote the diamond crystal nucleation and subsequently to initiate diamond layer growth (Barros et al., 2011). NCD films were grown in a resonance cavity microwave plasma enhanced chemical vapor deposition system (MWPECVD) using 1 % CH<sub>4</sub> mixture in hydrogen at substrate temperature of 700 °C (see Experimental methods for details: [50, 64]). The morphology of NCD films was composed of well-developed faceted nano-crystals of random orientation and is shown in Figure 4-6A. Figure 4-6B shows the Raman spectra of NCD films. The sp<sup>2</sup> and disordered carbon originating at the grain boundaries, as typical from NCD films, was as low as 0.7 % as determined by the numerical fitting of Raman spectra (for detail [65]). The inset of Figure 4-6C shows an XPS survey scan of an oxidized NCD surface, acquired immediately after the MWPECVD preparation and oxidizing the NCD diamond film in ozone. Clearly, the spectrum displays ultra-clean diamond surface dominated only by the emission from carbon and oxygen. The C-1s core level (binding energy 284 eV) and in addition to C-lines, an O-1s signal are visible (531 eV) which can be assigned to the oxygen-terminated surface. Such surfaces were further used for neuron adhesion study.

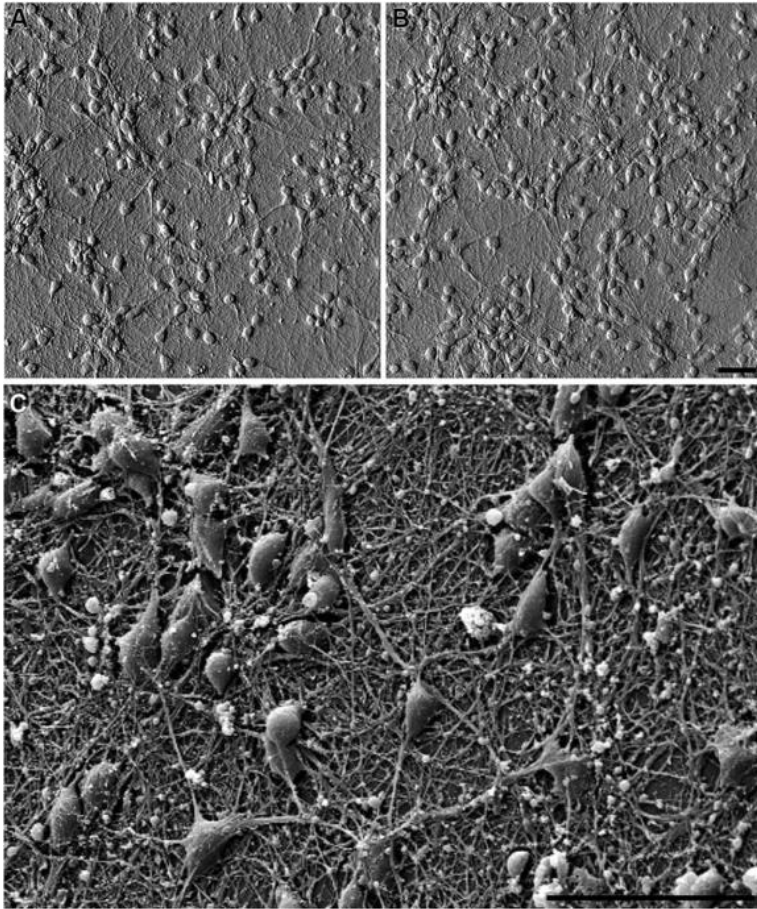


**Figure 4-8** - Embryonic hippocampal neurons (7 DIV) cultured on: (A) PDL-laminin functionalized glass and (B) PDL-laminin functionalized NCD. No difference in adhesion and growth is seen on the two substrates; bar = 50  $\mu\text{m}$ . (C) SEM image of embryonic hippocampal neurons cultured on PDL-laminin functionalized NCD. Note the dense growth of neuritis; bar = 50  $\mu\text{m}$ .

#### *Incompatibility of NCD Substrate for Primary Neuron Adhesion and Growth*

We tested the compatibility of bare NCD surface for adhesion and growth by culturing primary embryonic (E17) or newborn rat hippocampal cells on NCD, with hydrogen-(H-hydrophobic) and oxygen (O-hydrophilic)-termination. As a control to these experiments, we cultured neurons in the same experimental sessions on bare- and PDL-laminin functionalized glass substrates. The criteria used for comparing the cultures qualities were: adhesion of the cells to the substrate, the

development of neurites on the substrate, survival time of the culture, and neuronal network functioning as revealed by calcium imaging of evoked network activity.

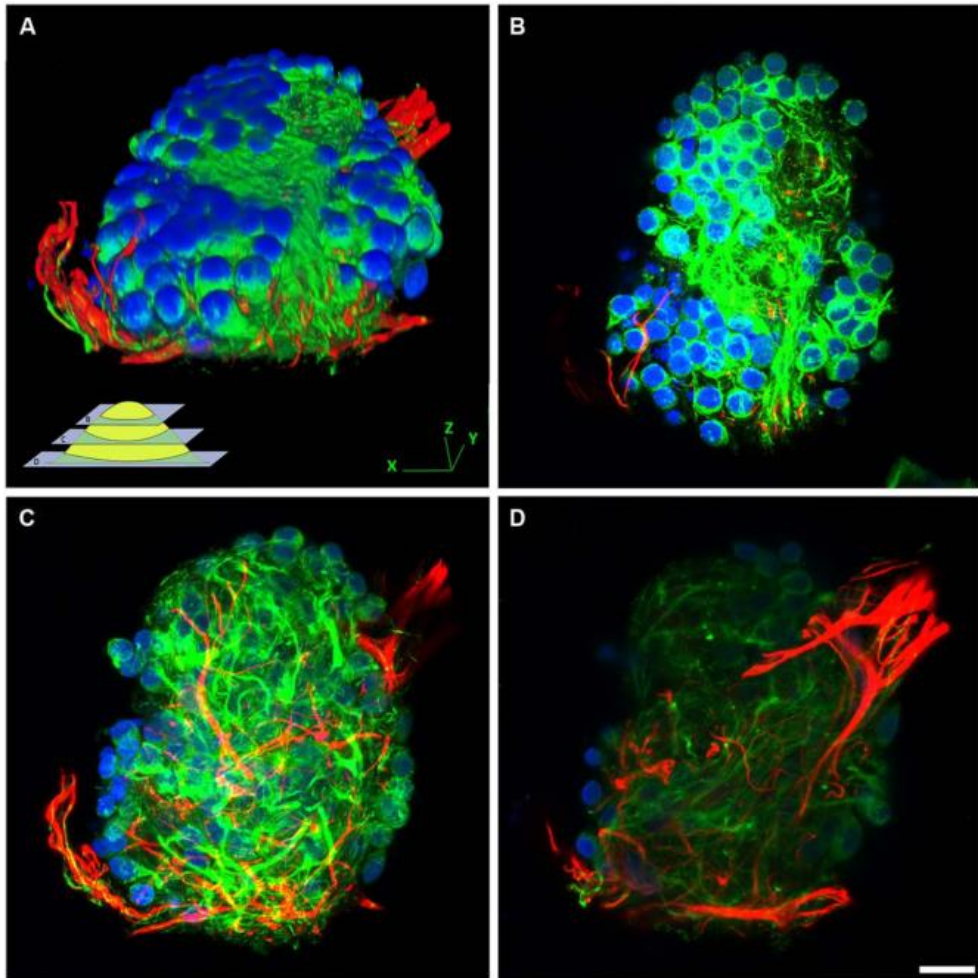


**Figure 4-9** - The structural organization of cell-aggregates formed on bare NCD substrate. Confocal image of immunolabeled (green- NF, redGFAP, blue- DAPI) hippocampal neurons and glia cultured on bare NCD, 10 DIV. (A) Three dimensional reconstructed view of a cell-cluster. The insert illustrates the focal planes of the images shown in B, C, and D. (B) Top layer of the cell cluster (a focal slice of 18  $\mu\text{m}$ ), consists mainly of neuronal cell bodies. (C) Middle part of the cell-cluster (thickness of 19.5  $\mu\text{m}$ ), consists of neurites. (D) Bottom part of the cell cluster (slice thickness of 12.5  $\mu\text{m}$ ), close to the substrate level, showing glial processes; bar = 20  $\mu\text{m}$ .

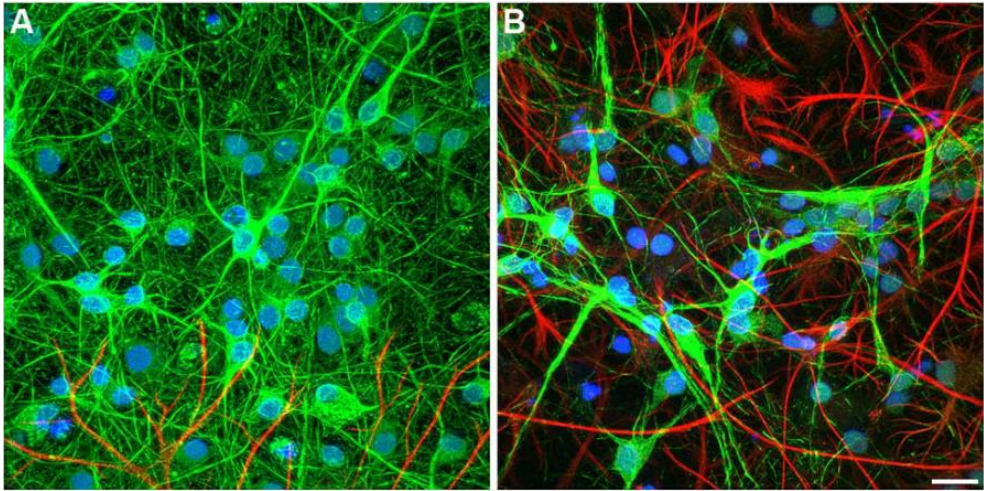


**Figure 4-10** - Confocal image of immunolabeled hippocampal cells. (A) embryonic, (B) newborn neurons cultured on PDL-laminin functionalized NCD, 10 DIV. The embryonic culture consists of mainly of neurons whereas newborns culture consist of mixed neuron-glia cells. Both embryonic and new born cultures survive on functionalized NCD for over 3 weeks; bar = 20  $\mu\text{m}$ . (green- NF, redGFAP, blue- DAPI)

Hippocampal cells (neurons and glia) grown on bare NCD, or on bare glass substrates revealed poor adhesion and cell clustering (Figure 4-7). The cell clusters were interconnected by a small number of extensions. This is in contrast to control cultures of embryonic or new born hippocampal cells grown on PDL-Laminin functionalized glass-substrate which adhered well to the substrate and generated an elaborate network of neuritis (Figure 4-8A). The self-assembly of cells into clusters, rather than adhesion of individual cells to the substrate, reduces the contact surface area between the cells and the substrate, and enhances cell-cell contact. Such self-assembly of aggregates reflects significant adhesion-incompatibility between the cells and the substrate relative to the adhesion among cells. Three dimensional reconstructions of confocal microscope optical sections obtained at 0.25  $\mu\text{m}$  steps revealed that in newborn cultures (that are rich with glia) the cells that interface with the substrate are mainly glia, whereas the neuronal cell bodies occupy the upper layers facing the bathing solution (Figure 4-9). Cultures prepared from embryos (E17) are almost glia-free, nevertheless they also form aggregates. These clusters detach from the substrate and degenerate within a number of days. No significant differences in

cell-substrate adhesion were noticed among hippocampal cells cultured on bare glass substrate and the various NCD types used.

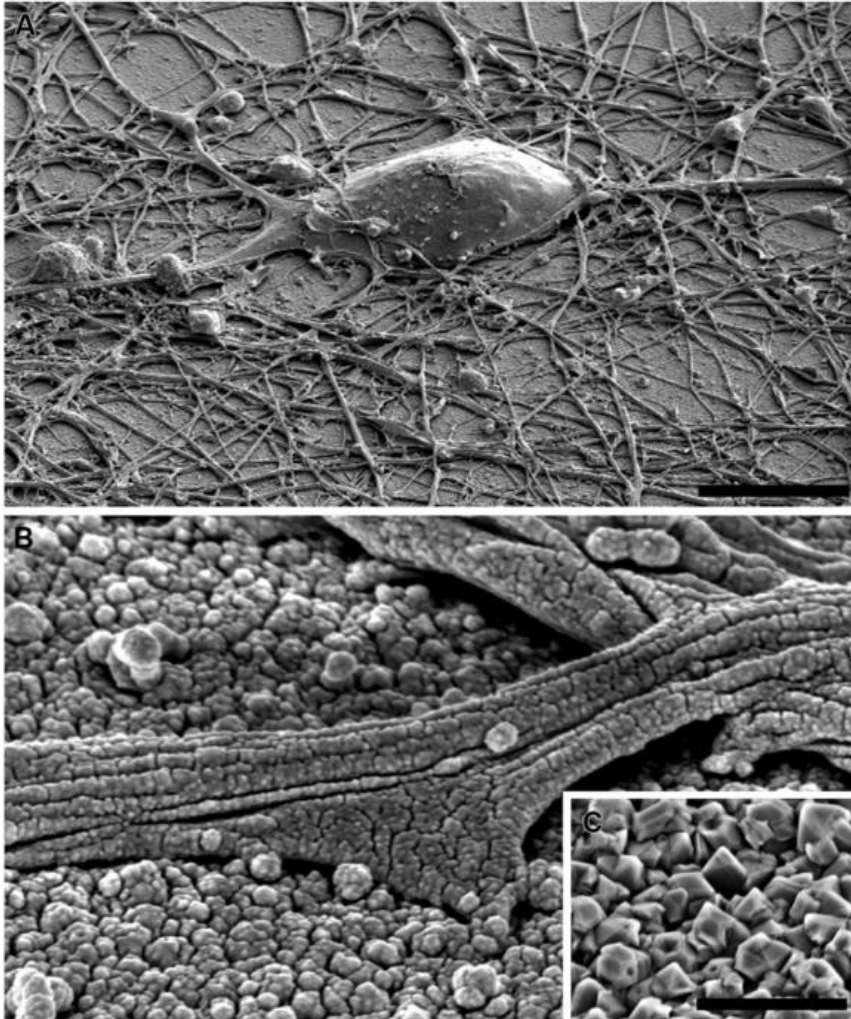


**Figure 4-11** - SEM image of embryonic hippocampal neurons cultured on PDL-laminin functionalized NCD, 7 DIV. (A) low magnification of a neuron; bar = 10  $\mu$ m. (B) a neurite adhering to the ND layer. (C) NCD imaged without gold spattering; bar = 500 nm.

We conclude that post mitotic primary hippocampal neurons and glia grown on un-functionalized NCD or glass form cells aggregates as they do not adhere well to the substrate.

### *Hippocampal Cell Adhesion and Growth on Functionalized NCD Substrates*

We next examined whether chemical functionalization of NCD surface solves the problem of cell-adhesion incompatibility to NCD substrates. To that end we employed the classical and robust PDL-laminin glass surface coating procedure. We found that functionalization of NCD substrates by PDL-laminin generates an adhesive and permissive substrate for primary neurons culturing (Figure 4-8, Figure 4-10, and Figure 4-11). Under these conditions, both embryonic and new born hippocampal cells adhere and extend a dense network of neuritis on the substrate. No significant differences in adhesion and survival over the time of observations were noted between neurons grown on functionalized glass or the various NCD substrates using morphological criteria (Figure 4-8) and functional assessments (see Neuronal Network Activity on Functionalized NCD Substrates). Thus, for cultures prepared from 17 days old embryos: on DIV 3 the averaged density of neurons on a standard area of functionalized glass (number of counted areas  $n = 5$ ) was  $683 \pm 94$  for control and on functionalized NCD  $718 \pm 173$ . These values are not significantly different ( $\alpha = 0.05$ ,  $p = 0.7$ ). Likewise, the cell densities on DIV 7 and 10 did not change overtime on both the functionalized glass and NCD substrates exhibiting on DIV 7 densities of  $528 \pm 123$  in control and  $496 \pm 151$  on functionalized NCD ( $p = 0.7$ ), and on DIV 10  $527 \pm 151$  in control and  $630 \pm 137$  on functionalized NCD ( $p = 0.29$ ). The density of cultured cells (neurons and astrocytes) prepared from new born rats did not reveal any differences between the functionalized glass and NCD substrate but revealed a significant increase in the number of astrocytes on day 10 of the culture. Thus, on DIV 3 the averaged density of cells in the control was  $247 \pm 14$  and on NCD  $273 \pm 105$  ( $\alpha = 0.05$ ,  $p = 0.6$ ), on DIV 7 in control the average was  $177 \pm 15$  and on functionalized NCD  $229 \pm 46$  ( $p = 0.01$ ). On DIV 10 of the cultures prepared from new borne rats a large and significant increase in the density of the cells was observer on both glass and NCD substrates. The averaged density on glass was  $437 \pm 46$  and on NCD  $524 \pm 153$  ( $p = 0.26$ ). The significant increase in the number of cells from DIV 7 to 10 is due to glia cell proliferation.

### *Neuronal Network Activity on Functionalized NCD Substrates*

The physical, chemical, and morphological nature of the substrates to which cells adhere and on which cells develop may have significant effects on cells morphology, their biophysical properties (electroanatomy) and, in the case of neurons, their synaptic functions and the overall network activities (for example [118]) To assess whether neurons grown on NCD functionalized with PDL-Laminin maintain excitable membrane properties that promote propagation of action potentials along neurites, form functional connectivity that permit polysynaptic communication, we imaged the fluorescent signals generated by the calcium indicator fluo-4 in response to a long lasting train of stimuli delivered to a single neuron at the center of the field of view. To that end, the neurons were loaded with acetoxymethyl (AM) ester fluo-4 and then after removal of the excess fluo4-AM and incubation period to allow hydrolyze of the ester, a neuron located at the center of field was stimulated by a fire polished microelectrode. Live confocal imaging of the fluo-4 fluorescent revealed the propagation of the fluorescent signal from the stimulated cell to neighboring cell bodies along neurites (Figure 4-12). Analysis of the number of neurons activated by the stimulation in control (neurons cultured on functionalized glass substrate) and neurons grown on functionalized NCD were similar ( $45 \pm 13.55$  in control and  $61.17 \pm 41.04$  on the NCD substrate. t-test for unequal variances  $n = 5$  and  $6$ , respectively, is for  $\alpha = 0.05$ ,  $p = 0.42$ ). The maximal distance of the fluorescent signals propagation was the same ranging between  $254$  and  $423 \mu\text{m}$  ( $322 \pm 75$  in control and  $317 \pm 66$  on the NCD substrate. t-test for unequal variances  $n = 5$  and  $6$ , respectively, is for  $\alpha = 0.005$ ,  $p = 0.91$ ). We conclude that the overall network connectivity of cells grown on functionalized NCD is similar to those grown on functionalized glass.

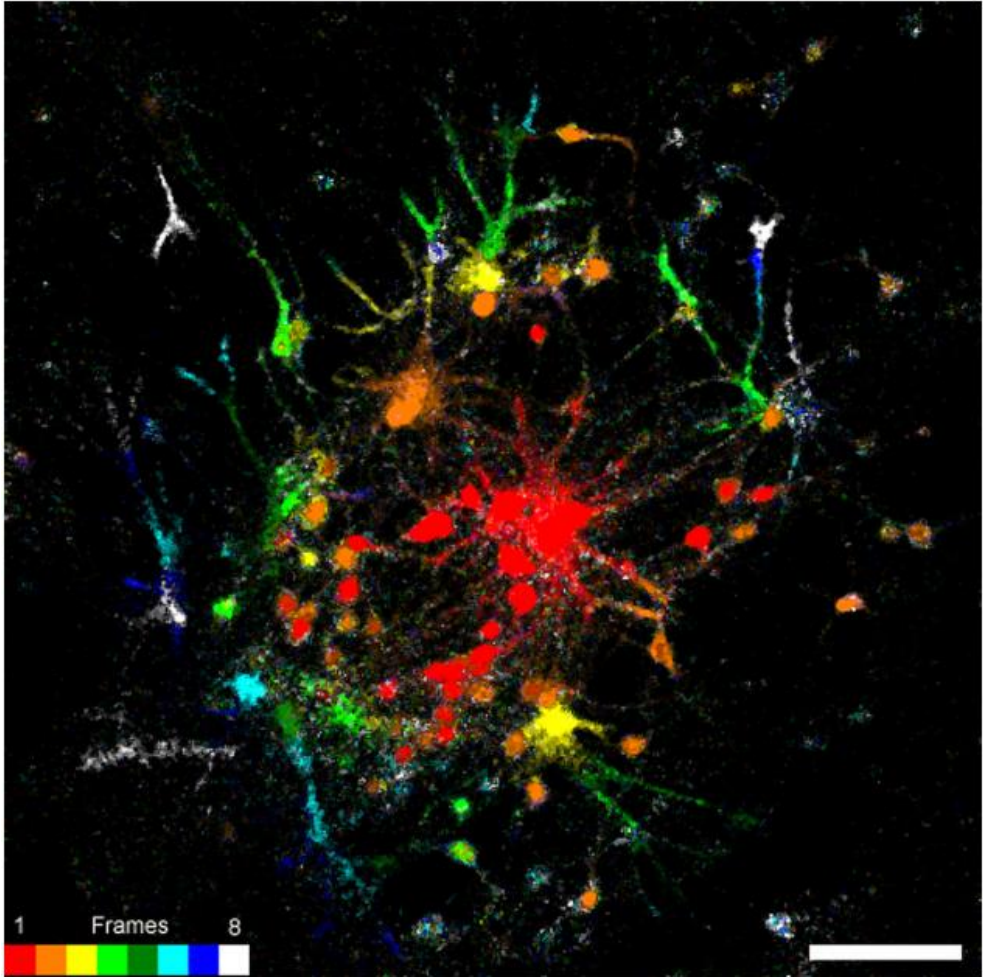


**Figure 4-12** - Connectivity map of 14 days old cultured embryonic neurons on PDL-laminin functionalized NCD surface. Nine consecutive confocal images were grabbed. The first before the onset of stimulation and the rest during and after the stimulation. Consequent images were subtracted (image  $n+1$  – image  $n$ ) to generate eight subtracted images. The resulting images were color coded according to the lookup table attached to the figure. Note that the fluo-4 fluorescent signals propagated radially (from red to white along the pseudo color lookup table). The average number of cells that were excited by stimulation of a single neuron and the maximal distance of signal propagation was similar in cultures grown on functionalized glass and NCD. Bar = 20  $\mu$ m.

## Discussion

The main observations of the present study are that in contrast to the general impression generated by earlier studies we found that post-mitotic primary rat hippocampal neurons and glial cells do not adhere and develop when cultured in defined medium on bare, oxidized and H-terminated NCD substrates. Nevertheless, classical chemical functionalization of the NCD substrate by PDL-laminin renders the substrate with permissive growth properties for these cells. Under these culturing conditions primary hippocampal neurons develop excitable membrane properties and excitatory synapses that communicate among them.

The incompatibility of bare NCD as a substrate for primary neuron culture reported here is in contradiction with earlier studies reporting that cell lines as well as hippocampal neurons adhere and develop on various NCD substrates without chemical surface functionalization prior to cell seeding. We devote the following paragraph to briefly propose a possible mechanism to account for this contradiction.

Under *in vivo* conditions cells are attached to each other by extracellular matrix (ECM) and cell adhesion molecules (CAMs) [119]. Whereas the ECM and the CAM are secreted and expressed (respectively) by all cell types derived from multicellular organisms, their molecular, biochemical nature and levels of expression differ in different cell types and under different physiological conditions (for example see [120]). These differences are so substantial that *in vitro* cell culturing methods take advantage of the differences to isolate certain cell types from others. This is done, for example, by seeding a heterogeneous cell suspension on a common un-functionalized glass or plastic substrates. Under these conditions some cell types adhere to the bare substrate while others remain in suspension for a longer period of time [121]. The selective cells adhesivity reflects differences in the nature and rates of ECM secretion and CAM expression. The non-adhering or the adhering cells can then be collected. Differences in ECM molecular nature and secretion are also observed under *in vivo* conditions. For example, regrowth of peripheral axons depends to a large extent on ECM secreted by supporting Schwann cells [122]. For these reasons, most classical and

contemporary primary neuron culturing-procedures heavily rely on conscious chemical functionalization of the substrates prior to cells seeding.

It is conceivable that cell lines and primary proliferating cell types that are characterized by effective ECM secretion adhere and divide when plated on chemically un-functionalized surfaces. On the other hand, generations of cell biologists have established that in vitro culturing of primary neurons on glass substrate require surface functionalization prior to seeding. Therefore, the reports of Thalhammer et al. (2010) and Edgington et al. (2013) who demonstrated that primary neurons which do not adhere to NCD adhere and grow on non-functionalized DND are somewhat surprising [57, 58]. The adhesion to DND could be explained by assuming that in these studies the DND surface was unconsciously functionalized by serum protein during the incubation step of the substrate in the seeding medium which contained 10 % FBS. Interestingly, the protocol used by us also involved a ~20 h incubation period in 5 % FBS. Nevertheless, as evident by our study, this and even extended periods of incubation, were insufficient to confer adhesive properties to our NCD substrate. The neurons did not adhere to  $sp^3$  carbon rich NCD grains, nor to  $sp^2$  carbon rich grain boundaries. Both oxygen terminated (negative surface charge) or H-terminated bare NCD surfaces (positive surface charge) yielded the same negative result.

A possible mechanism that could account for this phenomenon could be related to differences in protein absorption capacities of DND and NCD films as the DND used by Thalhammer et al. (2010) and Edgington et al. (2013) are composed of round diamond particles of diameter ~8–10 nm while NCD films used in this study are composed of faceted crystals with Rms ~15–17 nm [57, 58].

In conclusion, we demonstrate that bare NCD based substrates are not providing permissive adhesion and growth substrate for cultured primary neurons and glia. The literature demonstrates that cell lines and other proliferating cells can adhere and proliferate on ND substrates relying on their innate ECM resources. In contrast, cells that do not secrete effective ECM (as primary neurons) will not adhere to NCD substrate and degenerate. We conclude that, whereas bare NCD has a broad range of advantageous material properties unusual cell adhesion properties are not included among them. Nevertheless, simple functionalization

strategies make NCD a permissive substrate for adhesion and growth of post mitotic primary neurons. As functionalized NCD surfaces supports well neural adhesion its unique electrical mechanical and chemical properties is a highly attractive material for construction of in vitro and in vivo MEAs and BMIs.

### **Acknowledgments**

The study was supported by a grant from the European commission FP7-NMP SL-280778-2 (MERIDIAN). Silviya M. Ojovan and Mathew McDonald were supported by the EC-FP7 Marie Curie ITN PITN-GA-264872 (NAMASEN). Part of the study was carried out at the Smith family and Prof. Elkes laboratory for collaborative research.

**Conflict of Interest Statement:** The authors declare that the research was conducted in the absence of any commercial or financial relationships that could be construed as a potential conflict of interest.

## **4.5 Polyethyimine surface treatment**

### **4.5.1 Contributions to Section 4.5 “Polyethyimine Surface Treatment”**

The work of this section has not yet been published, but was a result of a collaboration between IMO-MEC and the University of Antwerp. This work was done in tandem to that of the collaboration with HUJI. Similarly, it was found that untreated NCD surfaces with either hydrogen or oxygen terminated surfaces were insufficient for neural cell growth and thus an alternative approach was developed. The idea for the use of PEI, which is a common adhesion promotor used on glass coverslips, was developed by Farnoosh Vahidpour at IMO-MEC. My role was to fabricate the diamond coverslips and perform material characterization. Farnoosh Vahidpour developed the PEI protocol on diamond substrates and evaluation of the surface after coating. The biological analysis, including Cell counting, viability assay, cell staining, and electrophysiology recordings were performed by Lowry Curley at the University of Antwerp

Polyethyimine is a polymer that is commonly used as a surface pretreatment of substrates used for neuronal cell cultures, including glass cover slips and plastic substrates. The accepted mechanism is that PEI creates a positive surface charge, which allows cells to lay down adhesive proteins, enabling good adhesion and outgrowth [123]. It was hypothesized that this common surface treatment could be adapted for use on NCD substrates to enhance the adhesion for primary neuron cultures. In this section, it is shown that PEI indeed provides an effective surface treatment for NCD substrates. My work involved in this work was the fabrication of NCD substrates, with the PEI treatment developed by my colleague Farnoosh Vahidpour with help from Lowry Curly at the University of Antwerp. Lowry Curly also performed the cell culturing and biological analysis. Further detail about the surface treatment of PEI on diamond can be found in the work of Farnoosh Vahidpour.

### **4.5.2 Substrate fabrication**

NCD thin films were grown over 70 square 5 mm x 5 mm fused silica substrates. Ca. 150 nm thick diamond films were grown using the ASTeX-3 MWPECVD reactor with a gas mixture of H<sub>2</sub> (99 %)/CH<sub>4</sub> (1 %) and substrate temperature of 650 °C. Substrates were cleaned using standard RCA1/RCA2 cleaning steps, as detailed in section 3.1.1, and then seeded with a diamond nanoparticle solution (see section 3.1.2). After the growth was finished, pure hydrogen plasma was run in the system for 30 min and subsequently cooled in hydrogen, to produce hydrogen terminated surfaces. Additionally, NCD films were grown on 100 7 mm x 7 mm glass substrates (EAGLE XG, Corning Inc., Corning NY, USA) by partners at Nano 6. The NCD films were grown using a MWPECVD reactor with linear antenna delivery, as described in [124]–[126]. These films were grown at a lower temperature (500 °C) and higher methane concentration which lead to much smaller diamond grains and thus higher sp<sup>2</sup> incorporation. For the purposes of this experiment, the set of samples grown with ASTeX-3 are referred to as HQD (high-quality diamond) and the set received from Nano 6 as LQD (low-quality diamond). For control substrates, conventional glass cover slips were used.

### **4.5.3 Substrate preparation**

For sterilization, NCD substrates were autoclaved using high pressure saturated steam at 121 °C for 30 min. Three different surface preparation techniques were employed to test cellular adhesion of the substrates: i) a protein pretreatment with 10 % fetal bovine serum (FBS) in Modified Essential Medium (Sigma-Aldrich) for 2 h prior to neuronal seeding, performed according to published protocols [111]; ii) Cleaning in an air plasma cleaning system (Pico, Diener Electronics, Jettingen, Germany) to increase surface hydrophilic, performed at 50 % power for 90 s; and (iii) coating by polyethyleneimine (PEI, Sigma-Aldrich) to provide a positive surface charge, performed using a 1 mg/ml PEI solution for 12 h, followed by extensive rinsing with de-ionized water and air dried prior to neuronal seeding.

#### 4.5.4 Primary neuronal cultures

Primary cortical neurons were obtained by standard methods, in agreement with national and institutional guidelines on animal experimentation, from newborn Wistar rats (Charles River, France). Superficial cortical slices were first isolated and minced into small pieces and then exposed to a 0.025 % trypsin solution for enzymatic digestion of the extracellular matrix, with further mechanical dissociation using a pipette. Finally, the cells were centrifuged and resuspended prior to cell seeding in growth medium containing Modified Essential Medium supplemented with 2 M glucose, 200 mM l-glutamine, 50 µg/mL gentamycin and 5 % horse serum (Sigma-Aldrich). For NCD and glass control substrates, a cell plating density of ~500 cells/mm<sup>2</sup> was employed (increased to ~2000 cells/mm<sup>2</sup> for patch-clamp intracellular recording experiments).

Cells were maintained in a 100 % relative humidity incubator, at 37 °C and 5 % CO<sub>2</sub> for a period of time ranging from 1 to 14 days *in vitro* (DIV), using growth medium. The culture medium was changed three times per week, by removing 0.5 ml and adding 0.5 ml of fresh medium. Glial growth was not inhibited.

#### 4.5.5 Cell biological analysis

For assessment of the cell adhesion and biocompatibility of each substrate, cell density, % viability, and immunocytochemistry experiments were performed on sister cultures at 1, 7 and 14 DIV. To determine the cell density, a Live/Dead assay kit (Sigma-Aldrich) was performed. The number of living or dead cells adhering to the substrates was quantified using pictures from four different regions for each substrate, under fluorescent microscopy with an EVOS FL using RFP (531/40 Ex; 593/40 Em) and GFP (470/22 Ex; 510/42 Em) filters (Invitrogen, Belgium). The averages across 6 separate samples were used for cell density values. To determine the percent of viable cells in relation to control, a 2,3-Bis-(2-Methoxy-4-Nitro-5-Sulfophenyl)-2H-Tetrazolium-5-Carboxanilide (XTT) cell viability colorimetric assay kit (Sigma-Aldrich) was used to metabolically determine cellular activity. The results from these two methods are summarized in Figure 4-13.

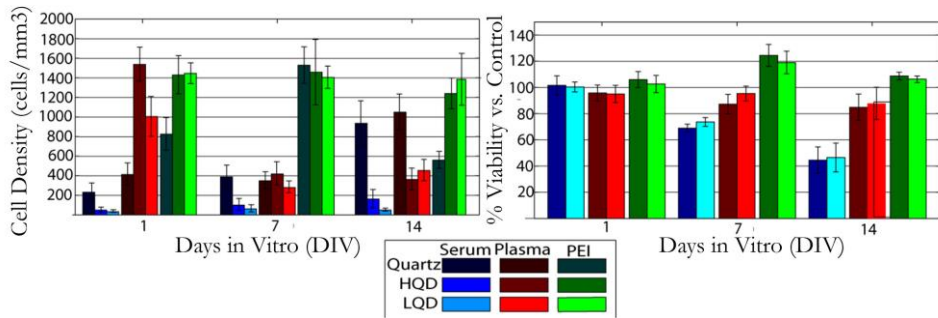


**Figure 4-13** – Biological analysis of diamond substrates vs. control, by cell-counting (left) and % viability with XTT assay (right). Error bars depict standard deviation.

Immunocytochemistry was undertaken by fixation of cells in 4% paraformaldehyde, followed by permeabilization and blocking steps. Primary antibody staining was employed overnight (AbCam, UK) to reveal neurons and neurites (mouse monoclonal  $\beta$  III tubulin), and glial cells (monoclonal glial fibrillary acidic protein). Secondary staining was performed for one hour with 488 goat anti-mouse and 568 goat anti-chicken antibodies (Invitrogen). Samples were mounted using Vectashield Hard Set with 4',6-diamidino-2-phenylindole (DAPI, revealing nuclei of neurons and glial cells) (Vector Laboratories, USA). Figure 4-14 compares the results of the different surface treatments for the different substrates. Large numbers of glial cells were present on quartz substrates, with neuronal clumping following plasma treatment. For NCD substrates, dense glia and neurons were only present with PEI treatment. PEI treatment induced structural network connectivity, with improved outgrowth on NCD.

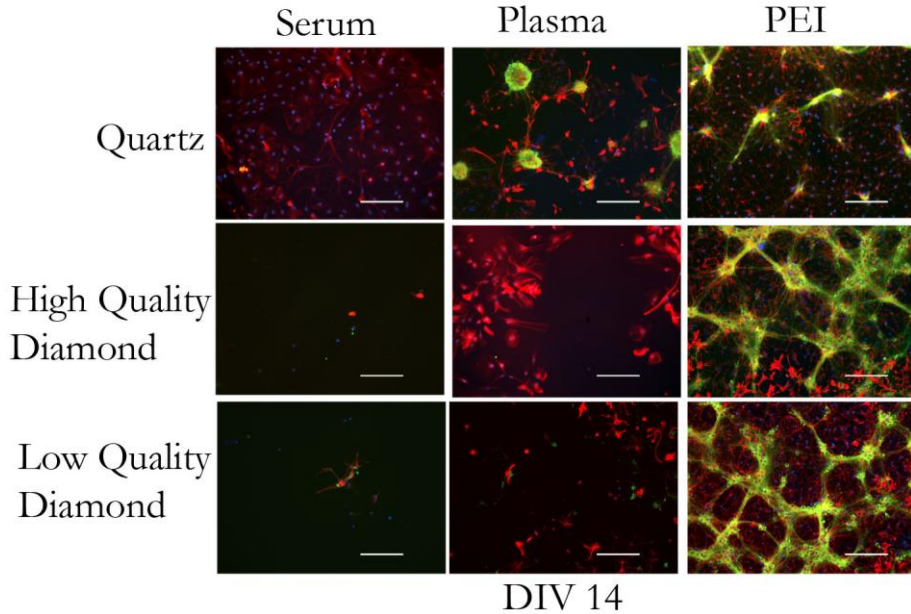


**Figure 4-14** – Staining of cell nuclei (DAPI, blue), glia (GFAP, red) and neurons ( $\beta$  III Tubulin, green) at 14 DIV.

#### 4.5.6 Cellular electrophysiology

Whole-cell patch clamp recordings from the cell somata of neurons cultured between DIV 14 and 21 was performed. Cells were identified visually by infrared differential interference contrast (DIC) videomicroscopy (SliceScope, Scientifica UK). Borosilicate glass pipettes (World Precision Instruments, USA) were prepared with a micropipette puller (P-97, Shutter Instruments, USA) for the recordings. The micropipettes had a resistance of  $\sim 8 \pm 2 \text{ M}\Omega$ , and were filled with intracellular solution containing 115 mM K-gluconate, 20 mM KCl, 10 mM HEPES, 10 mM phosphocreatine, 4 mM ATP-Mg, and 0.3 mM GTP, with a pH 7.25–7.3 titrated with KOH [127]. An extracellular solution was continuously perfused during recordings at a rate of 1.5 ml/min and contained 145 mM NaCl, 4 mM KCl, 2 mM Na-pyruvate, 5 mM Hepes, 5 mM glucose, 2 mM  $\text{CaCl}_2$ , and 1 mM  $\text{MgCl}_2$ , whose pH was adjusted to 7.4 with NaOH [128]. Recordings were performed in current-

clamp by an Axon Multiclamp™ 700B Microelectrode Amplifier (Molecular Devices, USA) at 15-20 kHz. Artefact compensation was done using active electrode compensation within the real-time system [129]. Figure 4-15 shows patch-clamp recordings on NCD and quartz control substrates. Intracellular traces on both samples recorded spontaneous action potentials and excitatory postsynaptic potentials, indicative of network activity. Table 4-3 summarizes the membrane properties determined with patch-clamp recordings, which show similar results between NCD and control quartz substrates. This indicated healthy active neurons integrated within a larger neural network.

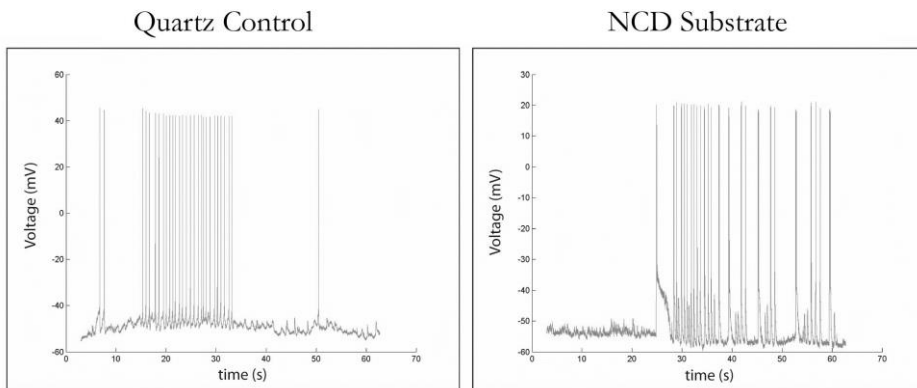


**Figure 4-15** – Intracellular (patch-clamp) recordings of primary cortical neurons on NCD and quartz control substrates.

**Table 4-3** – Patch-clamp data comparing membrane potentials on various substrates. Measurements taken from DIV 14-21.

|                          | HQD     |       |   | LQD     |       |    | Quartz  |       |    |
|--------------------------|---------|-------|---|---------|-------|----|---------|-------|----|
|                          | Average | SEM   | N | Average | SEM   | N  | Average | SEM   | N  |
| <b>Input resistance</b>  | 166.60  | 32.86 | 7 | 200.29  | 22.99 | 19 | 178.18  | 11.65 | 15 |
| <b>Resting Potential</b> | -70.46  | 2.16  | 5 | -57.00  | 2.01  | 19 | -55.53  | 1.49  | 16 |
| <b>ΔP Threshold</b>      | -31.95  | 0.43  | 5 | -36.38  | 3.04  | 13 | -38.21  | 1.92  | 15 |
| <b>ΔP Frequency</b>      | 0.15    | 0.03  | 5 | 0.38    | 0.08  | 16 | 0.19    | 0.05  | 14 |
| <b>Tau</b>               | 31.22   | 9.21  | 7 | 20.33   | 2.95  | 18 | 19.59   | 4.03  | 14 |
| <b>Input resistance</b>  | 166.60  | 32.86 | 7 | 200.29  | 22.99 | 19 | 178.18  | 11.65 | 15 |

# 5 Planar diamond MEAs

Having demonstrated that diamond can be used as a platform for neuronal growth, the next step was to test diamond on functional MEAs. This chapter presents the work done on MEAs that were produced with planar electrodes to test both the NCD as a passivation layer and BNCD as an electrode material. Section 5.1 covers tests performed on MEAs coated with an NCD passivation layer and conventional TiN electrodes. In section 5.2, BNCD electrodes are introduced in combination with NCD passivation layer to provide a full diamond functional interface. This information is presented as an article which has been published in J. Mater. Research.

The technology detailed here is similar in some aspects to [130], and I will highlight here the major differences between the works. In comparison, these devices have been developed with metal conducting paths as opposed to BNCD conducting paths, which gives much lower impedance, and a better connection to the external circuitry. Furthermore, the electrode design is different, derived from a MultiChannel Systems GmbH 60 electrode design, to allow direct comparison to those in the literature. Finally, all studies performed with these devices have been performed using primary neuron cultures as opposed to brain slices.

My contribution to this work has involved the development of an independent fabrication method for these devices. I have designed the devices and measured and modeled the electrochemical properties and based on these results the design was optimised. The cell culture experiments and data analysis has been performed by Lowry Curly and Antonina Monaco at the University of Antwerp with my assistance.

## **5.1 MEAs with NCD Passivation layer**

### **5.1.1 MEA Fabrication**

Custom glass substrate-integrated MEAs were obtained from Multichannel Systems (Reutlingen, Germany). These MEAs were fabricated with arrays of 60 flat titanium nitride (TiN) microelectrodes (30  $\mu\text{m}$  in diameter, 100  $\mu\text{m}$  in spacing), with 8 X 8 regular layout, as previously described [131], [132]. All MEAs consisted of gold leads with TiN electrodes on a glass substrate. For control MEAs, a 500 nm layer of silicon nitride, deposited by plasma enhanced chemical vapor deposition, was used as the passivation layer. On the test MEAs, the insulating layer was obtained by growing NCD in a linear antennae MWPECVD system, as described in section 4.5.2. Following NCD growth, the positive lift-off resist process (section 3.4.1) was used to define the electrodes for opening. A 75 nm layer of chromium was sputtered to act as an etch mask after lift-off. An oxygen plasma was used to transfer the 8 X 8 electrode pattern into the NCD thin film by, ultimately exposing the underneath TiN microelectrodes and the external contact pads. Chromium was subsequently removed using Cr-Etch 18 (Micro Resist Technology, Berlin, Germany) and the exposed NCD surface was further treated in H<sub>2</sub> plasma to clean the surface.

### **5.1.2 Substrate Preparation**

The same substrate preparation steps were performed on MEAs as in section 4.5.3, with the PEI functionalization chosen as the surface preparation treatment.

### **5.1.3 Primary Neuronal cultures**

Neuronal cultures follow the same protocol as in section 4.5.4, with the exception that for control MEAs and NCD-MEAs, a cell plating density of  $\sim 3000$  cells/mm<sup>2</sup> was employed. Control MEAs and NCD-MEAs were sealed by fluorinated Teflon membranes, allowing gas exchange but no water evaporation and further reducing the risk of cultures contamination [133]. This allowed extracellular

electrophysiological recordings in a separate low-humidity (i.e. electronic-friendly) incubator at 37 °C, 5 % CO<sub>2</sub>, ensuring long-term stability of recording conditions.

#### **5.1.4 Network Electrophysiology**

Control MEAs and NCD-MEAs were used to non-invasively monitor the electrical activity of neuronal networks developing *ex vivo* on their substrates, using the 60 TiN microelectrodes on each MEA. Two control MEAs and two NCD-MEAs were seeded with sister cultures and recordings were taken at 7, 12, 13, 14, 19, 20 and 21 DIV.

Each of the MEAs was mounted into the recording amplifier (Multichannel Systems, Reutlingen, Germany) and allowed an accommodation time of 10 minutes before 15 minutes of spontaneous electrical activity was acquired at 25 kHz/channel, after 1200x amplification. Data was stored on the disk using MC Rack software (Multichannel Systems, Reutlingen, Germany), and processed by custom C++ software for identification of firing of action potentials. Raw extracellular voltage waveforms  $V_k(t)$ , acquired from each of the  $k=1, 2, \dots, 60$  electrodes, were digitally bandpass filtered (a causal elliptic filter - no phase shift) between 0.2 and 3kHz.

A threshold-based algorithm, set at 5 times the median of the filtered signal, was used to identify the time of occurrence  $\{t_k^i\}$  of an action potential, detected at the  $k$ -th channel [134]. The detected multiunit events were logged to the disk by including the time-stamp of the spike, as well as the preceding 1 ms and following 1.8 ms of the corresponding non-rectified voltage trace (i.e.  $V_k(t)$ ,  $t \in [t_k^i - 1; t_k^i + 1.8]$ ). All spike-train analysis was performed using MATLAB (The MathWorks, Inc., Natick, MA, USA). Figure 5-1 shows a summary of action potential detection from one 15 minute recording period.

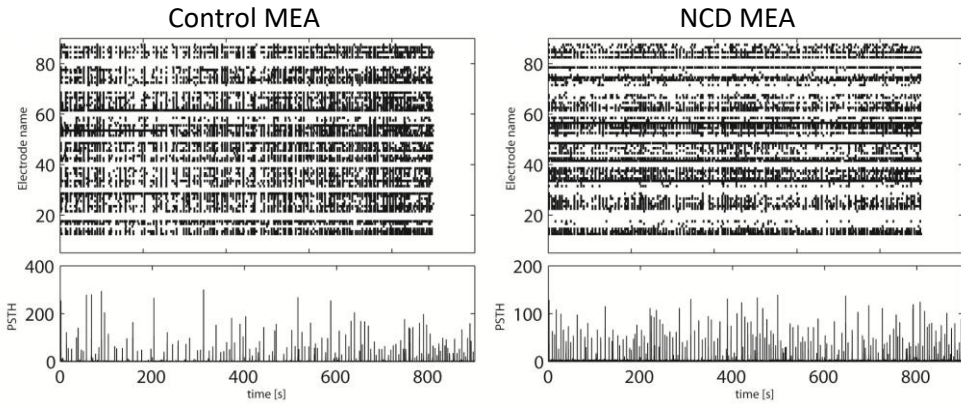


**Figure 5-1** – Summary of all the action potentials recorded at 14 DIV, at each individual electrode (above) and as a histogram of spikes (below).

The mean firing rate (MFR) and burst frequency were chosen to compare the effect of using an NCD interface as opposed to the control MEA. Here we define the MFR of a culture as the average of the means of the spiking frequency per each recorded channel. For defining the occurrence of synchronized burst spikes across multiple electrodes, criteria was chosen according to previous literature [135]. This was done by using a threshold for the instantaneous firing probability of all channels subdivided into bins of size  $\Delta t$  and multiplied, bin by bin, by the instantaneous number of co-active channels. This allowed for coordination of multichannel spike-trains to the  $t_k$ -time of individual bursts for monitoring temporal evolution of the firing rate during a network burst. For the MFR and burst frequency, the total recording time (15 minutes) was subdivided into ten 90 s intervals and the variation was calculated for standard deviation purposes. The results of the MFR and burst frequency measurements are presented in Figure 5-2.

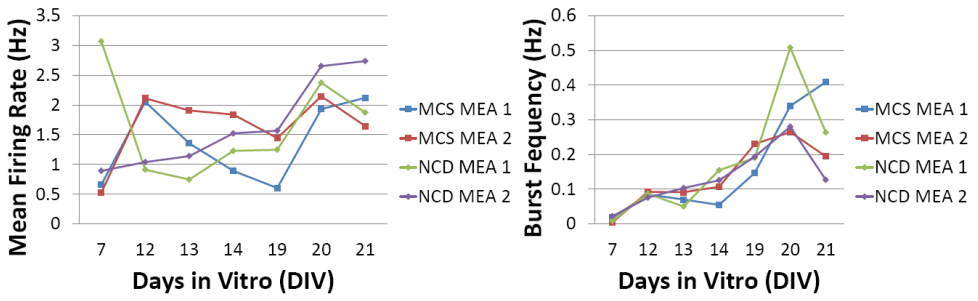


**Figure 5-2** – Mean firing rate and burst frequency of cortical neurons on NCD-MEAs and control MEAs.

## 5.2 Article: Diamond microelectrode arrays for in-vitro neuronal recordings

**MRS Communications, Volume 7, Issue 3, Sept 2017, Pages 683-690**

Matthew McDonald<sup>1</sup>, Antonina Monaco<sup>2</sup>, Farnoosh Vahidpour<sup>1</sup>, Ken Haenen<sup>1</sup>, Michele Giugliano<sup>2,3</sup>, and Milos Nesladek<sup>1,4</sup>

<sup>1</sup> Institute of Materials Research, Hasselt University, 3590, Diepenbeek, Belgium

<sup>2</sup> Department of Biomedical Sciences, University of Antwerp, B-2610, Wilrijk, Belgium

<sup>3</sup> Brain Mind Institute, Swiss Federal Institute of Technology Lausanne, Switzerland; and Dept. Computer Science, University of Sheffield, S1 4DP, UK

<sup>4</sup> Interuniversity Microelectronics Center (IMEC), B-3001, Heverlee, Belgium

### Abstract

A novel microfabrication technique for micro-electrode arrays (MEAs) with a full diamond-cell interface is demonstrated. Boron-doped nano-crystalline diamond is used as a conductive electrode material on metal tracks insulated by intrinsic nano-crystalline diamond (NCD). MEAs successfully recorded spontaneous electrical activity in rat primary cortical neuronal cultures. Patch-clamp measurements show no alterations to cell membrane passive properties or active firing response, for cell developing *ex vivo* on diamond. Impedance analysis revealed low impedance magnitude of BNCD electrodes, suitable for multi-unit neuronal recordings. Additionally, the impedance phase of the fabricated electrodes shows a high degree of capacitive coupling, ideal for neuron stimulation.

### Introduction

Diamond has become a material of increasing interest for electronic devices over the last decade, particularly as a biological sensing platform, due to its many attractive material properties [136]. Nano-crystalline diamond (NCD) thin films can be grown by chemical vapor deposition (CVD) on various substrates to fabricate functional devices using standard microfabrication techniques. Diamond is a wide band gap semiconductor that can be doped to give metal-like

conductivity, allowing development of biocompatible electrodes which are electrochemically robust, giving an extremely wide chemical potential window [30]. Furthermore, the wide bandgap of un-doped diamond allows it to be used as an insulating material in the voltage range of biological signals.

Microelectrode arrays (MEAs) were developed in the 1970s, and have become an indispensable tool in the field of electrophysiology for non-invasively investigating electrical activity of excitable cells, such as neurons and cardiomyocytes, both *in vivo* and *in vitro*. Moreover, MEAs enable the recording of spontaneous extracellular electric signals, allowing the interactions within populations of synaptically connected neurons to be studied, including their collective response to drugs, crucial for therapeutic drug-screening. MEAs can also be used to directly stimulate neurons, in order to study evoked response and the underlying networks organization, connectivity, and response dynamics [137]. However, most of the MEAs show both the capacitive and injection currents. The injection currents, depending on the current used, may deteriorate the neural tissue due to the local pH changes. The capacitive current is of high interest due to absence of any non-displacement currents.

Here we report on the fabrication of MEAs using boron-doped nano-crystalline diamond (BNCD) microelectrodes with a passivation layer made of intrinsic nano-crystalline diamond. BNCD exhibits many advantages as an electrode material compared to common gold, platinum and TiN materials, including high chemical and mechanical stability, a 3 V-wide electrochemical water potential window, and high biocompatibility [86, 87]. Moreover, BNCD has been shown to be an effective electrode material for biological sensors [77, 87–90]. NCD is also highly biocompatible [58, 86], as well as transparent, and insulating, making it a suitable material as a passivation layer to provide a complete diamond sensing platform surface. Recently, full diamond MEAs were used for detection of action potential of myocardial cells which generally have substantially higher amplitudes than for neurons<sup>6</sup>. One of the limits of such technology is the high resistance of the electrodes. Our work led to electrodes with purely capacitive coupling and resistance comparable to the state of the art non-diamond MEAs. Our method of fabrication combined with optimal layout and specific diamond surface

functionalization allowed for extracellular recording of neural signals from hippocampal neurons.

## Materials and Methods

### *Design and fabrication of MEAs*

The MEA design was derived from commercial planar MEAs (MultiChannel System GmbH, Reutlingen, Germany) to allow comparison of performance with commercial MEAs. It incorporates a regular 8 X 8 arrangement of 40  $\mu\text{m}$  diameter circular microelectrodes with a pitch of 200  $\mu\text{m}$ , as shown in Figure 5-3. Figure 5-4 shows the fabrication process for the MEA, which starts with a wafer of size 49 mm made from quartz glass in order to withstand the stresses induced from high temperature diamond growth. The fabrication technique has the advantage of using a single photolithographic step to open the electrodes in the insulating NCD layer and grow the conductive BNCD layer; this allows for the insulating and conductive layers to be at the same level, with virtually no step height between them. Additionally, the MEAs are made on a transparent quartz substrate so that neurons are easily visualized using standard microscopy.

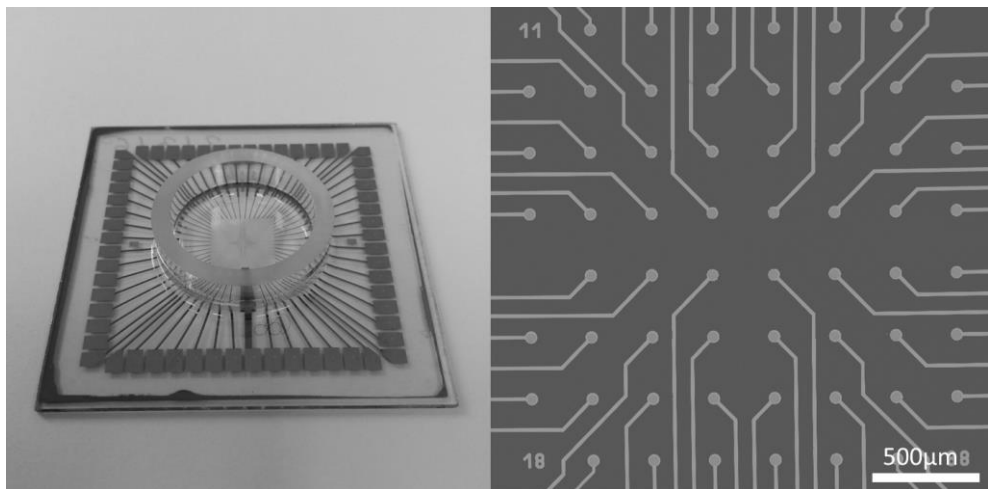


**Figure 5-3** - Fully packaged BNCD/NCD MEA (left) and SEM image of the active sensing area (right).

Quartz substrates were initially prepared by standard RCA1 and RCA2 cleaning [141]. Metal tracks were defined on the substrate using standard photolithography lift-off techniques. A thin (~5 nm) titanium adhesion layer was sputtered, followed by 300 nm gold and a second (~20 nm) adhesion layer of titanium. The surface was seeded for diamond growth by spin coating a 0.33 g/L solution of detonation diamond nanoparticles on the substrate (NanoAmando®B, NanoCarbo Research Institute, Japan) [52]. The NCD passivation layer was then grown using a gas mixture of 3 % methane and 97 % hydrogen in a MPECVD (Microwave Plasma Enhanced Chemical Vapor Deposition) growth reactor (Seki Technotron corp. AX6500). NCD was grown at a plasma temperature of 600-650 °C, by maintaining a pressure of 15 Torr and 2000 W with total gas flow of 300 sccm. A second lift-off process was used to sputter a hard mask of aluminum nitride (AlN) which defined the electrode area. Oxygen reactive ion etching (RIE) was used to open holes in the passivation layer and expose titanium/gold electrodes below. The substrate was then selectively seeded with detonation diamond nanoparticles, which attached to the electrode while being repelled by the surface charge of AlN [52]. BNCD electrodes were then grown with a gas mixture of hydrogen, methane and trimethylboron (TMB) in a MWPECVD growth reactor (Seki Technotron corp. AX6500). BNCD was grown at plasma temperature of 750 °C at 30 Torr and 3500 W with total gas flow of 500 sccm. Finally, the contacts were opened by placing a silicon wafer over the center area and etching the diamond covering the electrodes with an oxygen plasma treatment.

Additionally, a set of 1 cm x 1 cm NCD coated quartz substrates were prepared to test if the fabrication procedure left any artefacts that could have negative effects on the electrophysiological properties of the cells. Substrates went through all the same fabrication steps as MEAs, except for metal track deposition or photolithography to define microelectrode-opening holes.

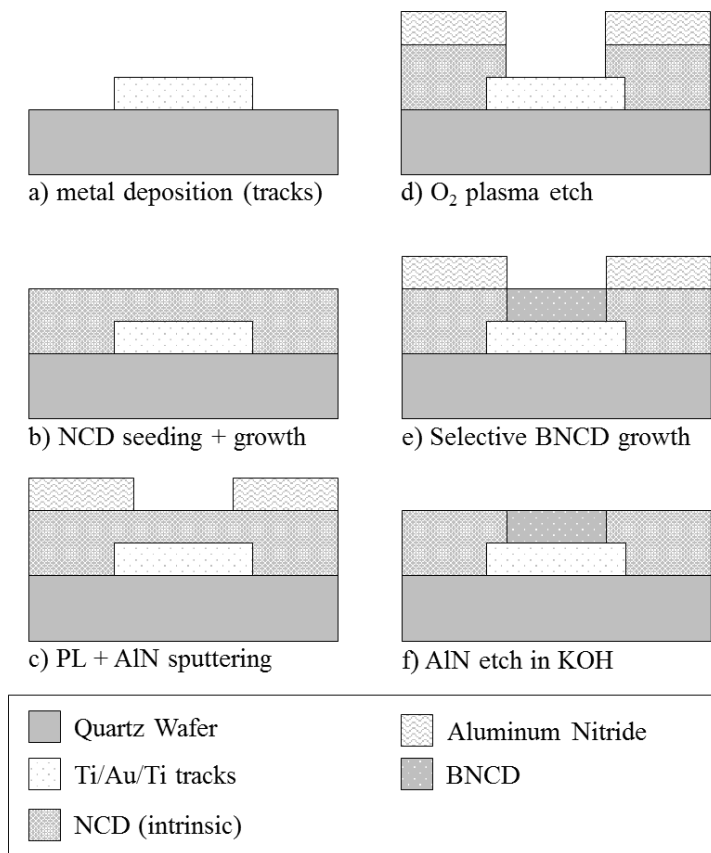


**Figure 5-4** – Fabrication process of MEAs with BNCD electrodes and NCD passivation layer. a) a Ti/Au/Ti metal tri-layer is deposited using lift-off photolithography to form the metal tracks, b) the surface is seeded with diamond nanoparticles and 180nm NCD layer is grown by MPECVD, c) photolithography is used to define a hard mask made of AlN, d) the NCD layer is etched through to the underlying metal track by oxygen plasma, e) the surface is selectively seeded with diamond nanoparticles and the BNCD electrode is grown, f) AlN is etched in a KOH solution.

#### *Rat primary cortical neurons cultures*

Prior to cell seeding, BNCD-MEAs and commercial ITO-based glass MEAs (Multichannel Systems GmbH), employed as control, were treated with 70 % ethanol for 10 minutes and air-dried overnight. Quartz substrates and glass coverslips used for patch clamp experiment were autoclaved upon high-pressure saturated steam at 121 °C for 30 min. MEAs, substrates and coverslips were then

coated with Polyethylenimine (PEI) by incubation under 0.1 % w/v of PEI in milli-Q water at room temperature for at least 8h; samples were then rinsed thoroughly with milli-Q water and air dried [86, 92]. The PEI treatment is based on our previous results, in which we demonstrated the PEI or Poly-D-lysine is necessary pre-condition for vital neuron growth [142].

Rat primary cortical cultures were obtained by postnatal (P0) Wistar rats (Charles River, France) using standard methods and following the guidelines of the Ethics Committee of the University of Antwerp. Cortices were dissected, sliced, digested in a trypsin solution, mechanically dissociated, centrifuged and suspended in Modified Essential Medium supplemented with 5 % horse serum, 50 µg/mL gentamycin, 200 mM l-glutamine and 2 M glucose.

Cells were seeded at nominal densities of 6500 cells/mm<sup>2</sup> on MEAs, and of 1500 cells/mm<sup>2</sup> on glass coverslips and quartz substrates. All chemicals were purchased by Sigma Aldrich (Belgium).

## Electrophysiology

### *Cellular electrophysiology*

Whole-cell patch-clamp recordings were carried out at 34 °C from neuronal somas after 9 Days in Vitro (DIV) using an Axon Multiclamp Amplifier (Molecular Devices, USA) controlled by LCG software [143]. During recordings, glass coverslips and BNCD-coated quartz substrates were kept in artificial cerebrospinal fluid, containing (in mM): 145 NaCl, 5 Hepes, 5 Glucose, 4 KCl, 2 CaCl<sub>2</sub>, 2 Na-pyruvate and 1 MgCl<sub>2</sub>; pH adjusted to 7.4 with NaOH.

Patch pipettes were pulled from borosilicate glass and filled with intracellular solution, containing (in mM): 135 K-gluconate, 10 Hepes, 10 PC-Na<sub>2</sub>, 4 NaCl, 4 ATP-Mg<sup>2+</sup>, 0.3 GTP-Na<sub>2</sub> and 0.2 EGTA; pH adjusted to 7.3 with KOH. Electrical impedance of patch pipettes was 6-8 MΩ. Recordings were analyzed using custom MATLAB scripts (The Math-works, USA). Statistical analysis was performed using the Lilliefors test, to assess normality of data sets, and the Student's t-test to

evaluate statistical significance; data are presented as mean  $\pm$  standard error of the mean (SEM).

### *Network electrophysiology*

Neuronal network activity was recorded at 17, 19, 21, 24 and 28 DIV from 2 control ITO-MEAs and 7 BNCD-MEAs, mounted into a recording amplifier (Multichannel System GmbH). Spontaneous electrical activity was recorded for 30 min; traces were acquired and stored on disk for offline analysis by MCRack (Multichannel Systems, Germany) and subsequently analyzed by QSpice Tools [144].

Individual microelectrodes of a MEA were defined as active, when the frequency of occurrence of detected biological events (spikes) at that single electrode exceeded 0.05 Hz.

## **Results and Discussion**

### *Morphological characterization*

Important characteristics of functional MEA electrodes are the impedance and capacitance. These parameters depend on the material and geometrical properties used for the construction of the functional electrodes as well as for the isolating layer. Diamond has the advantage of being able to be used both as a conductive and an isolating material. While undoped diamond is highly isolating, the conducting diamond is obtained by p-type doping with boron. The thickness of the doped and undoped diamond layers determines the capacitive and isolating properties respectively. The thickness of the diamond layers is also important from the fabrication point of view, for definition of the lithographic and etching steps. The thickness of diamond passivation layer was therefore carefully monitored by in-situ interferometry and was optimized to approximately 180 nm, which was sufficient to insulate the metal tracks. BNCD electrodes, were between

180-200 nm, which was found by using profilometry to measure the step height above the diamond passivation layer. The average electrode diameter was approximately 30  $\mu\text{m}$ , giving an active area of  $\sim 707 \mu\text{m}^2$ . Scanning electron microscopy was used to measure the morphology and grain-size of the diamond layers. NCD and BNCD crystals are highly faceted, with an average grain size of  $\sim 100 \text{ nm}$  and  $\sim 200 \text{ nm}$ , respectively (Figure 5-5).

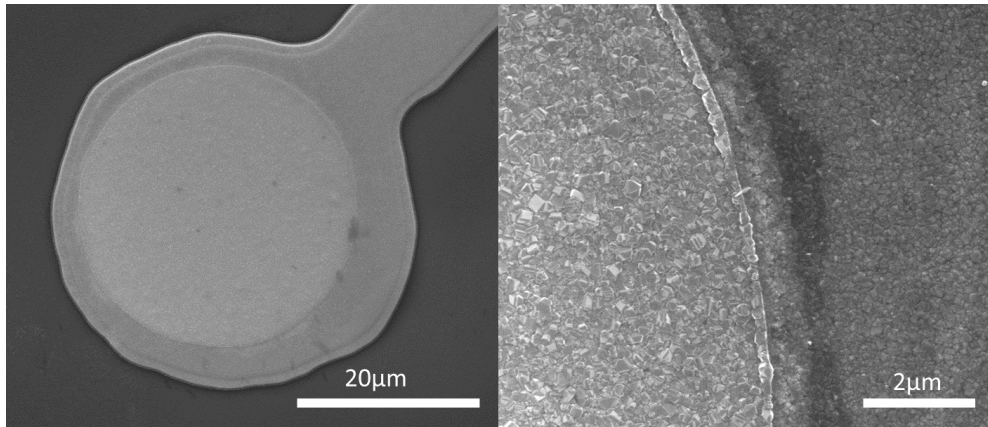


**Figure 5-5** – SEM image of BNCD electrode (left) and SEM image showing fine grain structure of BNCD electrode vs. NCD passivation layer.

The grain size is an important parameter for obtaining an optimal diamond film surface in terms of crystal quality (and consequently good electrical properties) and surface roughness of the electrode surface. Consequently, the grain size was controlled by the growth parameters such as the methane concentration in the gas mixtures during growth. A concentration of 3 % methane was used for the NCD growth to provide a smoother continuous film with low stress, to ensure no pinholes or cracking in the layer [145]. A methane concentration of 1 % was used in the gas mixture for BNCD to obtain a larger diamond grain size in order to maximize the conductivity [28]. A boron to carbon ratio of 9,000 ppm in the gas mixture was used to ensure sufficient boron doping levels for high electrode conductivity. The resultant layers had conductivities of ca. 400  $\Omega/\text{square}$ .

## *Electrochemical characterization*

One of the critical requirements for microelectrodes to detect multi-unit neuronal activity is to have a low enough impedance in the frequency range of 0.1-1 kHz, enabling adequate spatial selectivity and sensitivity [146]. Impedance of BNCD electrodes is expressed in terms of the equivalent Randles circuit and depends on the BNCD impedance (doping and the electrode geometry) as well as on forming the electric charge double layer on the electrode immersed in bio-analyte. To simulate the working conditions, electrochemical impedance spectroscopy (EIS) was used to perform the electrical characterization of the devices prior to cell seeding. IS was performed in 1 M phosphate buffer in frequency sweep mode with 0.1 V peak to peak sine wave from 1 MHz to 1 Hz (Solartron SI1260 Impedance/Gain Analyzer). Electrodes show typical shape and characteristics of diamond electrodes [147]; with impedance values around 300k $\Omega$  at 1kHz (Figure 5-6). The lowest obtained impedance was  $\sim$ 100 k $\Omega$  for electrodes with 30  $\mu$ m diameter active area (identical to commercial MEAs) Interestingly, IS showed -80 $^\circ$  to -90 $^\circ$  phase angle, in the range of 100-10,000 Hz (Figure 5-7), which shows an almost completely capacitive coupling of the electrical current, ideal for the stimulation of cells [148]. Most electrode materials, such as gold [149], ITO [150], or carbon nanotubes [42], have a charge injection behavior that is a combination of Faradic and capacitive currents. When MEAs are used for stimulation, charge injection through Faradic currents can result in damage to the surrounding cell tissues [149]. Diamond is a highly inert material which has a large electrochemical window ( $\sim$ 3 eV) and low double-layer capacitance (ca. 7  $\mu$ F/cm $^2$ ), resulting in an almost perfect capacitive charge injection [151]. The capacitive coupling is ideal in terms of the neural interfaces stability as no active ionic, i.e. Faradic currents flow between the cell membrane and the electrode, which would otherwise impact on electrochemical degradation of the cell tissue.

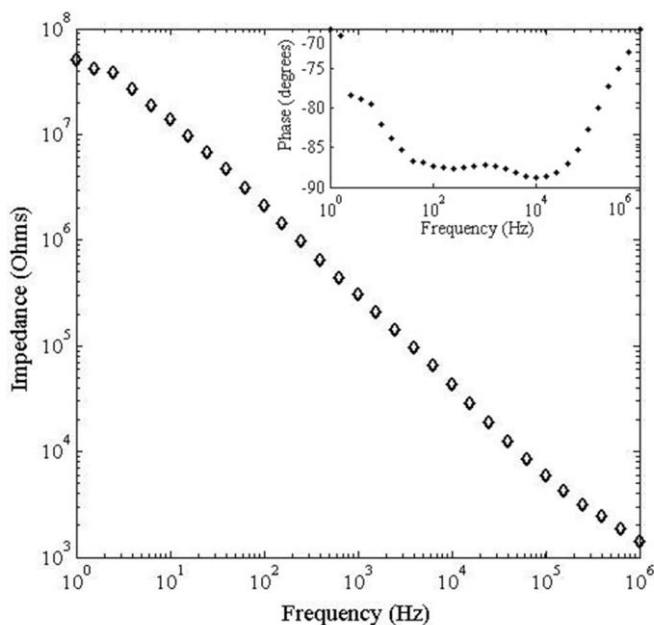


**Figure 5-6** – Bode plot of a BNCD electrode with active area of 707  $\mu\text{m}^2$ . Insert shows the frequency response of the electrode.

Additionally, impedances of all MEAs were tested at 1 kHz using an impedance testing device MEA-IT (Multichannel Systems GmbH). Impedance values were measured before and after attachment of a glass ring with a PDMS-based glue (Sylgard 184, Dow Corning) for creating a culture chamber on the MEA. Figure 5-7a,b shows the impedance magnitude and phase for all of the 59 electrodes on a representative MEA, showing that the average impedance increases drastically after exposure to PDMS, while the average phase stays relatively constant. The average impedance value for each MEA in the set, before and after ring attachment, is reported in Figure 5-7c. Though the standard ring mounting procedure was followed, using a PDMS based elastomer, impedance dramatically increased, and reaching values up to 1250 k $\Omega$ . Reasons for this increase might lie in the fact that PDMS has been known to outgas monomers that can diffuse across the substrate surface and significantly impact electrode performance [104, 105]. Diamond surface is extremely sensitive on forming a strong bond to charged molecules or polymers [154] that might lead to formation of an isolating layer on

the surface, leading to impedance enhancement. Though the thickness of the polymer layer can be reduced significantly by liquid chemistry, the last monolayer of polymer is strongly bound chemically to diamond surface and practically irremovable by for example, stripping in liquid SDS. Partial electrode performance was recovered by performing a cleaning in CF<sub>4</sub> plasma to try to remove PDMS residues [155]. This procedure led to a lower electrode impedance, though still higher when compared to those of MEAs before ring attachment.

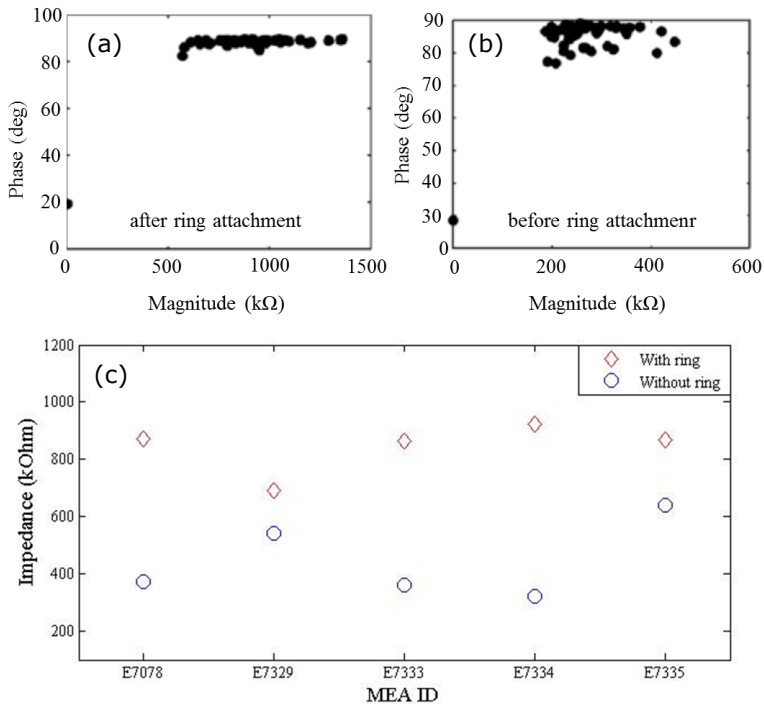


**Figure 5-7** – a) Plot of impedance magnitude and phase of all microelectrodes before and after b) attaching a glass ring as a culture chamber. c) Impedance magnitudes for 5 MEAs, averaged over all their microelectrodes.

### *Cellular electrophysiology*

In order to assess whether NCD affects neuronal viability, single-cell, or network's properties, whole-cell patch clamps recordings were performed under the voltage-clamp configuration on neurons grown on NCD substrates. Results (Figure 5-8)

show that neurons grown on NCD substrates have membrane passive properties (i.e., time constant, input resistance, and membrane potential) and active response firing properties comparable to control conditions (n=6 cells).

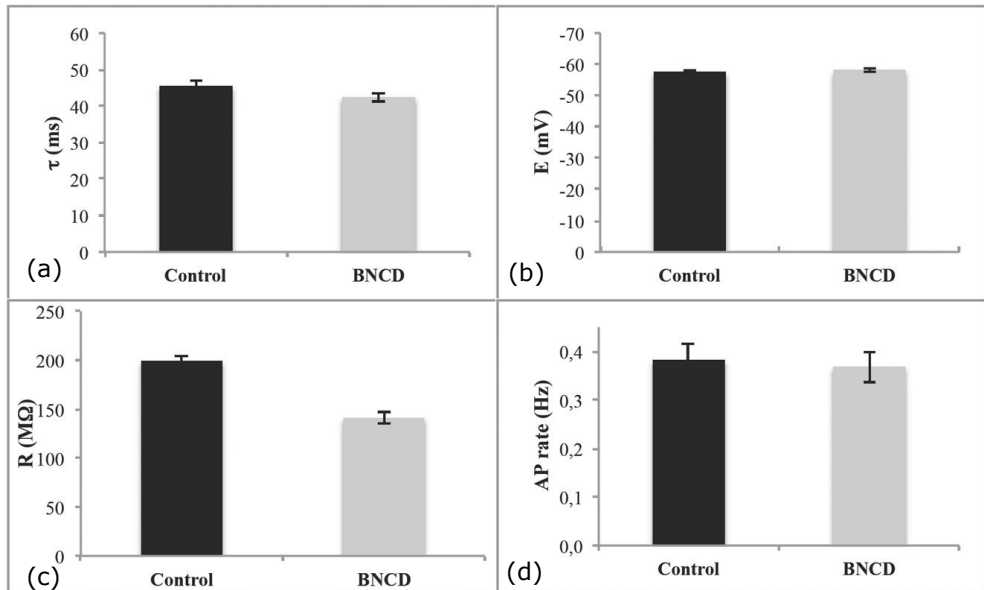


**Figure 5-8-** Effect on neurons cell properties by culturing on BNCD films compared to control condition (n=6). a) time constant  $\tau$ , b) membrane resting potential E, c) input resistance R, d) action potential rate. Error bars correspond to standard deviation of the data.

### Functional tests

To devise functionality of MEAs, a set of experiments is currently undergoing with the diamond MEAs, involving the extracellular recording and stimulation of rat primary cortical neuronal cultures. Preliminary results indicate that BNCD electrodes, with NCD passivation layer, can detect single spikes and bursts with amplitudes in the 20-30  $\mu\text{V}$  range with noise levels of ca.  $\pm 6 \mu\text{V}$  (See Figure 5-9). Comparison among the functional BNCD channels to ITO reference electrodes shows similar noise levels, as well as similar spike amplitudes, though ITO references performed slightly better, however ITO electrodes are a mix of capacitive and resistive Faradic behavior [150]. ITO references electrodes showed amplitudes in the range of 40-50  $\mu\text{V}$  with a noise level of ca.  $\pm 6 \mu\text{V}$ . Furthermore,

it appears that spike detection may be better on the reference electrodes, though further analysis is required to determine whether this is due to lower spike detection, or a physiological change due to the diamond surface. We attribute this result to the high impedance caused by the PDMS during ring attachment, leading to a lower spike amplitude and lower spike detection, rather than any change to the network function. The electrode resistance rises up from  $\sim 400$  to  $\sim 1250 \Omega$  after the ring attachment. After  $\text{CF}_4$  plasma cleaning, the resistance decreased to  $\sim 800 \Omega$ . Currently we are developing plasma technologies to remove the polymer monolayers from the diamond surface without any re-deposition of etched organic molecules to the surface.

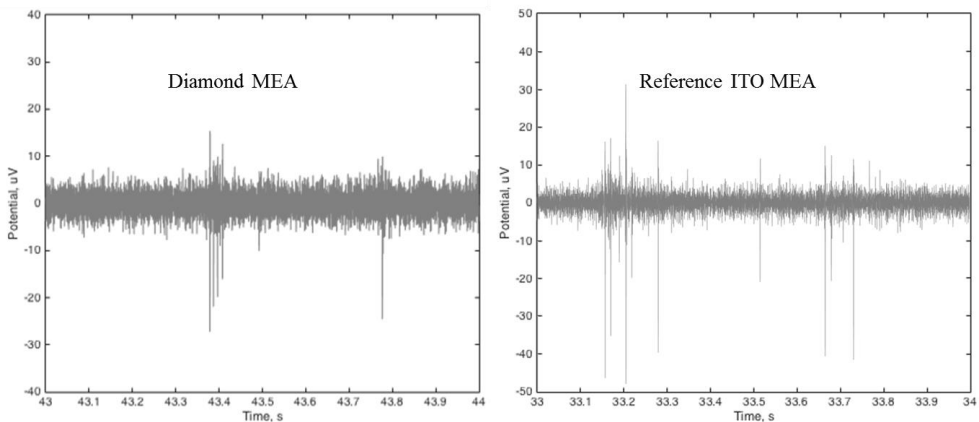


**Figure 5-9** - Spiking activity recorded on a diamond MEA compared to a control MEA with ITO electrodes.

While diamond has continuously been shown to be a good substrate for neuron growth [138], we have demonstrated here that it can also be used as an effective isolation layer at thicknesses of  $<180$  nm. This allows the cell culture to be in direct contact with only one material minimizing any contact potential as well as provides homogeneous neuron coverage. This property is important for studying neural networks as it is known that neural growth is strongly dependent on the material on which the neural cultures are cultivated [156]. PEI is a polymer commonly used in the pretreatment of glass for cell culturing as it adds surface charges that promote neural adhesion. Poly-L-lysine (PLL) was also used as a

pretreatment to cell culturing on diamond MEAs as it was found to also promote strong neural adhesion and growth on NCD substrates [138].

Furthermore, we show that it is possible to fabricate MEAs on optically transparent substrates and produce highly homogeneous layers with negligible leakage current from cracks or pinholes. Our new fabrication process has been designed to allow a variable height of the electrode compared to the isolation layer, from  $\sim 100$  nm below to  $> 1$   $\mu\text{m}$  above. An electrode height close to the thickness level of the passivation layer minimized the cleft size between the cell and device. This improves coupling when the cell is tightly bound to the passivation layer, by bringing the electrode as close to the cell as possible. A greater signal-to-noise ratio (SNR) should be possible by resolving the issue of increased impedance from gluing glass rings to the MEA and a strategy for this is being developed. The impedance could further be improved by using nanostructuring techniques to increase the surface area; this could easily be added into the current fabrication process with no additional lithography step needed [11]. Recently we have already achieved  $\sim 10\times$  increase of the BNCD capacitance, making it attractive for ultrasensitive MEAs based on purely capacitive coupling [7]. In summary, this fabrication process can be used to make functional MEAs from a fully diamond interface on transparent substrates for neural recordings that perform similarly to ITO reference MEAs; with room in the process to enhance the electrode interface.

In conclusion, we have developed a novel fabrication for MEAs made of thin diamond films on transparent substrates, which allow detection of neural signals with advantage of diamond biocompatibility, surface neutrality, capacitive coupling and excellent electrochemical characteristics.

## **Acknowledgements**

Financial support from the FP7 of the European Commission (NMP project "MERIDIAN" n. 280778-02, IEF "INCA-NANEP" n. 328214, ITN "NAMASEN" n. 264872), the Flanders Research Foundation (FWO, contract n. G088812N) is acknowledged. We also thank Mr. D. Van Dyck and Mr. M. Wijnants for technical assistance.



## 6 3D Diamond MEAs

The main aim of this thesis will be presented in this chapter, with research on 3D diamond nanostructures being presented. This work builds on the technology that was presented on planar electrode MEAs by introducing 3D diamond microstructures which I have developed. The goal of adding these structures is to induce an engulfment type mechanism of the cell in order to reduce the interface and drastically improve signal quality. The improvement upon existing devices with 3D microstructures is the use of a diamond interface, which should give an extremely robust device with a large electrochemical potential window. Diamond allows for a stable surface that will not degrade or biofoul in *in vivo* environments. The preliminary work shown in this section details a fabrication method for developing these devices and some preliminary work performed on testing them with primary neuron cultures.

The basic methods for fabricating the nanostructures will be discussed. Two type of devices have been fabricated: (1) gold mushroom arrays coated with NCD, and (2) functional MEAs using a NCD insulating layer with BNCD mushroom shaped electrodes. The first type of device is used to study the neuronal engulfment when NCD is used as an interfacial material. This was done by using the same gold mushroom structures as Micha et al. [38], [3], [76], with a thin BNCD layer as to change the interface while minimizing geometric change. The interface between these structures with the cultured cells was investigated using a focused ion beam to cut a cross section and imaged with SEM. The second type of device presented here has been used to measure electrical signals from cultured neurons, showing improved signal-to-noise ratios.

## **6.1 Fabrication of diamond coated nanostructured arrays**

In the first approach I used chips with arrays of gold mushrooms that were obtained from the Hebrew University of Jerusalem, with fabrication process described in [3]. The gold mushroom arrays were fabricated on float glass of size 10x3x0.2 mm, each with three regions of different mushroom sizes. Each region had mushrooms with a stem thickness of either 1  $\mu\text{m}$ , 2  $\mu\text{m}$ , or 3  $\mu\text{m}$  and approximate head diameter of 1.6  $\mu\text{m}$ , 3.1  $\mu\text{m}$ , or 4.5  $\mu\text{m}$  respectively. The pitch width between mushrooms was 10  $\mu\text{m}$ .

Samples were cleaned in boiling acetone/IPA (section 3.1.1) and seeded with a nanoparticle solution (section 3.1.2). Boron doped diamond was then grown on the chips using the ASTeX-2 reactor. Because the samples were prepared on float glass, growth temperatures were kept below 450  $^{\circ}\text{C}$  in order to prevent substrate deformation and delamination of diamond films. This was achieved by using a low pressure and microwave power of 10 Torr and 2100 W respectively. Due to a low temperature, a high concentration of 5%  $\text{CH}_4$  in the gas mixture was used in order to achieve higher growth rates. Additionally, a higher B:C ratio was used due to a lower boron incorporation as lower temperatures. The resultant films were approximately 70 nm thick with an ultra-fine grain structure typical of UNCD. SEM images of the gold mushrooms before and after diamond deposition are shown in Figure 6-1.

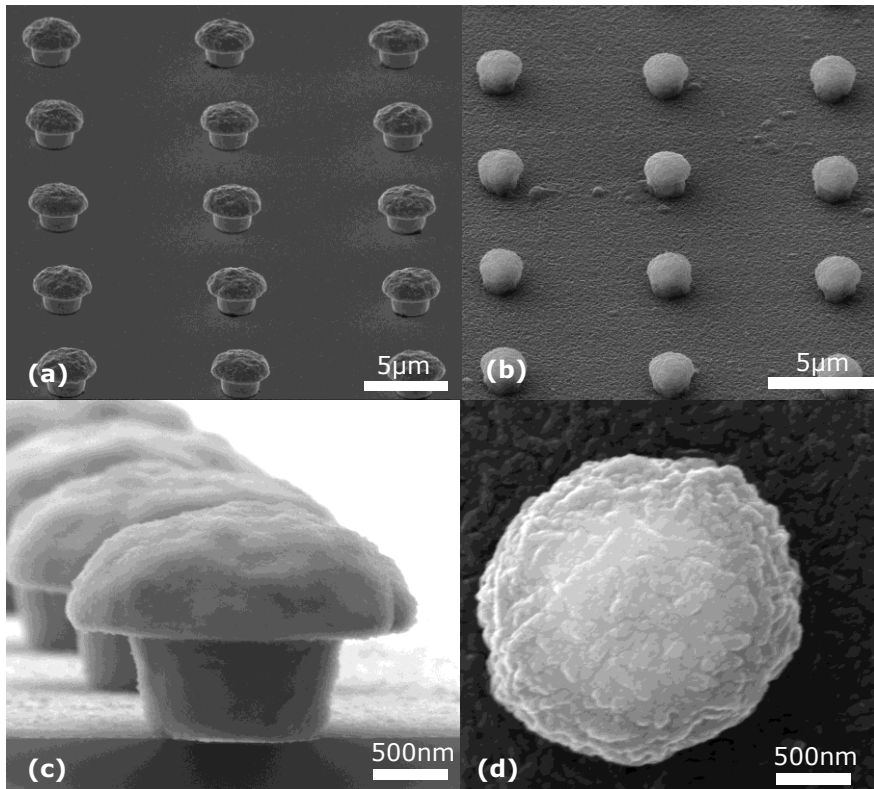


**Figure 6-1** – SEM images of mushroom chips showing (a) uncoated gold mushrooms (b) diamond coated gold mushrooms (c) cross section of chip, showing side view of a diamond coated mushrooms, and (d) fine grain structure of UNCD on gold mushroom.

## 6.2 Fabrication of 3D nanostructured diamond electrodes

In the second stage we have developed 3D nanostructures fully fabricated from diamond technology which was designed for this purpose. By using B-doped NCD the idea was to use the full potential of BNCD material in functional 3D neural interfaces. The basic fabrication process of the MEAs with is shown schematically in Figure 6-2

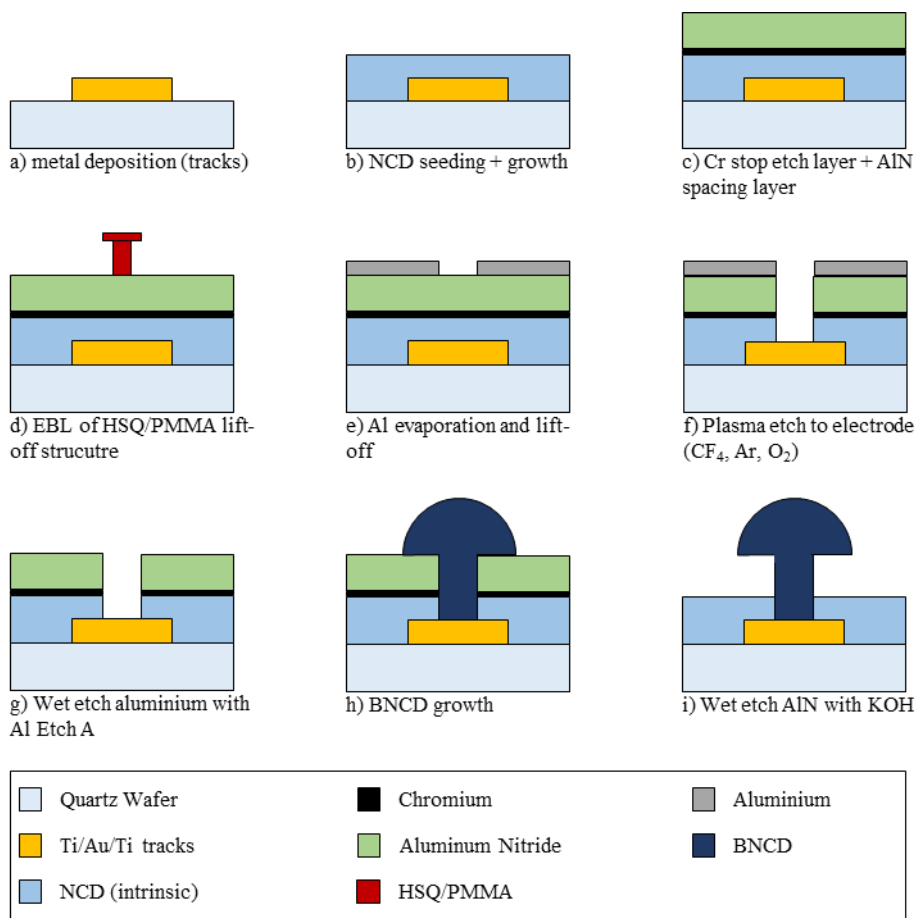


**Figure 6-2** – Fabrication steps involved in creating diamond MEAs with 3D mushroom shaped diamond electrodes.

The MEAs were fabricated using a 49mm X 49mm substrate made of quartz glass of size, in order to withstand the higher temperatures of diamond growth. The design for the metal tracks was based on a commercial planar MEA (MultiChannel System GmbH, Germany), which was also the same design used for the planar BNCD electrodes described in Chapter 5. This design was used to allow for direct comparison between the two geometries of electrodes in this thesis, as well as MEAs using this design found in the literature. Metal tracks were deposited using a lift-off technique employing the negative-tone photolithographic process, detailed in Section 3.4.1. A thin layer (~10 nm) of titanium was first sputtered as

an adhesion layer, followed by a  $\sim 250$  nm layer of gold and a second adhesion layer of titanium ( $\sim 10$  nm). The first titanium adhesion layer is used because gold does not adhere well to glass, and the second is used because diamond can not form a carbide interlayer with gold and thus does not adhere well. Titanium can be used to create a thin carbide layer and provide good adhesion, though it should be thin as to avoid high impedances from the titanium-carbide. The MEA was then seeded with diamond nanoparticles, using the method in section 3.1.2, in preparation for diamond growth. A NCD passivation layer was then grown on MEAs in the ASTeX-3 system using a gas mixture of 3 % methane in an excess of hydrogen. The growth temperature was  $650$  °C with a thickness of  $\sim 170$  nm. A 20 nm stop etch layer of chromium was then sputtered followed by an 800 nm spacing layer of aluminum nitride and annealed at  $500$  °C for an hour. The annealing step was performed to improve wet-etch selectively between AlN and Al layers. This spacing layer was used to determine the height of the mushroom stalk. A lift-off structure was then defined using the electron-beam lithography (EBL) procedure detailed in section 3.4.1. The size of the structure written by the e-beam determines the width of the mushroom stalk and this was chosen to be  $\sim 500$  nm. An aluminum hard mask ( $\sim 250$  nm) was then evaporated onto the device and the EBL structures were lifted off with acetone. The AlN layer was then etched anisotropically using a  $\text{CF}_4$  plasma (conditions given in Table 3-1) until the chromium stop-etch layer was reached. The chromium layer was etched using ion-milling in argon plasma. Finally, to reach the metal part of the electrode, the NCD was etched using oxygen plasma. The aluminum hard masked was removed using a selective acid wet etch (80 %  $\text{H}_3\text{PO}_4$  + 5 %  $\text{HNO}_3$  + 5 %  $\text{CH}_3\text{COOH}$  + 10 %  $\text{H}_2\text{O}$ ). It was found that seeding was not necessary for diamond growth at the titanium interlayer. This is thought to be due to the carbide formed in the titanium layer during NCD growth which retains the structure and is sufficient for diamond nucleation. Without seeding, no diamond grows on the AlN spacing layer and thus allows for a selective growth of the mushroom starting from the metal electrode. Long enough growth creates an overgrowth which grows isotropically in all directions forming the mushroom head. Thus, the deposition time determined the size of the mushroom head, and a diameter of  $\sim 1.5$   $\mu\text{m}$  was targeted. In-situ thickness measurement was not possible due to the small size of the structures and thus the size was estimated from growth rates measured on

flat substrates. BNCD was grown in the ASTeX-2 reactor at 700 °C using a gas mixture of 1 % methane in excess hydrogen with a boron:carbon ratio of 8000 ppm. The size of the mushroom head was checked with SEM after the growth to ensure adequate size before the AlN spacing layer was removed in a KOH solution. Finally, the contact pads were opened by covering the center with a piece of silicon and oxygen etching the NCD from the pads. SEM images of the fabrication process for defining and growing the mushroom are shown in Figure 6-3.

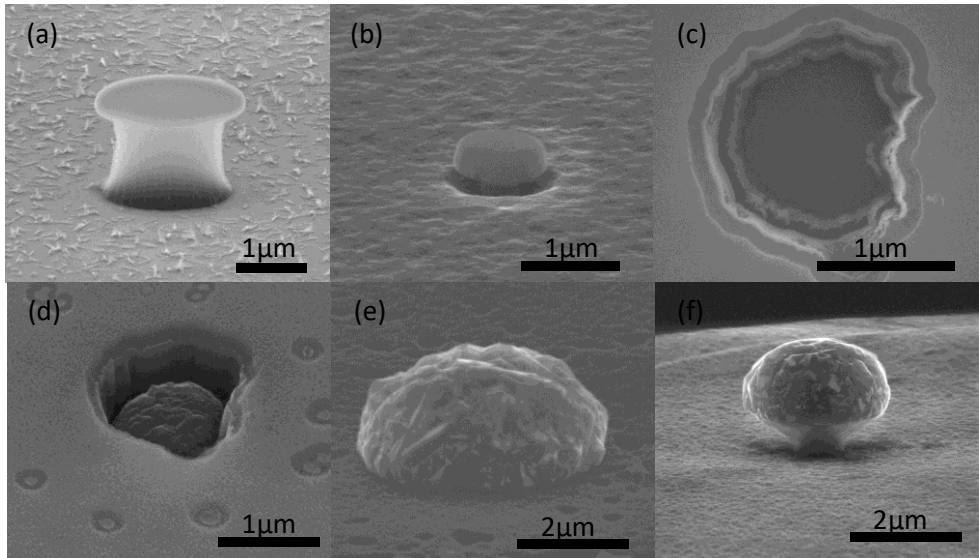


**Figure 6-3** - (a) Lift-off structures with EBL (b) Aluminum mask evaporation (c) lift-off and etching through SiO<sub>2</sub>/NCD to open electrode (d) Growth of BNCD stem through opened hole (e) continued BNCD growth to create mushroom head (f) removal of SiO<sub>2</sub> to reveal final structure.

Several issues were encountered during the development of the fabrication procedure that slowed the progress and could be improved upon in future works. Firstly, the EBL process was limited by oxygen plasma etching, which was isotropic. This meant that the thickness of the PMMA layer was limited by the desired diameter, since a layer too thick would be under-etched too much by the time it etched through the thick layer. Anisotropic oxygen plasma etching was

attempted, but we found issues with re-sputtering of the HSQ layer which caused many undesired pillar structures to take shape across the surface. Perhaps a further refinement of this lithographic process could allow structures with higher aspect ratio to be created. The limited height of PMMA caused issues of the EBL structures becoming completely enclosed when sputtering AlN layers and unable to be released. It is believed that this was due to high surface mobility after AlN deposition, which allowed AlN to be preferentially deposited at the EBL structure, causing it to be higher than the intended layer and enclose the structure completely. This issue was resolved by tuning the deposition parameters to reduce surface mobility, which was successful. However, there were also issues of thin film stress which only became apparent after the final growth of the BNCD mushrooms at high temperatures. After growth, the NCD insulating layer and AlN film would often crack and peel off, which is believed to be due to the differences in thermal expansion between the AlN and FS substrate. The MWPECVD reactors used for this research were limited in the ability to control the cooling rate, as the minimum temperature able to be sustained by the plasma is in the range of  $\sim 450$  °C. The issues of thin film stress during cooling were at the end of this project and not fully resolved. However, a number of devices were able to be fabricated in which the NCD layer remained intact. On these few devices,  $\sim 50$  % of the mushroom shaped electrodes remained in good shape.

## **6.3 Neural cell culturing**

The section here describes the work done at the Hebrew University of Jerusalem by the group of Micha Spira in preparing the 3D microelectrode samples for cell culturing and the actual cell culturing of primary hippocampal neurons on the devices.

### **6.3.1 Sample Preparation**

For MEAs, glass rings for cell culturing were attached using a PDMS based glue (Sylgard 184, Dow Corning) and cured on a hotplate at 40 °C for 12 hours. During

curing, the active area was protected by a photoresist, in order to negate the effects of PDMS contamination on the electrode surface, and subsequently removed with acetone. Both MEAs and mushroom arrays were subject to 5 minutes of oxygen plasma cleaning in a commercial plasma asher machine.

Before cell culturing, all samples were washed and incubated in ethanol 75 % for 2 h for sterilization. Samples were then thoroughly rinsed with double distilled water and functionalized for 12 h prior to cell seeding. Two surface treatments were used for mushroom arrays (1) 0.1 mg/ml PDL (Sigma–Aldrich) and 25 µg/ml laminin (Sigma–Aldrich) in sodium borate, and (2) 0.1 mg/ml PEI in milli-Q water at room temperature. For cell culturing on MEAs, the first surface treatment (PDL/laminin) was used.

### **6.3.2 Cell Culture**

Rat hippocampal neurons were chosen for both engulfment studies and electrical recording studies using the diamond mushroom MEAs. Neurons were obtained from either 17 day old embryos or from one day old newborn rats, as described by Kaech and Banker [157]. For the embryonic hippocampal neurons, pregnant rats were anesthetized, embryos removed, and then decapitated. After removal, the neurons were treated with papain for 45 minutes (Sigma-Aldrich), and serially triturated. Resultant neuron density before plating was in the range of 250,000-500,000 cells/mL. Cells were seeded in an attachment/seeding medium consisting of Neurobasal medium, 2 % B27, 1 % GlutaMAX, 5 % FBS (all from Life Technologies), and 1 % Penicillin-Streptomycin Amphotericin B Solution (Biological Industries). After 24 hours (1 DIV), the seeding medium was replaced with serum-free maintenance/feeding medium, consisting of Neurobasal medium, 2 % B27, 1 % GlutaMAX, and 1 % Penicillin-StreptomycinAmphotericin B Solution. In order to prevent proliferation of glial cells, 5 µM ara-c (Sigma–Aldrich) was added at 3 DIV. Every 3-5 days, half of the maintenance medium was replaced by astogial conditioned medium. The neural culture was kept at a constant 37 °C in a humidified atmosphere with 5 % CO<sub>2</sub>. Cultures were kept for 16 DIV. All procedures were approved by the Committee for Animal

Experimentation at the Institute of Life Sciences of the Hebrew University of Jerusalem.

## **6.4 Cross section of diamond coated arrays**

In order to investigate the interface between cells and the 3D nanostructured array, scanning electron microscopy was used to study cross-sections through the nanostructures. These cross-sections were prepared using focused-ion beam (FIB) techniques after cultured neurons had been fixed and dehydrated. This was done by using a FIB to deposit metal material and subsequently remove material in the selected area for cross-section. Cross sectioning and imaging studies were performed by Jaroslava Lavkova at the University of Prague.

After cell culturing, the substrates were washed twice with a warm phosphate buffer solution (PBS) and then cells were chemically fixed by placing in a solution of 3.2 % glutaraldehyde in PBS at room temperature for 15 minutes before washing again with PBS. Dehydration was then done in a series of 10 % to 100 % ultrapure ethanol solutions in ultrapure water for 5 minutes at each step. At the concentration of 95 % ethanol, 3 repetitions of the solution were used for 5 minutes each. Finally, at 100 % ethanol, the samples were placed in a chamber for critical point drying (CPD). CPD was performed by lowering the temperature of the chamber to 10 °C and the pressure to between 50-100 bar. Under these conditions, CO<sub>2</sub> is a liquid and was used to replace the ethanol in the chamber. The temperature of the chamber was then slowly increased to 40 °C. CO<sub>2</sub> converts to gaseous form as the temperature increases past the critical point temperature of ca. 31 °C [158]. The gaseous CO<sub>2</sub> was evacuated at 40 °C and drying was complete.

Focused ion-beam (FIB) is a technique used that is similar to SEM in that it used a focused beam of charged particles. However, FIB uses a beam composed of heavy ions instead of electrons, which can be used for site-selective deposition or ablation. The focused-ion beam used in this work consisted of a beam of gallium ions accelerated at 30 kV with currents ranging from 80 pA to 0.40 nA. Ion beam induced deposition (IBID) can be used to deposit materials on the surface by using

the interaction of the beam with a precursor gas. The gas is introduced to the system and chemisorbs to the surface. The ion beam decomposes the gas into a volatile component and a non-volatile component which remains on the surface. Platinum was deposited on the samples using IBID with a Pt-rich amorphous carbon gas. The metal layer was used to preserve the structure of the underlying cell during ablation with the ion-beam to create the cross-section.

## 6.5 Results

### 6.5.1 Engulfment study

The purpose of this engulfment study was to confirm that neurons will engulf mushrooms with a diamond interface, similarly to how they have been shown to do so for gold and SiO<sub>2</sub> mushrooms [5], [159]. For this reason, a qualitative observation of engulfment was made and no detailed analysis of the degree of coupling was performed. Figure 6-4 shows typical cross sections from the three sizes of mushrooms (1 μm, 2 μm, and 3 μm) used, where a neuron was identified to be sitting on top of a mushroom. In the literature, it has been shown that the degree of coupling of the cell to mushroom electrode is dependent on the absolute size, as well as the aspect ratios of the stem diameter, stem height, and cap diameter. Spira et al. have demonstrated that a cap diameter of 1.5-2 μm is sufficiently small to produce an engulfment level of ca. 90% with the level dropping off for larger diameters[159]. This is similar to what we see with diamond the coated mushrooms: an almost complete engulfment for the smallest (1 μm stem diameter) with decreasing coverage as the size is increased. Furthermore, as described found by Spira et al., a narrow cleft is formed between the cell's plasma membrane and the upper surface of the mushroom, independent of the mushroom diameter [159]. Thus, it is qualitatively determined that a diamond interface can be used to promote neuronal engulfment similarly to that shown in previous literature.

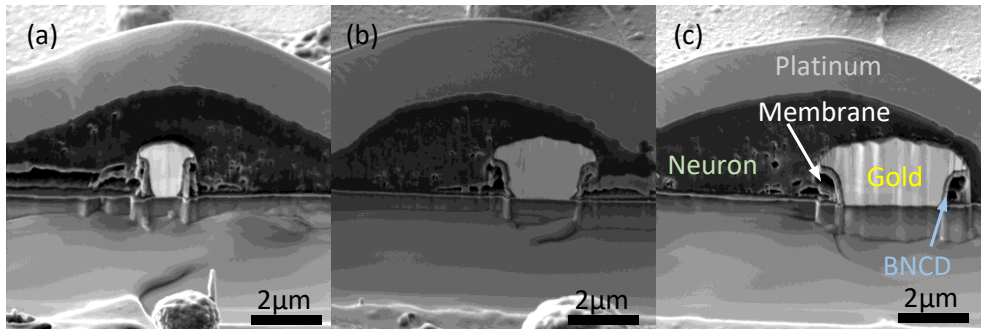


**Figure 6-4** – Cross section of NCD coated gold mushrooms of different sizes (a) 1  $\mu\text{m}$  (b) 2  $\mu\text{m}$ , and (c) 3  $\mu\text{m}$ . The cell membrane on all three sections shows tight binding to the upper curved portion of the mushroom. The cleft between stalk of the mushroom and the cell membrane shows increasing width with the diameter of the mushroom.

### 6.5.2 Cell recordings

For neuronal recordings from hippocampal cells, the devices described in section 6.2 were used. The fabrication method of the devices is still undergoing development and only one successful MEA has been fabricated for this cell recording studies. This MEA had 29 of the fabricated mushroom electrodes remaining of a possible 59. Even with this single MEA, the preliminary results look quite promising, and future work should be focused to create more of the MEA devices in order to solidify these results and be able to perform analytics on the data. Because of the limited data from this study, we are restricted to a qualitative analysis of the data. Recordings of spontaneous electrical activity were made at 10, 12, 14, and 16 DIV. The background noise level of the system was typically ca. 20  $\mu\text{V}$ . A square wave pulse lasting 20 ms with amplitude of 1 mV was used in the bathing solution for calibration. A wide band filter of 1-10 kHz was used for the recordings. Cell recordings were performed by the group of Micha Spira at the Hebrew University of Jerusalem.

Figure 6-5 shows recordings from at 12 DIV and 16 DIV of seven selected electrodes that showed good activity throughout the entire cell culture. This comparison shows how gradually the bursts are generated as the cell culture matures and becomes more networked.

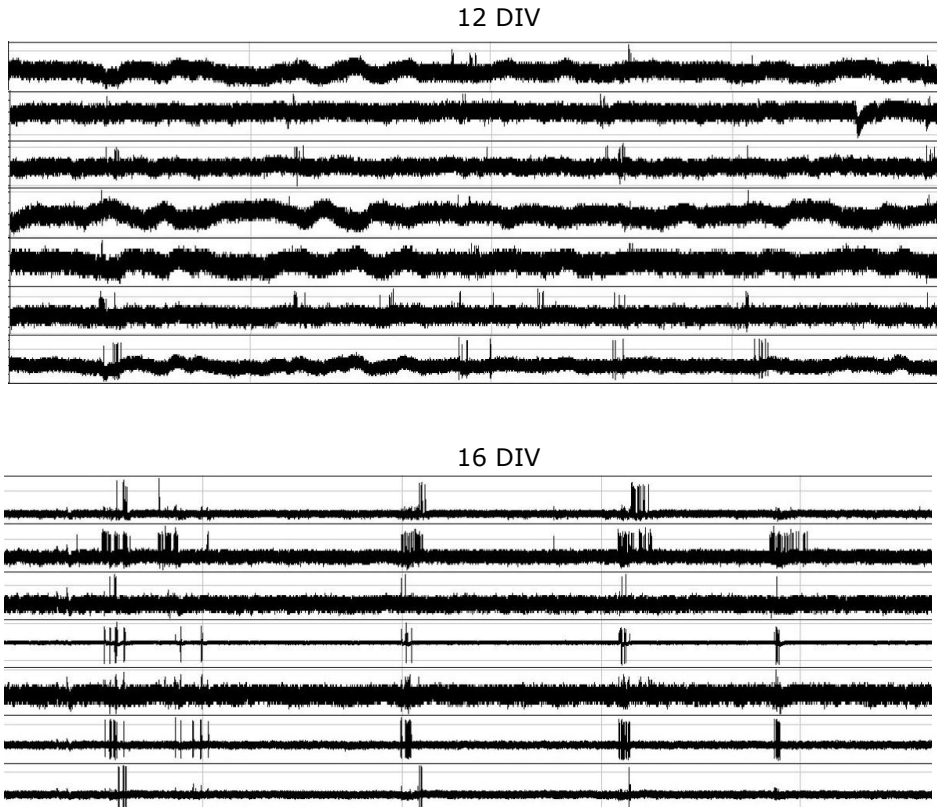


**Figure 6-5** – Recordings from 7 active mushroom shaped diamond electrodes after 12 DIV (above) and 16 DIV (below), taken over 90s time period, to show activity. Amplitudes range between channels varies from 40  $\mu$ V to 200  $\mu$ V.

Though the number of electrodes in this study was relatively small, they seem to be dominated by positive monophasic and positive biphasic spikes, as opposed to predominantly the negative monophasic spikes characteristic of planar electrodes; see Figure 6-6. These results are in agreement with those of hippocampal cell recordings on gold mushroom shaped electrodes [115]. According to Spira et al., this difference in dominant spike polarity can be explained by two possible mechanisms. The first is that the two shapes record from different areas of the cell: planar electrodes predominantly from the axons or excitable soma while mushrooms predominantly record from dendrites or inexcitable cell bodies. The reasoning is that a negative field potential reflects local extracellular inward

current and a positive field potential reflects outward current, corresponding to excitable areas and unexcitable areas respectively [115], [160]. Another explanation is that the mushrooms are indeed recording attenuated intracellular signals, similar to perforated patch-clamp, due to a high seal resistance of the engulfment and expression of conducting ion channels at the junction [3], [115], [160]–[163].

Compared to the measurements made on planar diamond electrodes (Section 7.2), these measurements show an order of magnitude increase in measured potential. This increased sensitivity gives greater resolution of the neuron spikes, allowing the full action potential to be seen.

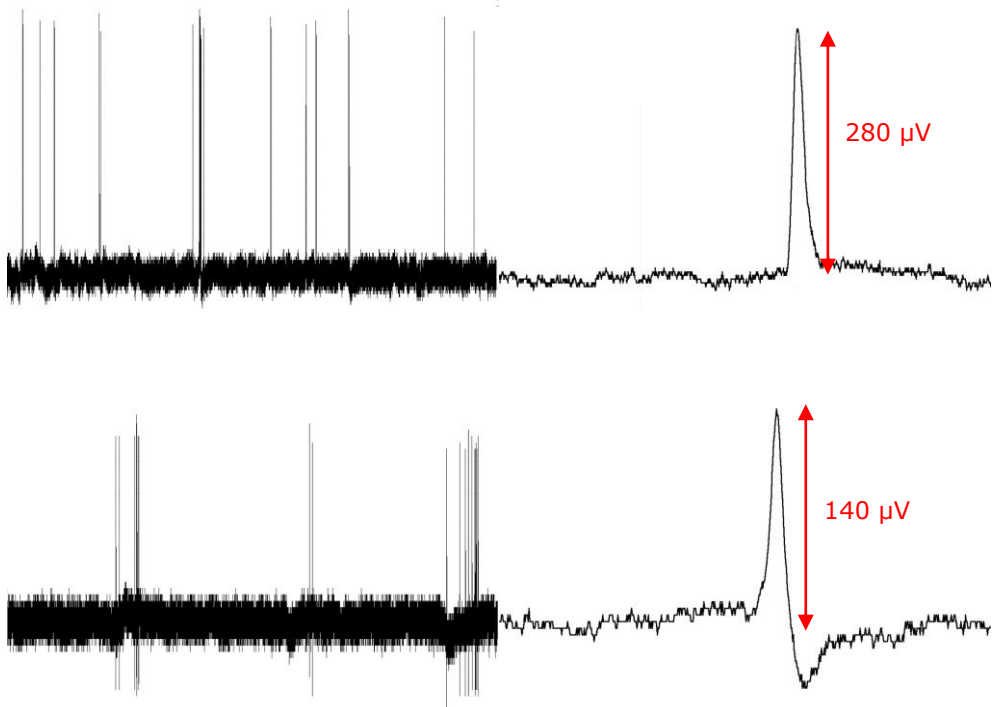


**Figure 6-6** – Recordings from two different mushroom shaped diamond electrodes showing predominantly positive monophasic spikes (above) and positive biphasic spikes (below). The spikes on the right side of the figure are from those on the left side, but with a zoomed in time scale.



# 7 Conclusions and Outlook

## 7.1 Conclusions

The main work in the context of this thesis addresses three main topics building towards the goal of a protruding mushroom shaped electrode diamond device for neuronal interfacing. The first topic addresses the issues in developing a reliable method for the promotion of neuronal growth and adhesion on nanocrystalline diamond surface. Secondly, boron-doped diamond is shown to be an effective electrode material and NCD as an effective insulating material for MEAs. Finally, preliminary results from 3-dimensional mushroom shaped BCND electrodes show that they can be used to promote engulfment of the electrodes and provide high quality recordings.

In chapter 4 it is shown that while diamond is typically a good surface for cell culturing, it was found that some additional treatment was necessary for primary neural cells. It was found that neuroblastoma cells, which are representative of neural cells, show good adhesion and growth on untreated diamond surfaces. Both hydrogen- and oxygen-terminated NCD and BNCD surfaces promoted neuronal cell adhesion and proliferation compared to fused silica controls, even with medium free of fetal bovine serum. However, this cell type is proliferating and results could not be extrapolated to non-proliferating primary neural cells. Indeed, when primary neural cells were used, it was necessary to first treat the surface with either PEI or a PDL/laminin surface treatment before cells would adhere well. Bare NCD substrates were not permissive to cell adhesion and growth for primary neuron & glial cell cultures. While this shows that bare NCD does not have unusual cell adhesion for this cell type, it does have a host of beneficial material properties that can be taken advantage of with simple functionalization strategies. Treatments of PEI or a PDL/laminin are standard treatments for glass substrates and are thought to enhance adhesion through creating a positive surface charge. It is thought that this same mechanism is responsible for its enhanced adhesion on NCD surfaces as well.

The first MEA devices were introduced in chapter 5 which were produced with planar electrodes in order to confirm the ability of both NCD and BNCD to be integrated onto a MEA device. NCD was successfully used as an insulating material with TiN electrodes to record from neurons, with similar results to TiN electrodes with a standard SiN passivation layer. Similar devices were then used with a thin layer of BNCD added to the active electrode surface of a gold electrode. Results showed that these devices could be used to successfully record from neurons, though the impedance of the electrodes was quite high. This is thought to be due mostly to adhesion of PDMS monomers to the surface during attachment of the glass culturing ring. Further work should be done to solve this issue in order to achieve a better impedance, which would also help recordings from 3D shaped electrodes.

Finally, the main aim of my thesis project, of 3D mushroom diamond electrode based MEA devices, was detailed in chapter 6. During my PhD project, a lot of time was spent developing the fabrication technique for 3D mushroom shaped diamond electrodes and thus little time was left for testing of the devices. However, it was possible to develop, in parallel, an array of gold mushrooms and coat them with BNCD to confirm engulfment by neurons. It was found that qualitatively, in the same way that neurons engulf gold mushrooms from the literature, they similarly engulf them when presented with a NCD interface. It was possible to test a single MEA with the diamond mushroom shaped electrodes, and though it is a small sample size, the results already look promising. The recorded action potentials are predominantly of positive potentials, showing both monophasic and biphasic signals, with amplitudes between 100-300  $\mu\text{V}$ . This is typical of the mushroom shaped gold electrodes found within the literature and significantly higher than planar electrodes. These results are very promising and reveal recordings of attenuated intracellular signals may be possible extracellularly using these devices, however, more devices are necessary to confirm these results. Future work should focus on creating more of these devices for testing. Advantage of using the diamond electrodes is a high potential window allowing and low background current allowing to reduce the cell and tissue necrosis due to pH changes due to Faradaic current compound.

While gold mushroom shaped electrodes have been shown to be effective in producing intracellular quality signals from cell cultures, it may be necessary to look at different materials for long-term *in-vivo* recordings. Diamond is a highly stable material that shows little fouling or degradation, and is ideal as a long term interface for implantable devices. Furthermore, boron doped diamond displays an incredibly high potential window, which makes it a good candidate for stimulation applications. For these reasons, combined with the positive preliminary data, it is believed these devices can make an impact in this field and that work should be carried out to further develop these devices. In conclusion, we have developed a novel fabrication for MEAs made of thin diamond films on transparent substrates, which allow detection of neural signals with advantage of diamond biocompatibility, surface neutrality, capacitive coupling and excellent electrochemical characteristics.

## **7.2 Outlook**

The future of diamond as a platform for neuronal sensing looks promising, based on the results of this work and the growing number of successful work related to this field [2, 6–9, 47, 76, 136, 162,163]. We have helped to advance this field by helping verify some major milestones towards using this technology. Multiple publications have come out of this work specifically aimed at showing the effectiveness of diamond as a platform for neuronal growth, as well as multiple others that successfully use diamond as this platform. Furthermore, we have shown that diamond can effectively be used as the main interface for electrical sensing devices, as both an insulating passivation layer and a conductive planar electrode; adding another important piece of the puzzle. One of challenge faced at this stage is the relatively high impedance of NCD compared to other electrode materials leading to comparatively lower spike signals. In future work, the impedance of planar electrodes could be enhanced by using nanostructuring techniques to increase the surface area; which could be incorporated into the presented fabrication process with no additional lithography step required [11]. In some recent work, we have utilized the high surface area of TiN electrodes and coated them with BNCD to achieved a nearly 10x increase of the BNCD

capacitance, making it attractive for ultrasensitive MEAs based on purely capacitive coupling [7]. While there is much progress that could be made advancing planar microelectrodes, the main goal of this thesis was to expand upon a new approach of using small protruding structures to promote cell engulfment and obtaining high-resolution signals. This work built upon the gold structures original created to prove this, in order to take advantage of diamond's material properties including high biocompatibility, inertness, non-fouling, and high potential windows for capacitive coupling. Much time was spent developing a microfabrication process to make these structures from diamond and many challenges were faced along the way. The EBL lift-off process was one challenge with which further refinement could potentially allow high aspect ratio structures. Another improvement that could be made to this process is an optimization of all the deposition parameters for the multiple layers, including the AlN layer that was used to as a template for the BNCD structures. While the procedure was already optimized for layer thickness and deposition parameters, further refinement could potentially allow better aspect ratio with the existing EBL process, and may reduce some of the issues with thin-film stress that was encountered. Stress in the films was one of the major issues encountered during development of the fabrication process, which resulted in many catastrophic device failures due to differences in thermal expansion after diamond growth at high temperatures. This could potentially have been resolved by selecting silicon as a substrate material instead of fused silica; however, it was highly beneficially to have a transparent device, so work was focused on fused silica as the substrate. Stress may also have been avoided through replacement of the AlN spacing layer with another material, such as SiO<sub>2</sub>; however, deposition and plasma etching of SiO<sub>2</sub> was not readily available at the institute. Many of these issues in fabrication were limitations of the fabrication technology available at the institute where the research was conducted, and could potentially be resolved using state-of-the-art equipment. Even though more work needs to be done in optimizing this process, it proved to be successful in creating some functional devices capable of recording from neuronal cells. We were successful in showing that these structures made of BNCD can be used to capture high resolution signals from neurons, similar to the results found for gold mushroom shaped electrodes. This was the ultimate goal of the project, and while we have the first trials done showing positive results, more

devices and studies are necessary to provide a solid proof of this work. I believe that there is promising potential for these type of devices, and it is my hope that the work on this project continues.



# References

- [1] E. R. Kandel, J. H. Schwartz, T. M. Jessell, S. A. Siegelbaum, and A. J. Hudspeth, *Principles of Neural Science, Fifth Edition*. McGraw-Hill Education, 2012.
- [2] M. E. J. Obien, K. Deligkaris, T. Bullmann, D. J. Bakkum, and U. Frey, "Revealing neuronal function through microelectrode array recordings," *Front. Neurosci.*, vol. 8, no. January, pp. 1–30, Jan. 2015.
- [3] A. Hai, J. Shappir, and M. E. Spira, "Long-Term , Multisite , Parallel , In-Cell Recording and Stimulation by an Array of Extracellular Microelectrodes," no. C, pp. 559–568, 2010.
- [4] A. Hai, A. Dormann, J. Shappir, S. Yitzchaik, C. Bartic, G. Borghs, J. P. M. Langedijk, and M. E. Spira, "Spine-shaped gold protrusions improve the adherence and electrical coupling of neurons with the surface of micro-electronic devices.," *J. R. Soc. Interface*, vol. 6, no. 41, pp. 1153–65, Dec. 2009.
- [5] N. Position, F. Santoro, S. Dasgupta, J. Schnitker, T. Auth, E. Neumann, G. Panaitov, G. Gompper, and A. Offenha, "Interfacing Electrogenic Cells with 3D," *ACS Nano*, no. 7, pp. 6713–6723, 2014.
- [6] H. Chan, D. M. Aslam, S. Member, J. A. Wiler, and B. Casey, "A Novel Diamond Microprobe for Neuro-Chemical and -Electrical Recording in Neural Prosthesis," vol. 18, no. 3, pp. 511–521, 2009.
- [7] M. Alcaide, A. Taylor, M. Fjorback, V. Zachar, and C. P. Pennisi, "Boron-Doped Nanocrystalline Diamond Electrodes for Neural Interfaces: In vivo Biocompatibility Evaluation," vol. 10, no. March, pp. 1–9, 2016.
- [8] M. E. J. Obien, K. Deligkaris, T. Bullmann, and D. J. Bakkum, "Revealing neuronal function through microelectrode array recordings," *Front. Neurosci.*, vol. 8, no. January, pp. 1–30, 2015.
- [9] M. McDonald, D. Croux, F. Vahidpour, L. Curley, P. Pobedinskas, K. Haenen, M. Giugliano, Z. Vi, L. Kavan, M. Nesl, I. For, and S. Sio, "All-diamond functional surface micro-electrode arrays for brain-slice neural analysis," *Phys. Status Solidi A*, vol. 214, no. 2, 2017.
- [10] "Diamond microelectrode arrays for in vitro neuronal recordings," vol. 7, no. 3, pp. 683–690, 2018.
- [11] G. Piret, C. Hébert, J.-P. Mazellier, L. Rousseau, E. Scorsone, M. Cottance, G. Lissorgues, M. O. Heuschkel, S. Picaud, P. Bergonzo, and B. Yvert, "3D-nanostructured boron-doped diamond for microelectrode array neural interfacing.," *Biomaterials*, vol. 53, pp. 173–83, Jun. 2015.
- [12] P. Bergonzo, A. Bongrain, E. Scorsone, A. Bendali, L. Rousseau, G. Lissorgues, P. Mailley, Y. Li, T. Kauffmann, F. Goy, B. Yvert, J. A. Sahel, and S. Picaud, "3D shaped mechanically flexible diamond microelectrode arrays for eye implant applications: The MEDINAS project," vol. 32, pp.

- 91–94, 2011.
- [13] J. Sung and J. Lin, *Diamond Nanotechnology: Synthesis and Applications*. Pan Stanford, 2010.
- [14] I. Fleming, *Molecular Orbitals and Organic Chemical Reactions: Reference Edition*. Wiley, 2010.
- [15] S. J. Sque, "Bulk and Transfer Doping of Diamond," 2007.
- [16] C. Stavis, T. L. Clare, J. E. Butler, A. D. Radadia, R. Carr, H. Zeng, W. P. King, J. A. Carlisle, A. Aksimentiev, R. Bashir, and R. J. Hamers, "Surface functionalization of thin-film diamond for highly stable and selective biological interfaces," *Proc. Natl. Acad. Sci.*, vol. 108, no. 3, pp. 983–988, 2011.
- [17] J. Pernot, P. N. Volpe, F. Omnès, P. Muret, V. Mortet, K. Haenen, and T. Teraji, "Hall hole mobility in boron-doped homoepitaxial diamond," *Phys. Rev. B*, vol. 81, no. 20, p. 205203, May 2010.
- [18] J. Pernot, C. Tavares, E. Gheeraert, E. Bustarret, M. Katagiri, and S. Koizumi, "Hall electron mobility in diamond," *Appl. Phys. Lett.*, vol. 89, no. 12, p. 122111, 2006.
- [19] N. D. Lai, D. Zheng, F. Treussart, and J.-F. Roch, "Optical determination and magnetic manipulation of a single nitrogen-vacancy color center in diamond nanocrystal," *Adv. Nat. Sci. Nanosci. Nanotechnol.*, vol. 1, no. 1, p. 15014, 2010.
- [20] M. Mrozek, A. M. Wojciechowski, D. S. Rudnicki, J. Zachorowski, P. Kehayias, D. Budker, and W. Gawlik, "Coherent population oscillations with nitrogen-vacancy color centers in diamond," *Phys. Rev. B*, vol. 94, no. 3, p. 35204, Jul. 2016.
- [21] T. Teraji, "Chemical vapor deposition of homoepitaxial diamond films," *Phys. Status Solidi*, vol. 203, no. 13, pp. 3324–3357, Oct. 2006.
- [22] K. E. Spear, J. P. Dismukes, and E. Society, *Synthetic Diamond: Emerging CVD Science and Technology*. Wiley, 1994.
- [23] R. Jukka, "Diamonds are a Thermal Designer's Best Friends," *Electronics Cooling*, 2002. .
- [24] M. Paul, "Diamond thin films : a 21st-century material," *Phil. Trans. R. Soc. Lond. A*, no. 358, pp. 473–495, 2000.
- [25] R. E. Clausing, L. L. Horton, J. C. Angus, and P. Koidl, *Diamond and Diamond-like Films and Coatings*. Springer US, 2012.
- [26] S. Yugo, T. Kanai, T. Kimura, and T. Muto, "Generation of diamond nuclei by electric field in plasma chemical vapor deposition," *Appl. Phys. Lett.*, vol. 58, no. 10, pp. 1036–1038, Mar. 1991.
- [27] V. Vermeeren, S. Wenmackers, P. Wagner, and L. Michiels, *DNA sensors with diamond as a promising alternative transducer material.*, vol. 9, no. 7. 2009.
- [28] S. D. Janssens, P. Pobedinskas, J. Vacik, V. Petráková, B. Ruttens, J. D'Haen, M. Nesládek, K. Haenen, and P. Wagner, "Separation of intra- and intergranular magnetotransport properties in nanocrystalline diamond

- films on the metallic side of the metal-insulator transition," *New J. Phys.*, vol. 13, 2011.
- [29] G. M. Klemencic, S. Mandal, J. M. Werrell, S. R. Giblin, O. A. Williams, G. M. Klemencic, S. Mandal, J. M. Werrell, and S. R. Giblin, "Superconductivity in planarised nanocrystalline diamond films," *Sci. Technol. Adv. Mater.*, vol. 18, no. 1, pp. 239–244, 2017.
- [30] A. Kraft, G. Gmbh, and K. Str, "Doped Diamond : A Compact Review on a New , Versatile Electrode Material," *Int. J. Electrochem. Sci.*, vol. 2, pp. 355–385, 2007.
- [31] S. Turner, Y.-G. Lu, S. D. Janssens, F. Da Pieve, D. Lamoen, J. Verbeeck, K. Haenen, P. Wagner, and G. Van Tendeloo, "Local boron environment in B-doped nanocrystalline diamond films," *Nanoscale*, vol. 4, no. 19, pp. 5960–5964, 2012.
- [32] S. D. Janssens, P. Pobedinskas, V. Petráková, M. Nesládek, K. Haenen, and P. Wagner, "Influence of methane concentration on the electric transport properties in heavily boron-doped nanocrystalline CVD diamond films," *MRS Proc.*, vol. 1282, p. mrsf10-1282-a15-04, 2011.
- [33] "Medical gallery of Blausen Medical 2014," *WikiJournal of Medicine*, 2014.
- [34] "Action Potential," *Wikipedia*. [Online]. Available: [https://en.wikipedia.org/wiki/Action\\_potential](https://en.wikipedia.org/wiki/Action_potential).
- [35] "Baby's Brain," *The Urban Child Institute*. [Online]. Available: <http://www.urbanchildinstitute.org/why-0-3/baby-and-brain>.
- [36] Y. Zhao, S. Inayat, D. A. Dikin, J. H. Singer, R. S. Ruoff, and J. B. Troy, "Patch clamp technique: Review of the current state of the art and potential contributions from nanoengineering," *Proc. Inst. Mech. Eng. Part N J. Nanoeng. Nanosyst.*, vol. 222, no. 1, pp. 1–11, Mar. 2008.
- [37] N. a. Kotov, J. O. Winter, I. P. Clements, E. Jan, B. P. Timko, S. Campidelli, S. Pathak, A. Mazzatenta, C. M. Lieber, M. Prato, R. V. Bellamkonda, G. a. Silva, N. W. S. Kam, F. Patolsky, and L. Ballerini, "Nanomaterials for Neural Interfaces," *Adv. Mater.*, vol. 21, no. 40, pp. 3970–4004, Oct. 2009.
- [38] M. E. Spira and A. Hai, "Multi-electrode array technologies for neuroscience and cardiology," *Nat. Nanotechnol.*, vol. 8, no. 2, pp. 83–94, Feb. 2013.
- [39] M. Systems, "Microelectrode Arrays." [Online]. Available: <https://www.multichannelsystems.com/products/microelectrode-arrays>.
- [40] A. Novellino and J. Zaldivar, "Recurrence Quantification Analysis of Spontaneous Electrophysiological Activity during Development: Characterization of In Vitro Neuronal Networks Cultured on Multi Electrode Array Chips," *Adv. Artif. Intell.*, 2010.
- [41] R. Gerwig, K. Fuchsberger, B. Schroepfel, G. S. Link, G. Heusel, U. Kraushaar, W. Schuhmann, A. Stett, and M. Stelzle, "PEDOT – CNT composite microelectrodes for recording and electrostimulation applications : fabrication , morphology , and electrical properties," vol. 5, no. May, pp. 1–11, 2012.
- [42] R. Gerwig, K. Fuchsberger, B. Schroepfel, G. S. Link, G. Heusel, U.

- Kraushaar, W. Schuhmann, A. Stett, and M. Stelzle, "PEDOT-CNT Composite Microelectrodes for Recording and Electrostimulation Applications: Fabrication, Morphology, and Electrical Properties," *Front. Neuroeng.*, vol. 5, no. May, p. 8, Jan. 2012.
- [43] A. Hai, J. Shappir, and M. E. Spira, "In-cell recordings by extracellular microelectrodes," *Nat. Methods*, vol. 7, no. 3, pp. 200–2, Mar. 2010.
- [44] S. F. Cogan, "Neural Stimulation and Recording Electrodes," *Annu. Rev. Biomed. Eng.*, vol. 10, no. 1, pp. 275–309, Jul. 2008.
- [45] M. Alcaide, A. Taylor, M. Fjorback, V. Zachar, and C. P. Pennisi, "Boron-Doped Nanocrystalline Diamond Electrodes for Neural Interfaces: In vivo Biocompatibility Evaluation," *Front. Neurosci.*, vol. 10, p. 87, 2016.
- [46] E. M. Hudak, D. W. Kumsa, H. B. Martin, D. J. Garrett, K. Ganesan, A. Stacey, A. R. Harris, S. J. Morgan, and J. Chen, "Conducting polymer coated neural recording electrodes Biofouling resistance of boron-doped diamond neural stimulation electrodes is superior to titanium nitride electrodes in vivo."
- [47] R. (Universität T. Gerwig, "Development and characterization of PEDOT-CNT microelectrode arrays for advanced neuronal recording , stimulation and sensing," Eberhard Karls Universität Tübingen, 2012.
- [48] R. Gerwig, K. Fuchsberger, B. Schroepel, G. S. Link, G. Heusel, U. Kraushaar, W. Schuhmann, A. Stett, and M. Stelzle, "PEDOT–CNT Composite Microelectrodes for Recording and Electrostimulation Applications: Fabrication, Morphology, and Electrical Properties," *Front. Neuroeng.*, vol. 5, p. 8, May 2012.
- [49] V. Maybeck, R. Edgington, A. Bongrain, J. O. Welch, E. Scorsone, P. Bergonzo, R. B. Jackman, and A. Offenhäusser, "Boron-Doped Nanocrystalline Diamond Microelectrode Arrays Monitor Cardiac Action Potentials," *Adv. Healthc. Mater.*, vol. 3, no. 2, pp. 283–289, 2014.
- [50] E. C. Onyiriuka, C. B. Moore, F. P. Fehlner, N. J. Binkowski, D. Salamida, T.-J. King, and J. G. Couillard, "Effect of RCA cleaning on the surface chemistry of glass and polysilicon films as studied by ToF-SIMS and XPS," *Surf. Interface Anal.*, vol. 26, no. 4, pp. 270–277, 1998.
- [51] O. a. Williams, O. Douhéret, M. Daenen, K. Haenen, E. Ōsawa, and M. Takahashi, "Enhanced diamond nucleation on monodispersed nanocrystalline diamond," *Chem. Phys. Lett.*, vol. 445, no. 4–6, pp. 255–258, Sep. 2007.
- [52] P. Pobedinskas, G. Degutis, W. Dexters, W. Janssen, S. D. Janssens, B. Conings, B. Ruttens, J. D'Haen, H.-G. Boyen, a. Hardy, M. K. Van Bael, and K. Haenen, "Surface plasma pretreatment for enhanced diamond nucleation on AlN," *Appl. Phys. Lett.*, vol. 102, no. 20, p. 201609, 2013.
- [53] D. G. Stavenga, "Thin Film and Multilayer Optics Cause Structural Colors of Many Insects and Birds," *Mater. Today Proc.*, vol. 1, pp. 109–121, 2014.
- [54] "LOR and PMGI Resists."
- [55] V. M. Sundaram and S.-B. Wen, "An easy method to perform e-beam negative tone lift-off fabrication on dielectric material with a sandwiched

- conducting polymer layer," *J. Micromechanics Microengineering*, vol. 21, no. 6, p. 65021, Jun. 2011.
- [56] M. Yan, J. Lee, B. Ofuonye, S. Choi, J. H. Jang, and I. Adesida, "Effects of salty-developer temperature on electron-beam-exposed hydrogen silsesquioxane resist for ultradense pattern transfer," *J. Vac. Sci. Technol. B Microelectron. Nanom. Struct.*, vol. 28, no. 6, p. C6S23, 2010.
- [57] J. K. W. Yang and K. K. Berggren, "Using high-contrast salty development of hydrogen silsesquioxane for sub-10-nm half-pitch lithography," *J. Vac. Sci. Technol. B Microelectron. Nanom. Struct.*, vol. 25, no. 6, p. 2025, 2007.
- [58] K. Lister, "Pattern transfer of a 23 nm-period grating and sub-15 nm dots into CVD diamond," *Microelectron. Eng.*, vol. 73–74, pp. 319–322, Jun. 2004.
- [59] M. Häffner, a. Haug, a. Heeren, M. Fleischer, H. Peisert, T. Chassé, and D. P. Kern, "Influence of temperature on HSQ electron-beam lithography," *J. Vac. Sci. Technol. B Microelectron. Nanom. Struct.*, vol. 25, no. 6, p. 2045, 2007.
- [60] H. Yang, A. Jin, Q. Luo, J. Li, C. Gu, and Z. Cui, "Electron beam lithography of HSQ/PMMA bilayer resists for negative tone lift-off process," *Microelectron. Eng.*, vol. 85, no. 5–6, pp. 814–817, May 2008.
- [61] B. J. M. Hausmann, M. Khan, Y. Zhang, T. M. Babinec, K. Martinick, M. McCutcheon, P. R. Hemmer, and M. Lončar, "Fabrication of diamond nanowires for quantum information processing applications," *Diam. Relat. Mater.*, vol. 19, no. 5–6, pp. 621–629, May 2010.
- [62] P. Rai-Choudhury, *Handbook of Microlithography, Micromachining, and Microfabrication: Micromachining and microfabrication*. SPIE Optical Engineering Press, 1997.
- [63] "Scanning electron microscope," *Wikipedia*. [Online]. Available: [https://en.wikipedia.org/wiki/Scanning\\_electron\\_microscope#Detection\\_of\\_secondary\\_electrons](https://en.wikipedia.org/wiki/Scanning_electron_microscope#Detection_of_secondary_electrons).
- [64] "Elcectron Microanalysis Core Facility," *Northern Arizona University*. [Online]. Available: <https://nau.edu/cefns/labs/electron-microprobe/glg-510-class-notes/signals/>.
- [65] A. C. Ferrari and J. Robertson, "Raman spectroscopy of amorphous, nanostructured, diamond-like carbon, and nanodiamond," *Philos. Trans. R. Soc. London. Ser. A Math. Phys. Eng. Sci.*, vol. 362, no. 1824, p. 2477 LP-2512, Nov. 2004.
- [66] R. L. Grosse, "Handbook of Raman Spectroscopy: From the Research Laboratory to the Process Line Edited by Ian R. Lewis (Kaiser Optical Systems) and Howell G. M. Edwards (University of Bradford). Dekker: New York, Basel. 2001. xiv + 1054 pp. \$225. ISBN 0-8247-0557-2," *J. Am. Chem. Soc.*, vol. 124, no. 19, pp. 5601–5602, May 2002.
- [67] S. M. Leeds, T. J. Davis, P. W. May, C. D. O. Pickard, and M. N. R. Ashfold, "Use of different excitation wavelengths for the analysis of CVD diamond by laser Raman spectroscopy," *Diam. Relat. Mater.*, vol. 7, no. 2, pp. 233–237, 1998.

- [68] K. Okada, H. Kanda, S. Komatsu, S. Matsumoto, K. Okada, H. Kanda, S. Komatsu, and S. Matsumoto, "Effect of the excitation wavelength on Raman scattering of microcrystalline diamond prepared in a low pressure inductively coupled plasma Effect of the excitation wavelength on Raman scattering of microcrystalline diamond prepared in a low pressure inductively coupled plasma," vol. 1674, no. 2000, 2003.
- [69] T. Street, "Raman spectroscopy of amorphous , nanostructured , diamond-like carbon , and nanodiamond," vol. 2, no. Robertson 2002, pp. 2477–2512, 2004.
- [70] "Basics of Electrochemical Impedance Spectroscopy." [Online]. Available: <https://www.gamry.com/application-notes/EIS/basics-of-electrochemical-impedance-spectroscopy/>.
- [71] A. . Zia and S. C. Mukhopadhyay, "Electrochemical Sensing: Carcinogens in Beverages," Springer, 2016, pp. 21–37.
- [72] M. Pacios, R. Villa, and P. Godignon, "Carbon Nanotubes as Suitable Electrochemical Platforms for Metalloprotein Sensors and Genosensors," 2011.
- [73] J. A. Garrido, S. Nowy, A. Ha, and M. Stutzmann, "The Diamond / Aqueous Electrolyte Interface: an Impedance Investigation," no. 12, pp. 3897–3904, 2008.
- [74] F. Fendrych, A. Taylor, L. Peksa, I. Kratochvilova, J. Vlcek, V. Rezacova, V. Petrak, Z. Kluber, L. Fekete, M. Liehr, and M. Nesladek, "Growth and characterization of nanodiamond layers prepared using the plasma-enhanced linear antennas microwave CVD system," *J. Phys. D. Appl. Phys.*, vol. 43, no. 37, p. 374018, Sep. 2010.
- [75] Y. S. Singh, L. E. Sawarynski, H. M. Michael, R. E. Ferrell, M. a Murphey-Corb, G. M. Swain, B. a Patel, and A. M. Andrews, "Boron-Doped Diamond Microelectrodes Reveal Reduced Serotonin Uptake Rates in Lymphocytes from Adult Rhesus Monkeys Carrying the Short Allele of the 5-HTTLPR.," *ACS Chem. Neurosci.*, vol. 1, no. 1, pp. 49–64, Jan. 2010.
- [76] S. M. Ojovan, M. McDonald, M. McDonald, N. Rabieh, N. Shmuel, H. Erez, M. Nesladek, and M. E. Spira, "Nanocrystalline diamond surfaces for adhesion and growth of primary neurons, conflicting results and rational explanation.," *Front. Neuroeng.*, vol. 7, no. June, p. 17, Jan. 2014.
- [77] P. Ariano, O. Budnyk, S. Dalmazzo, D. Lovisolo, C. Manfredotti, P. Rivolo, and E. Vittone, "On diamond surface properties and interactions with neurons.," *Eur. Phys. J. E. Soft Matter*, vol. 30, no. 2, pp. 149–56, Oct. 2009.
- [78] M. Amaral, P. S. Gomes, M. a Lopes, J. D. Santos, R. F. Silva, and M. H. Fernandes, "Cytotoxicity evaluation of nanocrystalline diamond coatings by fibroblast cell cultures.," *Acta Biomater.*, vol. 5, no. 2, pp. 755–63, Feb. 2009.
- [79] F. Klauser, M. Hermann, D. Steinmüller-Nethl, O. Eiter, A. Pasquarelli, E. Bertel, T. Seppi, P. Lukas, and T. Lechleitner, "Direct and Protein-Mediated Cell Attachment on Differently Terminated Nanocrystalline Diamond," *Chem. Vap. Depos.*, vol. 16, no. 1–3, pp. 42–49, Mar. 2010.

- [80] V. N. Mochalin, O. Shenderova, D. Ho, and Y. Gogotsi, "The properties and applications of nanodiamonds," *Nat. Nanotechnol.*, vol. 7, p. 11, Dec. 2011.
- [81] A. Härtl, E. Schmich, J. A. Garrido, J. Hernando, S. C. R. Catharino, S. Walter, P. Feulner, A. Kromka, D. Steinmüller, and M. Stutzmann, "Protein-modified nanocrystalline diamond thin films for biosensor applications," *Nat. Mater.*, vol. 3, p. 736, Sep. 2004.
- [82] P. Ariano, O. Budnyk, S. Dalmazzo, D. Lovisolo, C. Manfredotti, P. Rivolo, and E. Vittone, "On diamond surface properties and interactions with neurons," *Eur. Phys. J. E*, vol. 30, no. 2, p. 149, 2009.
- [83] K. Fromell, P. Forsberg, M. Karlsson, K. Larsson, F. Nikolajeff, and L. Baltzer, "Designed protein binders in combination with nanocrystalline diamond for use in high-sensitivity biosensors," *Anal. Bioanal. Chem.*, vol. 404, no. 6, pp. 1643–1651, 2012.
- [84] L. Yang, L. Zhang, and T. J. Webster, "Carbon nanostructures for orthopedic medical applications," *Nanomedicine*, vol. 6, no. 7, pp. 1231–1244, Sep. 2011.
- [85] L. Bacakova, L. Grausova, J. Vacik, A. Fraczek, S. Blazewicz, A. Kromka, M. Vanecek, and V. Svorcik, "Improved adhesion and growth of human osteoblast-like MG 63 cells on biomaterials modified with carbon nanoparticles," *Diam. Relat. Mater.*, vol. 16, no. 12, pp. 2133–2140, 2007.
- [86] M. J. Papo, S. A. Catledge, Y. K. Vohra, and C. Machado, "Mechanical wear behavior of nanocrystalline and multilayer diamond coatings on temporomandibular joint implants," *J. Mater. Sci. Mater. Med.*, vol. 15, no. 7, pp. 773–777, 2004.
- [87] L. Booth, S. A. Catledge, D. Nolen, R. G. Thompson, and Y. K. Vohra, "Synthesis and Characterization of Multilayered Diamond Coatings for Biomedical Implants," *Materials (Basel)*, vol. 4, no. 5, pp. 857–868, May 2011.
- [88] W. C. Clem, S. Chowdhury, S. A. Catledge, J. J. Weimer, F. M. Shaikh, K. M. Hennessy, V. V. Konovalov, M. R. Hill, A. Waterfeld, S. L. Bellis, and Y. K. Vohra, "Mesenchymal stem cell interaction with ultra-smooth nanostructured diamond for wear-resistant orthopaedic implants," *Biomaterials*, vol. 29, no. 24, pp. 3461–3468, 2008.
- [89] Y.-C. Chen, D.-C. Lee, C.-Y. Hsiao, Y.-F. Chung, H.-C. Chen, J. P. Thomas, W.-F. Pong, N.-H. Tai, I.-N. Lin, and I.-M. Chiu, "The effect of ultra-nanocrystalline diamond films on the proliferation and differentiation of neural stem cells," *Biomaterials*, vol. 30, no. 20, pp. 3428–3435, 2009.
- [90] R. Pareta, L. Yang, A. Kothari, S. Sirinrath, X. Xiao, B. W. Sheldon, and T. J. Webster, "Tailoring nanocrystalline diamond coated on titanium for osteoblast adhesion," *J. Biomed. Mater. Res. Part A*, vol. 95A, no. 1, pp. 129–136, 2010.
- [91] M. Amaral, A. G. Dias, P. S. Gomes, M. A. Lopes, R. F. Silva, J. D. Santos, and M. H. Fernandes, "Nanocrystalline diamond: In vitro biocompatibility assessment by MG63 and human bone marrow cells cultures," *J. Biomed. Mater. Res. Part A*, vol. 87A, no. 1, pp. 91–99, 2008.
- [92] L. Yang, B. W. Sheldon, and T. J. Webster, "Orthopedic nano diamond

- coatings: Control of surface properties and their impact on osteoblast adhesion and proliferation," *J. Biomed. Mater. Res. Part A*, vol. 91A, no. 2, pp. 548–556, 2009.
- [93] D. J. Garrett, K. Ganesan, A. Stacey, K. Fox, H. Meffin, and Steven Praver, "Ultra-nanocrystalline diamond electrodes: optimization towards neural stimulation applications," *J. Neural Eng.*, vol. 9, no. 1, p. 16002, 2012.
- [94] Y.-C. Chen, D.-C. Lee, T.-Y. Tsai, C.-Y. Hsiao, J.-W. Liu, C.-Y. Kao, H.-K. Lin, H.-C. Chen, T. J. Palathinkal, W.-F. Pong, N.-H. Tai, I.-N. Lin, and I.-M. Chiu, "Induction and regulation of differentiation in neural stem cells on ultra-nanocrystalline diamond films," *Biomaterials*, vol. 31, no. 21, pp. 5575–5587, 2010.
- [95] A. Thalhammer, R. J. Edgington, L. A. Cingolani, R. Schoepfer, and R. B. Jackman, "The use of nanodiamond monolayer coatings to promote the formation of functional neuronal networks," *Biomaterials*, vol. 31, no. 8, pp. 2097–2104, 2010.
- [96] K.-H. Park and K. Yun, "Immobilization of Arg-Gly-Asp (RGD) sequence in a thermosensitive hydrogel for cell delivery using pheochromocytoma cells (PC12)," *J. Biosci. Bioeng.*, vol. 97, no. 6, pp. 374–377, 2004.
- [97] T. Lechleitner, F. Klauser, T. Seppi, J. Lechner, P. Jennings, P. Perco, B. Mayer, D. Steinmüller-Nethl, J. Preiner, P. Hinterdorfer, M. Hermann, E. Bertel, K. Pfaller, and W. Pfaller, "The surface properties of nanocrystalline diamond and nanoparticulate diamond powder and their suitability as cell growth support surfaces," *Biomaterials*, vol. 29, no. 32, pp. 4275–4284, 2008.
- [98] M. Amaral, P. S. Gomes, M. A. Lopes, J. D. Santos, R. F. Silva, and M. H. Fernandes, "Cytotoxicity evaluation of nanocrystalline diamond coatings by fibroblast cell cultures," *Acta Biomater.*, vol. 5, no. 2, pp. 755–763, 2009.
- [99] M. Kalbacova, B. Rezek, V. Baresova, C. Wolf-Brandstetter, and A. Kromka, "Nanoscale topography of nanocrystalline diamonds promotes differentiation of osteoblasts," *Acta Biomater.*, vol. 5, no. 8, pp. 3076–3085, 2009.
- [100] F. Klauser, M. Hermann, D. Steinmüller-Nethl, O. Eiter, A. Pasquarelli, E. Bertel, T. Seppi, P. Lukas, and T. Lechleitner, "Direct and Protein-Mediated Cell Attachment on Differently Terminated Nanocrystalline Diamond," *Chem. Vap. Depos.*, vol. 16, no. 1–3, pp. 42–49, 2010.
- [101] C. L. Frewin, M. Jaroszeski, E. Weeber, K. E. Muffly, A. Kumar, M. Peters, A. Oliveros, and S. E. Sadow, "Atomic force microscopy analysis of central nervous system cell morphology on silicon carbide and diamond substrates," *J. Mol. Recognit.*, vol. 22, no. 5, pp. 380–388, 2009.
- [102] L. Whitesell and S. L. Lindquist, "HSP90 and the chaperoning of cancer," *Nat. Rev. Cancer*, vol. 5, p. 761, Sep. 2005.
- [103] P. Spessotto, M. Cervi, M. T. Mucignat, G. Munguerra, I. Sartoretto, R. Doliana, and A. Colombatti, "β1 Integrin-dependent Cell Adhesion to EMLIN-1 Is Mediated by the gC1q Domain," *J. Biol. Chem.*, vol. 278, no. 8, pp. 6160–6167, Feb. 2003.
- [104] M. Daenen, L. Zhang, R. Erni, O. A. Williams, A. Hardy, M. K. Van Bael, P.

- Wagner, K. Haenen, M. Nesládek, and G. Van Tendeloo, "Diamond Nucleation by Carbon Transport from Buried Nanodiamond TiO<sub>2</sub> Sol-Gel Composites," *Adv. Mater.*, vol. 21, no. 6, pp. 670–673, Feb. 2009.
- [105] F. Fendrych, A. Taylor, L. Peksa, I. Kratochvilova, J. Vlcek, V. Rezacova, V. Petrak, Z. Kluiber, L. Fekete, and M. Liehr, "Growth and characterization of nanodiamond layers prepared using the plasma-enhanced linear antennas microwave CVD system," *J. Phys. D. Appl. Phys.*, vol. 43, no. 37, p. 374018, 2010.
- [106] Z. V. Živcová, O. Frank, V. Petrák, H. Tarábková, J. Vacík, M. Nesládek, and L. Kavan, "Electrochemistry and in situ Raman spectroelectrochemistry of low and high quality boron doped diamond layers in aqueous electrolyte solution," *Electrochim. Acta*, vol. 87, pp. 518–525, 2013.
- [107] Y. S. Singh, L. E. Sawarynski, H. M. Michael, R. E. Ferrell, M. A. Murphey-Corb, G. M. Swain, B. A. Patel, and A. M. Andrews, "Boron-Doped Diamond Microelectrodes Reveal Reduced Serotonin Uptake Rates in Lymphocytes from Adult Rhesus Monkeys Carrying the Short Allele of the 5-HTTLPR," *ACS Chem. Neurosci.*, vol. 1, no. 1, pp. 49–64, Jan. 2010.
- [108] X. Xiao, J. Wang, C. Liu, J. A. Carlisle, B. Mech, R. Greenberg, D. Guven, R. Freda, M. S. Humayun, J. Weiland, and O. Auciello, "In vitro and in vivo evaluation of ultrananocrystalline diamond for coating of implantable retinal microchips," *J. Biomed. Mater. Res. Part B Appl. Biomater.*, vol. 77B, no. 2, pp. 273–281, May 2006.
- [109] A. E. Hadjinicolaou, R. T. Leung, D. J. Garrett, K. Ganesan, K. Fox, D. A. X. Nayagam, M. N. Shivdasani, H. Meffin, M. R. Ibbotson, S. Prawer, and B. J. O'Brien, "Electrical stimulation of retinal ganglion cells with diamond and the development of an all diamond retinal prosthesis," *Biomaterials*, vol. 33, no. 24, pp. 5812–5820, 2012.
- [110] K. Ganesan, D. J. Garrett, A. Ahnood, M. N. Shivdasani, W. Tong, A. M. Turnley, K. Fox, H. Meffin, and S. Prawer, "An all-diamond, hermetic electrical feedthrough array for a retinal prosthesis," *Biomaterials*, vol. 35, no. 3, pp. 908–915, 2014.
- [111] A. Thalhammer, R. J. Edgington, L. a Cingolani, R. Schoepfer, and R. B. Jackman, "The use of nanodiamond monolayer coatings to promote the formation of functional neuronal networks.," *Biomaterials*, vol. 31, no. 8, pp. 2097–104, Mar. 2010.
- [112] J. Edgington, A. Thalhammer, J. O. Welch, A. Bongrain, P. Bergonzo, E. Scorsoni, R. B. Jackman, and R. Schoepfer, "Patterned neuronal networks using nanodiamonds and the effect of varying nanodiamond properties on neuronal adhesion and outgrowth," *J. Neural Eng.*, vol. 10, no. 5, p. 56022, 2013.
- [113] K. B Holt, C. Ziegler, D. J Caruana, J. Zang, E. Millan, J. Hu, and J. Foord, *Redox properties of undoped 5 nm diamond nanoparticles. Phys. Chem. Chem. Phys.* 10(2), 303-310, vol. 10. 2008.
- [114] S. Kaech and G. Banker, "Culturing hippocampal neurons," *Nat. Protoc.*, vol. 1, p. 2406, Jan. 2007.
- [115] A. Fendyur, N. Mazurski, J. Shappir, and M. E. Spira, "Formation of

- Essential Ultrastructural Interface between Cultured Hippocampal Cells and Gold Mushroom-Shaped MEA- Toward 'IN-CELL' Recordings from Vertebrate Neurons.," *Front. Neuroeng.*, vol. 4, no. December, p. 14, Jan. 2011.
- [116] M. E. Spira, R. Oren, A. Dormann, and D. Gitler, "Critical calpain-dependent ultrastructural alterations underlie the transformation of an axonal segment into a growth cone after axotomy of cultured *Aplysia* neurons," *J. Comp. Neurol.*, vol. 457, no. 3, pp. 293–312, Mar. 2003.
- [117] O. A. Williams, M. Nesladek, M. Daenen, S. Michaelson, A. Hoffman, E. Osawa, K. Haenen, and R. B. Jackman, "Growth, electronic properties and applications of nanodiamond," *Diam. Relat. Mater.*, vol. 17, no. 7, pp. 1080–1088, 2008.
- [118] A. Fabbro, M. Prato, and L. Ballerini, "Carbon nanotubes in neuroregeneration and repair," *Adv. Drug Deliv. Rev.*, vol. 65, no. 15, pp. 2034–2044, 2013.
- [119] M. Abedin and N. King, "Diverse evolutionary paths to cell adhesion," *Trends Cell Biol.*, vol. 20, no. 12, pp. 734–742, Jan. 2018.
- [120] C. S. Barros, S. J. Franco, and U. Müller, "Extracellular Matrix: Functions in the Nervous System," *Cold Spring Harb. Perspect. Biol.*, vol. 3, no. 1, p. a005108, Jan. 2011.
- [121] M. E. Danoviz and Z. Yablonka-Reuveni, "Skeletal Muscle Satellite Cells: Background and Methods for Isolation and Analysis in a Primary Culture System BT - Myogenesis: Methods and Protocols," J. X. DiMario, Ed. Totowa, NJ: Humana Press, 2012, pp. 21–52.
- [122] F. Gonzalez-Perez, E. Udina, and X. Navarro, "Chapter Ten - Extracellular Matrix Components in Peripheral Nerve Regeneration," in *Tissue Engineering of the Peripheral Nerve: Stem Cells and Regeneration Promoting Factors*, vol. 108, S. Geuna, I. Perroteau, P. Tos, and B. B. T.-I. R. of N. Battiston, Eds. Academic Press, 2013, pp. 257–275.
- [123] Y. Bledi, A. J. Domb, and M. Linial, "Culturing neuronal cells on surfaces coated by a novel polyethyleneimine-based polymer," *Brain Res Brain Res Protoc.*, vol. 5, pp. 282–289, 2000.
- [124] Y. Wei, X. Zuo, L. Chen, Y. Meng, S. Fang, J. Shen, and X. Shu, "Linear Plasma Sources for Large Area Film Deposition: A Brief Review," *Plasma Sci. Technol.*, vol. 16, no. 4, pp. 356–362, Apr. 2014.
- [125] K. Tsugawa, M. Ishihara, J. Kim, M. Hasegawa, and Y. Koga, "Large-Area and Low-Temperature Nanodiamond Coating by Microwave Plasma Chemical Vapor Deposition," vol. 16, no. 6, 2007.
- [126] A. Taylor, F. Fendrych, L. Fekete, J. Vlček, V. Řezáčová, V. Petrák, J. Krucký, M. Nesládek, and M. Liehr, "Novel high frequency pulsed MW-linear antenna plasma-chemistry: Routes towards large area, low pressure nanodiamond growth," *Diam. Relat. Mater.*, vol. 20, no. 4, pp. 613–615, Apr. 2011.
- [127] H. Köndgen, C. Geisler, S. Fusi, X.-J. Wang, H.-R. Lüscher, and M. Giugliano, "The dynamical response properties of neocortical neurons to temporally modulated noisy inputs in vitro.," *Cereb. Cortex*, vol. 18, no. 9,

- pp. 2086–97, Sep. 2008.
- [128] M. Giugliano, P. Darbon, M. Arsiero, H.-R. Lüscher, and J. Streit, "Single-neuron discharge properties and network activity in dissociated cultures of neocortex.," *J. Neurophysiol.*, vol. 92, no. 2, pp. 977–96, Aug. 2004.
  - [129] R. Brette, Z. Piwkowska, C. Monier, M. Rudolph-Lilith, J. Fournier, M. Levy, Y. Frégnac, T. Bal, and A. Destexhe, "High-Resolution Intracellular Recordings Using a Real-Time Computational Model of the Electrode," *Neuron*, vol. 59, no. 3, pp. 379–391, Aug. 2008.
  - [130] F. Vahidpour, L. Curley, I. Biró, M. McDonald, D. Croux, P. Pobedinskas, K. Haenen, M. Giugliano, Z. V. Živcová, L. Kavan, and M. Nesládek, "All-diamond functional surface micro-electrode arrays for brain-slice neural analysis," *Phys. status solidi*, vol. 214, no. 2, 2017.
  - [131] W. Nisch, J. Bock, U. Egert, H. Hammerle, and A. Mohr, "A thin film microelectrode array for monitoring extracellular neuronal activity in vitro," vol. 9, pp. 737–741, 1994.
  - [132] H. Hammerle, "A novel organotypic long-term culture of the rat hippocampus on substrate-integrated multielectrode arrays," pp. 229–242, 1998.
  - [133] S. M. Potter and T. B. Demarse, "A new approach to neural cell culture for long-term studies," vol. 110, pp. 17–24, 2001.
  - [134] R. Q. Quiroga, "Unsupervised Spike Detection and Sorting with Wavelets and Superparamagnetic Clustering," vol. 1687, pp. 1661–1687, 2004.
  - [135] J. Van Pelt, M. a Corner, P. S. Wolters, W. L. C. Rutten, and G. J. a Ramakers, "Longterm stability and developmental changes in spontaneous network burst firing patterns in dissociated rat cerebral cortex cell cultures on multielectrode arrays.," *Neurosci. Lett.*, vol. 361, no. 1–3, pp. 86–9, May 2004.
  - [136] C. E. Nebel, B. Rezek, D. Shin, H. Uetsuka, and N. Yang, "Diamond for bio-sensor applications," *J. Phys. D. Appl. Phys.*, vol. 40, no. 20, pp. 6443–6466, Oct. 2007.
  - [137] A. Stett, U. Egert, E. Guenther, F. Hofmann, T. Meyer, W. Nisch, and H. Haemmerle, "Biological application of microelectrode arrays in drug discovery and basic research.," *Anal. Bioanal. Chem.*, vol. 377, no. 3, pp. 486–95, Oct. 2003.
  - [138] A. Vaitkuvienė, M. McDonald, F. Vahidpour, J.-P. Noben, K. Sanen, M. Ameloot, V. Ratautaite, V. Kasetá, G. Biziuleviciene, A. Ramanaviciene, M. Nesládek, and A. Ramanavicius, "Impact of differently modified nanocrystalline diamond on the growth of neuroblastoma cells," *N. Biotechnol.*, vol. 32, no. 1, pp. 7–12, Jan. 2015.
  - [139] M. Cottance, S. Nazeer, L. Rousseau, G. Lissorgues, A. Bongrain, R. Kiran, E. Scorsone, P. Bergonzo, A. Bendali, S. Picaud, and S. Joucla, "Diamond Micro-Electrode Arrays (MEAs): a new route for in-vitro applications .," *DTIP*, no. April, pp. 16–19, 2013.
  - [140] S. Meijjs, M. Alcaide, C. Sørensen, M. McDonald, S. Sørensen, K. Rechendorff, A. Gerhardt, M. Nesládek, N. J. M. Rijkhoff, and C. P. Pennisi,

- "Biofouling resistance of boron-doped diamond neural stimulation electrodes is superior to titanium nitride electrodes in vivo," *J. Neural Eng.*, vol. 13, no. 5, p. 56011, 2016.
- [141] W. Kern, "The Evolution of Silicon Wafer Cleaning Technology," *J. Electrochem. Soc.*, vol. 137, no. 6, pp. 1887–1892, Jun. 1990.
- [142] S. M. Ojovan, M. McDonald, N. Rabieh, N. Shmuel, H. Erez, M. Nesladek, and M. E. Spira, "Nanocrystalline diamond surfaces for adhesion and growth of primary neurons, conflicting results and rational explanation," *Front. Neuroeng.*, vol. 7, no. June, pp. 1–9, Jun. 2014.
- [143] D. Linaro, J. Couto, and M. Giugliano, "Command-line cellular electrophysiology for conventional and real-time closed-loop experiments.," *J. Neurosci. Methods*, vol. 230, pp. 5–19, Jun. 2014.
- [144] M. Mahmud, R. Pulizzi, E. Vasilaki, and M. Giugliano, "QSpice tools: a generic framework for parallel batch preprocessing of extracellular neuronal signals recorded by substrate microelectrode arrays.," *Front. Neuroinform.*, vol. 8, no. March, p. 26, Jan. 2014.
- [145] T. Vandeveld, M. Nesladek, C. Quaeys, and L. Stals, "Optical emission spectroscopy of the plasma during CVD diamond growth with nitrogen addition," *Thin Solid Films*, vol. 290–291, pp. 143–147, 1996.
- [146] D. R. Merrill and P. A. Tresco, "Impedance Characterization of Microarray Recording Electrodes in Vitro," *IEEE Trans Biomed Eng.*, vol. 52, no. 11, pp. 1960–1965, 2005.
- [147] K. Honda, T. N. Rao, D. A. Tryk, A. Fujishima, M. Watanabe, K. Yasui, and H. Masuda, "Electrochemical Characterization of the Nanoporous Honeycomb Diamond Electrode as an Electrical Double-Layer Capacitor," *J. Electrochem. Soc.*, vol. 147, no. 2, pp. 659–664, 2000.
- [148] P. Fromherz and A. Stett, "Silicon-Neuron Junction: Capacitive Stimulation of an Individual Neuron on a Silicon Chip," *Phys. Rev. Lett.* 21, vol. 75, no. 8, pp. 1670–1674, 1995.
- [149] S. F. Cogan, K. A. Ludwig, C. G. Welle, and P. Takmakov, "Tissue damage thresholds during therapeutic electrical stimulation," *J. Neural Eng.*, vol. 13, no. 2, p. 21001, 2016.
- [150] F. O. Morin, Y. Takamura, and E. Tamiya, "Investigating neuronal activity with planar microelectrode arrays: achievements and new perspectives.," *J. Biosci. Bioeng.*, vol. 100, no. 2, pp. 131–43, Aug. 2005.
- [151] Z. V. Živcová, O. Frank, V. Petrák, H. Tarábková, J. Vacík, M. Nesládek, and L. Kavan, "Electrochemistry and in situ Raman spectroelectrochemistry of low and high quality boron doped diamond layers in aqueous electrolyte solution," *Electrochim. Acta*, vol. 87, pp. 518–525, Jan. 2013.
- [152] K. J. Regehr, M. Domenech, J. T. Koepsel, K. C. Carver, J. Ellison-zelski, W. L. Murphy, L. A. Schuler, E. T. Alarid, and J. David, "Biological implications of polydimethylsiloxane-based microfluidic cell culture," *Lab Chip.*, vol. 9, no. 15, pp. 2132–2139, 2009.
- [153] J. M. Nagarah, "Planar silicon patch-clamp electrodes integrated with polydimethylsiloxane microfluidics," University of California, Los Angeles,

USA, 2009.

- [154] H. Krysova, Z. Vlckova-Zivcova, J. Barton, V. Petrak, M. Nesladek, P. Cigler, and L. Kavan, "Visible-light sensitization of boron-doped nanocrystalline diamond through non-covalent surface modification.," *Pccp*, vol. 17, no. 2, pp. 1165–72, 2015.
- [155] J. Garra, T. Long, J. Currie, T. Schneider, R. White, and M. Paranjape, "Dry etching of polydimethylsiloxane for microfluidic systems," *J. Vac. Sci. Technol. A Vacuum, Surfaces, Film.*, vol. 20, no. 3, p. 975, 2002.
- [156] P. Fattahi, G. Yang, G. Kim, and M. R. Abidian, "A Review of Organic and Inorganic Biomaterials for Neural Interfaces," pp. 1846–1885, 2014.
- [157] S. Kaech and G. Banker, "Culturing hippocampal neurons.," *Nat. Protoc.*, vol. 1, no. 5, pp. 2406–15, Jan. 2006.
- [158] "Carbon Dioxide," *Wikipedia*. [Online]. Available: [https://en.wikipedia.org/wiki/Carbon\\_dioxide](https://en.wikipedia.org/wiki/Carbon_dioxide).
- [159] S. M. Ojovan, N. Rabieh, N. Shmoel, H. Erez, E. Maydan, A. Cohen, and M. E. Spira, "A feasibility study of multi-site, intracellular recordings from mammalian neurons by extracellular gold mushroom-shaped microelectrodes.," *Sci. Rep.*, vol. 5, no. August, p. 14100, Jan. 2015.
- [160] Y. Nam and B. C. Wheeler, "In Vitro Microelectrode Array Technology and Neural Recordings," vol. 39, no. 1, pp. 45–61, 2011.
- [161] M. Jenkner and P. Fromherz, "Bistability of Membrane Conductance in Cell Adhesion Observed in a Neuron Transistor," pp. 4705–4708, 1997.
- [162] P. Fromherz, "Semiconductor chips with ion channels , nerve cells and brain," vol. 16, pp. 24–34, 2003.
- [163] E. Claverol-tinture and J. Pine, "Extracellular potentials in low-density dissociated neuronal cultures," vol. 117, pp. 13–21, 2002.
- [164] B. Rezek, M. Krátká, E. Ukraintsev, O. Babchenko, A. Kromka, A. Brož, and M. Kalbacova, "Diamond as Functional Material for Bioelectronics and Biotechnology," 2011.
- [165] M. W. Varney, D. M. Aslam, A. Janoudi, H.-Y. Chan, and D. H. Wang, "Polycrystalline-Diamond MEMS Biosensors Including Neural Microelectrode-Arrays," *Biosensors*, vol. 1, no. 3, pp. 118–133, Aug. 2011.